CHALMERS
UNIVERSITY OF TECHNOLOGY

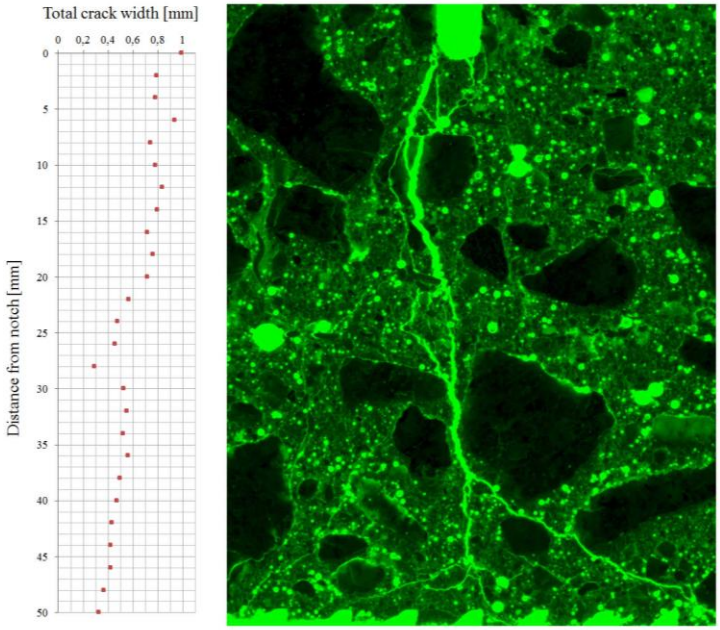

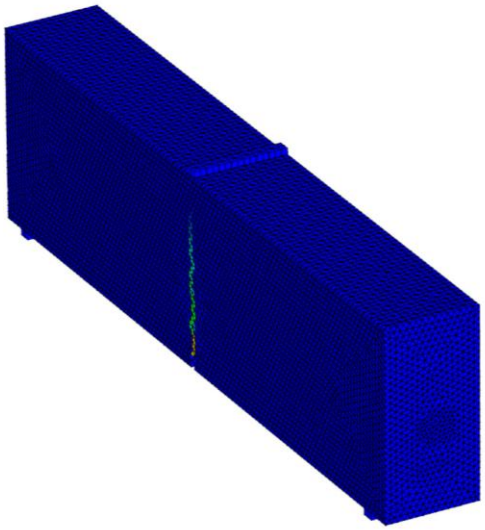

Crack Width Profiles for Fibre-reinforced Concrete Elements with Conventional Reinforcement

Master of Science Thesis in the Master's Programme
Structural Engineering and Building Technology

NICLAS GÖRANDER
CHRISTOPHER HALLDÉN

Department of Civil and Environmental Engineering
Division of Structural Engineering
Concrete Structures
CHALMERS UNIVERSITY OF TECHNOLOGY
Gothenburg, Sweden 2015
Master's Thesis 2015:80

MASTER'S THESIS 2015:80

Crack Width Profiles for Fibre-reinforced Concrete Elements with Conventional Reinforcement

Master of Science Thesis in the Master's Programme
Structural Engineering and Building Technology

NICLAS GÖRANDER

CHRISTOPHER HALLDÉN

Department of Civil and Environmental Engineering
Division of Structural Engineering
Concrete Structures
CHALMERS UNIVERSITY OF TECHNOLOGY

Göteborg, Sweden 2015

Crack Width Profiles for Fibre-reinforced Concrete Elements with Conventional Reinforcement
Master of Science Thesis in the Master's Programme
Structural Engineering and Building Technology
NICLAS GÖRANDER
CHRISTOPHER HALLDÉN

Examensarbete / Institutionen för bygg- och miljöteknik,
Chalmers tekniska högskola 2015:80

Department of Civil and Environmental Engineering
Division of Structural Engineering
Concrete Structures
Chalmers University of Technology
SE-412 96 Göteborg
Sweden
Telephone: + 46 (0)31-772 1000

Cover:
Picture of crack pattern and finite element model.

Chalmers Reproservice/Department of Civil and Environmental Engineering Göteborg, Sweden 2015

Crack Width Profiles for Fibre-reinforced Concrete Elements with Conventional Reinforcement
Master of Science Thesis in the Master's Programme
Structural Engineering and Building Technology
NICLAS GÖRANDER
CHRISTOPHER HALLDÉN
Department of Civil and Environmental Engineering
Division of Structural Engineering
Concrete Structures
Chalmers University of Technology

ABSTRACT

Fibre-reinforced concrete (FRC) is known to improve the cracking behaviour of conventionally reinforced concrete structures by reducing the crack spacing and crack width. However, it is still not fully known if fibres have any effect on the crack width profile between the reinforcement bar and the concrete surface or which effect this has on the structures service life.

This thesis aims to experimentally investigate and present the impact of fibres on the crack width profile for conventionally reinforced concrete elements and how well this behaviour can be modelled using finite element analysis.

In order to reach the aim of the thesis three-point bending tests were conducted and the actual crack width profiles were measured manually for surface cracks of ~0.6 mm and ~1 mm. The commercially available software DIANA was used to reproduce the bend tests. Additional material tests were made on the used concrete mixes to obtain material properties which were needed as input data for the finite element models. The results from finite element analysis showed that it was possible to a large extent to model the global behaviour of the tested beams, but the crack width profile could not be captured.

No clear effect on total crack width profile, attributable to the fibres, could be observed from the results. However, it was observed that the main cracks had a higher tendency to branch into several smaller cracks when fibres were added. Further, the study of crack width profiles indicated that benefits in terms of smaller individual cracks could have positive effect on FRC structures service life.

Key words: Crack width profile, Crack morphology, Crack width measurements, Combined reinforcement, SFRC, HyFRC, Finite element method, Inverse analysis

Sprickbreddsprofiler för fiberarmerad betong med konventionell armering

Examensarbete inom Structural Engineering and Building Technology

NICLAS GÖRANDER
CHRISTOPHER HALLDÉN
Institutionen för bygg- och miljöteknik
Avdelningen för Konstruktionsteknik
Betongbyggnad
Chalmers tekniska högskola

SAMMANFATTNING

Fiberarmerad betong är allmänt känt för att förbättra sprickbeteendet för konventionellt armerade betongkonstruktioner genom att reducera sprickavstånd och sprickbredd. Det är dock fortfarande inte känt om fibrer har någon påverkan på sprickbreddsprofilen mellan armeringsstången och betongytan eller vilket effekt detta kan ha på konstruktionens livslängd.

Målet med detta arbete är att experimentellt undersöka och presentera fibrers påverkan på sprickprofilen för konventionellt armerade betongbalkar och hur väl det beteendet kan modelleras med finita element metoden.

För att nå arbetets mål utfördes böjprovning (trepunkts) av armerade betongbalkar där den faktiska sprickbreddsprofilen mellan betongytan och armeringsstången mättes för sprickor med sprickbredden ~0.6 mm och ~1 mm vid betongytan. Den kommersiella programvaran DIANA användes för att reproducera böjtesterna. Kompletterande materialprovningar utfördes på de använda betongrecepten för att erhålla materialegenskaper till modellerna. Resultatet från finita elementanalyserna visade på att det globala beteendet för balkarna kunde reproduceras till stor del medan sprickprofilerna inte visade sig stämma överens med experimentella resultat.

Någon tydlig effekt av de använda fibrerna på den totala sprickbreddsprofilen kunde inte påvisas. Det gick dock att observera att huvudsprickan tenderade att förgrena sig i flera mindre sprickor när fibrer tillsattes i betongen. Effekten av flera mindre sprickor, istället för en stor, kan vara fördelaktigt med hänsyn till betongkonstruktionens livslängd.

Nyckelord: Sprickprofil, sprick-morfologi, sprickbreddsmätning, kombinationsarmering, stålfiberarmerad betong, hybridfiberarmerad betong, finita element metoden

Contents

Preface

The work for this thesis was performed between January and June 2015. The main work was carried out at the Division of Structural Engineering, Concrete Structures, at Chalmers University of Technology. Parts of the experimental work have taken place in the premises of Thomas Betong and SP in Borås. Due to efficiency reasons Christopher worked more with building the finite element model in DIANA and Niclas more with processing the data from experiments and measurements. However, both of us have been involved in all parts of the thesis and always working next to each other.

This thesis would never have gotten this far without the help and attention from our supervisors Carlos G. Berrocal, Ingemar Löfgren and David Fall. We specially want to thank Carlos for being next door every day feeding us with information and useful feedback. We also want to thank our opponents, Johan Forsgran and Andreas Lamton, who have given us valuable feedback through the whole project.

We would also like to address our gratitude to the members of the Department of Structural Engineering, with special thanks to Sebastian Almfeldt who helped us executing the experimental work. Also Jan Erik Lindqvist and the members of his team at SP/CBI Borås who helped us with a great deal of lab work.

Göteborg June, 2015

Niclas Görander Christopher Halldén

Notations

Roman upper case letters

A_c	Cross-sectional area of concrete
A_s	Cross-sectional area of steel bar
E_c	Modulus of elasticity of concrete
E_f	Modulus of elasticity of fibre
E_m	Modulus of elasticity of matrix
E_s	Modulus of elasticity of steel bar
F	Load
G_f	Fracture energy
L	Length of test specimen
N	Normal force
N_{cr}	Cracking load

Roman lower case letters

c	Concrete cover
d	Distance from compressive edge to reinforcement
f_{ct}	Tensile strength of concrete
f_R	Flexural tensile strength
f_{yk}	Characteristic yield stress
h	Height of concrete section
k	Coefficient
k_f	Ratio of residual and mean tensile strength
$l_{element}$	Characteristic length of a finite element
l_s	Transmission length
Δl	Length without stress transfer
s_r	Crack spacing
w	Crack width
w_{eff}	Effective crack width
w_k	Characteristic crack width
w_s	Crack width at reinforcement level
w_u	Ultimate crack width
x	Height of compression zone

Greek letters

α	Ratio
ε	Strain
ε_{cm}	Average strain of concrete
ε_{sm}	Average strain of steel bar
ϕ	Diameter
ρ	Ratio of reinforcement
σ	Stress
σ_c	Stress in concrete
σ_{fu}	Ultimate stress in fibre
σ_{mu}	Ultimate stress in matrix
σ_s	Stress in steel bar
τ_b	Bond stress

Abbreviations

3PBT	Three-point bend test
AR	Alkali resistant
CMOD	Crack mouth opening displacement
FE	Finite element
FEA	Finite element analysis
FEM	Finite element method
FRC	Fibre-reinforced concrete
HyFRC	Hybrid fibre-reinforced concrete
PC	Plain concrete
PVA	Poly-vinyl alcohol
RC	Reinforced concrete
SFRC	Steel fibre-reinforced concrete
SLS	Serviceability limit state
ULS	Ultimate limit state
UV	Ultra violet

1 Introduction

1.1 Background

In structural engineering Fibre-reinforced Concrete (FRC) has now been available for a considerable time but still it is not used very frequently in practice. Also its application is concentrated to few types of structures where the two most common are graded slabs and pavements for crack control i.e. not used in structures for structural purpose. The relatively small use of FRC in structural elements is said to be a result of the lack of standardized design codes (di Prisco et al. 2013). This have led to putting more pressure to develop codes that handle the design process of fibre-reinforced elements and recently ditto have been released. It is commonly known that fibres have a positive influence on limiting crack width. However, it is also of interest to assess the impact of fibres on the crack width profile and morphology to be able to determine if there are other benefits, not only crack width and crack spacing. To be able to use these possible properties of fibres, it is of interest to model and predict the behaviour of structures made of FRC. Finite element analysis is widely used to calculate and design structural elements but it can be executed in many ways, which makes this subject interesting for further research.

FRC can be composed in many different variations and the number of types of fibres is only increasing. With different materials come also different properties that can be combined. Fibre size is often divided into micro or macro scale, where fibres with a diameter greater than 0.1 mm are referred to as macro, to differ them mainly in size but also in their mechanical behaviour (Bentur & Mindess 2007). In order to find other suitable applications of FRC and what the possible structural benefits that combining different types of fibres can bring, it is of interest to further investigate to what extent the combination of different fibre sizes and materials might impact the crack width.

1.2 Aim and objectives

The general aim of this thesis was to deepen the knowledge regarding how fibres influence the crack width profile and morphology, and to investigate whether finite element analysis can be used to model the real behaviour of cracking concrete elements with fibre-reinforcement in combination with conventional reinforcement (ribbed reinforcement bars).

A modified three-point bending test based on RILEM beams (EN 14651 2005) was performed to investigate the effect that fibres had on the crack width profile and the crack pattern in the concrete cover, i.e., between the ribbed reinforcement bars and the concrete surface. Additionally, poly-vinyl alcohol (PVA) micro fibres were used together with the steel macro fibres to evaluate if a combination of different types of fibre had any beneficial effect on the crack width profile between the ribbed reinforcement bar and the concrete.

The specific objectives are:

- To assess the influence of fibres on the crack width profile and crack pattern between the reinforcement bar and concrete surface.
- To develop a non-linear finite element model that could verify the ability of finite element method to describe the real structural behaviour.

1.3 Scope and limitations

The thesis covers the cracking behaviour of FRC elements with ribbed reinforcement bars in serviceability limit state.

Three-point bending tests were performed on modified RILEM beams where fibres were used together with conventional reinforcement. The fibres that were used in the experiments were macro steel fibres with end-hooks and micro PVA fibres. The experiment was limited to three concrete mixes; plain concrete (PC), steel fibre-reinforced concrete (SFRC) and a hybrid mix consisting of steel fibre-reinforced concrete combined with PVA fibres (HyFRC). Self-compacting concrete with concrete strength class of C32/40 was used for all specimens. The tested beams with ribbed reinforcement were not loaded to failure but rather to a certain crack width at the surface. This was decided to achieve easy comparable values of the crack width profiles and simplify the crack width measurements.

There are several commercially available finite element analysis (FEA) programs today that can be used for modelling. In this thesis DIANA (TNO DIANA 2014) was used to model the beams. The FEM model was limited to reproducing the three-point bending test since those were the tests performed in the experiment.

1.4 Methodology

The project started with a literature study of previous research in the field of FRC and FEM modelling of FRC elements. This was done to better understand the basics of fibre-reinforcement and more precisely the crack behaviour of FRC elements, also to find out which approaches had previously been used to model FRC elements in DIANA and other FEA programs.

Parallel to the literature study an experimental program was conducted where crack widths were measured and material properties for the FEA were gathered. Also the obtained data in terms of structural behaviour could act as verification for the FE model. The experiments were conducted to be able to examine if the crack profile differed for FRC compared to that of plain concrete. To be able to easily cast, manage and study the structural elements used for experimental work a modified RILEM (RILEM TC 162-TDF 2000) beam was chosen for the experiments. The cracks were measured digitally using a microscope outfitted with a camera. Finally the values were sorted, discussed and presented to be comprehensible.

The final models that were developed utilized the input data obtained from experimental work and from inverse analysis the tensile strength of the fibre-reinforced concrete mixes were established. From the literature study other's experience from previous work was considered and problems that were already known could be avoided.

The methodology consists of three main tracks, here stated in short;

- Literature study of previously published work in the field of fibre-reinforced concrete and FE modelling.
- Experimental programme to gather new data in terms of crack widths to use for investigating the effect of fibres and input data for FE modelling.
- Finite element analyses of the test setups. Verification achieved by comparing numerical results and experimental data.

2 Fibre-reinforced Concrete

This chapter serves to introduce to the reader the basics of fibre-reinforced concrete, with focus on the materials used in this thesis. Furthermore, the physical behaviour of some fibres is presented as well as a definition of what makes a fibre structurally effective in fibre-reinforced concrete. Also the impact of corrosion on reinforced concrete structures and how their durability may be affected when fibre-reinforced concrete is used.

2.1 General

Starting with the basics of concrete it is commonly based on hydraulic binder (Portland cement), water and aggregates. By adding fibre to the mix the properties and the behaviour of the structure will change. In most cases fibres give little or no addition to concrete strength, but it leads to improvement in the post-cracking state since toughness is increased (Bentur & Mindess 2007). Initially, fibres were mostly used for crack control but presently there has been an increase of fibre usage to increase the toughness of concrete structures. Areas where the toughness have been utilized are dynamic and cyclic loading such as fatigue, seismic and temperature change. What is important to understand is that fibre-reinforced concrete is not a single material and the possibilities in terms of areas of application are plenty.

The main purpose of adding fibres into the concrete mix is to add residual strength to the material. Residual strength is associated with post-cracking capacity of a concrete element. By adding fibres and distributing them in the concrete mix they will alter the tensile behaviour of the element. Fibres bridging cracks will allow transfer of stress, which decrease the crack width and crack spacing and distributing the stresses over a larger area. The tensile post-cracking behaviour is generally classified into two categories, strain softening and strain hardening behaviour (Löfgren 2005). In Figure 2.1 three curves which represent the typical stress-deformation relation of these materials are presented. Which strain behaviour that will occur depends largely on fibre dosage, but there are many parameters that will decide what properties the composite, concrete mixed with fibres, will obtain. The following sections serve to introduce some fibre types and how they can affect the concrete properties.

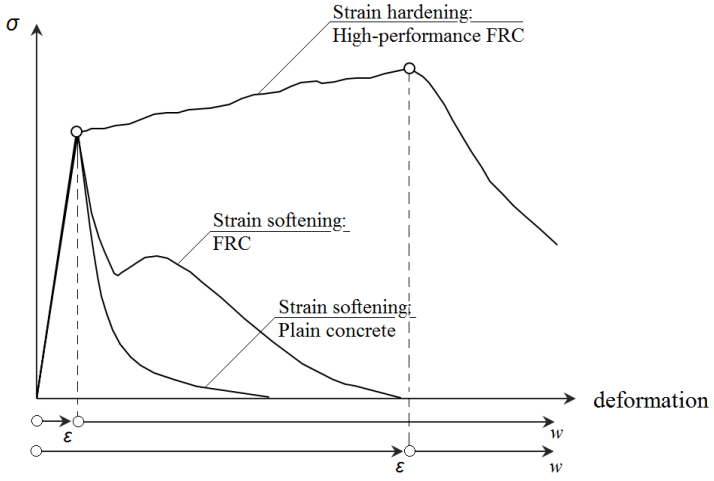

Figure 2.1 Schematic tensile behaviour of different concrete composites.

2.2 Fibre technology

As the technology of fibre-reinforced concrete has caught the interest of researchers worldwide it has resulted in a considerable amount of different types of fibres. Altered properties give new possibilities in terms of behaviour and performance when mixed into the concrete matrix. In Table 2.1 for an outtake of various available fibres and their properties are presented. The fibres described show that a wide range of material properties are available for non-structural and structural purposes depending on the characteristics and performance of the fibres

Table 2.1 A summary of various fibres physical properties (Löfgren 2005).

Type of fibre	Diameter [μm]	Specific gravity [g/cm^3]	Tensile strength [MPa]	Elastic modulus [GPa]	Ultimate elongation [%]
Metallic					
Steel	5-1000	7.85	200-2600	195-210	0.5-5
Glass					
AR glass	8-20	2.70	1500-3700	80	2.5-3.6
Synthetic					
Poly-vinyl alcohol (PVA)	3-8	1.2-2.5	800-3600	20-80	4-12
Natural – organic					
Cellulose	15-125	1.50	300-2000	10-50	20
Jute	100-200	1.02-1.04	250-350	25-32	1.5-1.9
Natural – inorganic					
Asbestos	0.02-25	2.55	200-1800	164	2-3
Basalt	9-23	2.65	4840	89	3.15
Wollastonite	25-40	2.87-3.09	2700-4100	303-530	-

As suggested by Naaman (Naaman 2003), short discontinuous fibres can be divided into three main categories which are; according to the fibre material, the physical/chemical properties and their mechanical properties.

- *Fibre material*; natural organic (i.e. cellulose), natural mineral (i.e. asbestos) and man-made (i.e. steel or synthetics)
- *Physical or chemical properties*; density, surface roughness, shape, chemical stability and non-resistivity when mixed into concrete, etc.
- *Mechanical properties*; tensile strength, ductility, elastic modulus, etc.

These three definitions are the base for fibres but there are more levels of describing and sorting fibres. To evaluate fibres effectiveness and possibilities to enhance the concrete matrix there are a number of property relations that are of importance and should be fulfilled (Naaman 2003). These relations basically are to assure that the fibres will enhance the material, by adding fibres with higher performance properties. Firstly the tensile strength of the fibre should be greater than for the concrete matrix,

Naaman states it should be of order two to four times greater of magnitude. Secondly, the elastic modulus should be at least three times greater. Thirdly the bond strength should be at least as high as the tensile strength of the concrete matrix. Fourthly the fibre should be ductile and add ductility to the matrix, see Figure 2.2 for an overview of these statements. Naaman also describes that Poisson ratio and thermal expansion coefficient should if possible be of the same order as the concrete matrix; this is to avoid a debonding due to possible large difference in deformation when any type of load is applied.

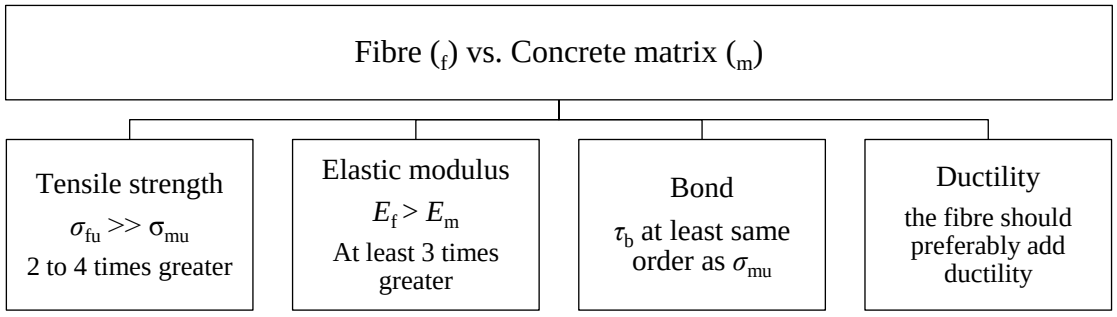

Figure 2.2 Desirable fibre properties according to Naaman (Naaman 2003).

Geometries have a great impact on the performance of the fibres, especially on the bond to the concrete. Different cross-sections create different cross-sectional area and perimeter, in an example from Löfgren (Löfgren 2005) it is shown that a fibre with triangular cross-section has a 28% larger perimeter (therefore contact surface) than a fibre with same area but with a circular cross-section. This implies the possibilities to improve the characteristics of fibres for better reinforcing performance in concrete. See Figure 2.3 (a) for typical fibre geometries and Figure 2.3 (b) for common cross-sections.

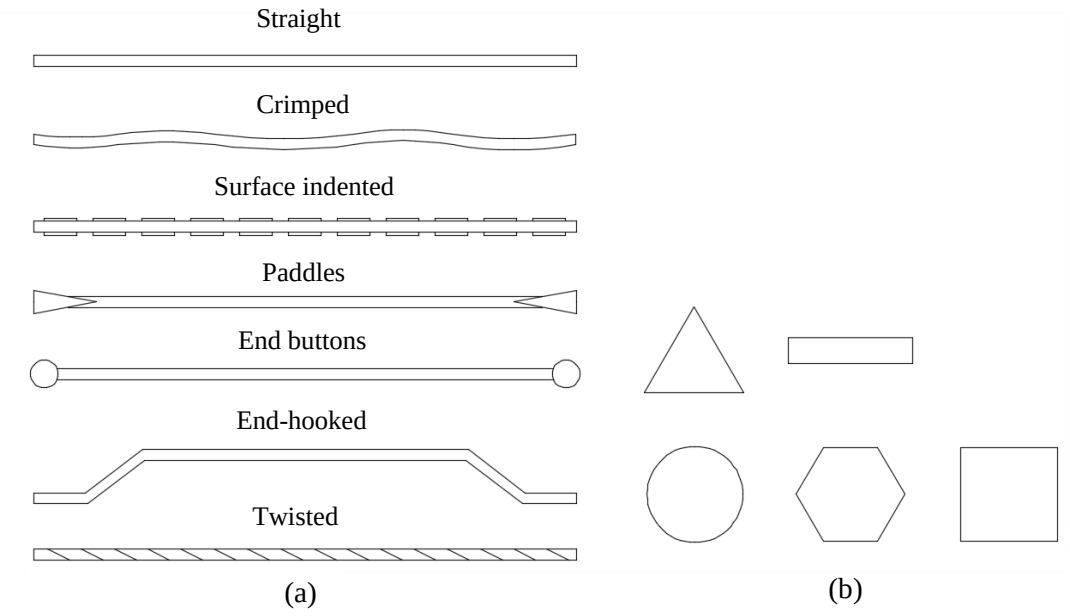

Figure 2.3 Fibre geometries (Naaman 2003) and cross-sections (based on Löfgren 2005).

Material properties are important when designing structures with fibre-reinforced concrete. When applied with structural purpose it is today more standardized how to evaluate the properties of the FRC since the recent release of new adopted standards. (see RILEM TC 162-TDF 2000; DAfStbUA SFB N 0146 2005; Model Code 2010). Also in 2014 the Swedish Standard SS 812310:2014 was published, which is not officially a part of Eurocode but functions as a complement to Eurocode 2 and they should be read as one to fully be able to perform a design. The Swedish Standard covers design of FRC structures using fibres made of steel and polymer and is defined by SS-EN 14889-1 and SS-EN 14889-2. That means use of fibres made out of other materials are not yet included.

When designing structures in fibre concrete it is of importance to be consistent with how to use the fibre concrete properties. As stated in the complement to Eurocode 2, Fibre Concrete – Design of Fibre Concrete Structures, the specific properties of the fibre concrete have to be known, either prescribed or by interpolation (within certain demands), "Initial testing shall be performed in each case where a new fibre concrete composition is to be used to provide a fibre concrete that achieves the specified properties or intended performance with an adequate margin" (Swedish Standards Institute 2014). The standard demands that extended testing should be performed if any of the parameters of the mix is changed.

2.2.1 Steel fibres

Steel fibres are the most used fibre material for FRC with structural purpose (Jansson 2011). The benefits of using steel come from the material properties. The possibilities to produce effective fibres in terms of geometry and material properties probably made it the most commonly used fibre material (Bentur & Mindess 2007).

Normally the fibre have circular cross-section with a diameter of 0.2-1.0 mm and a length/thickness ratio between 40 and 80, but the variations available are many. A typical feature is to have a mechanical anchor; this is due to the large impact on the fibre pull-out force (Löfgren 2005). By the choice of fibre type, the mechanical anchorage will affect which failure mode will occur when the structure is deformed. The general failure behaviour for steel fibre-reinforced concrete (SFRC) is pull-out, where the fibres bridging a crack deform and get pulled out of the concrete. There are several mechanisms present during pull-out that create crack bridging such as; friction between fibre and concrete, and deformation of any type of anchorage feature e.g. end-hooks. A potential problem for high strength steel fibres is that the capacity of the fibre itself is higher than the surrounding concrete. In other words, there is higher likelihood of anchorage failure and concrete damage, which in turn reduces the efficiency of the fibre.

The common end-hooked steel fibres fulfil the fibre vs. matrix relation (see Figure 2.2) to a great extent, but there is research on how to improve the performance of steel fibres. In a study by Naaman (Naaman 2003), which focused on improving the efficiency of fibres by changing shape, size and mechanical properties of the fibre, an improved fibre type was presented. This fibre shows a slip-hardening behaviour, whereas the commonly used steel fibre with end-hooks exhibits slip-softening behaviour. The new fibre type is associated with high performance FRC which is distinguished by a tension-hardening behaviour while conventional FRC, at normal

dosages, shows a tension-softening behaviour. Thus, the post-cracking behaviour of a FRC element heavily depends on the fibre amount and properties.

Material properties of steel fibres show great variety depending on manufacturer and intended application. Tensile strength can range, according to Löfgren (Löfgren 2005), between 200-2600 MPa and for ultimate elongation a great variety can be found also here when the range is 0.5-5%. Basically the properties are changeable in the way that suits the specific structure and application.

The most commonly used steel fibre is the end-hooked variant. Today it is used mainly within tunnelling, industrial floors but also for residential purposes.

2.2.2 Poly-Vinyl Alcohol fibres

Poly-vinyl alcohol (PVA) is a synthetic fibre which is achieved through hydrolysis of poly-vinyl acetate. Synthetic fibres like poly-vinyl alcohol fibres have different characteristics compared to steel fibres and therefore different functionality in the concrete matrix. The PVA fibres have high tensile strength (Zheng & Feldman 1995), with values comparable with high strength steel used for steel fibres. When comparing ultimate strain, PVA fibres range a little above steel with 4-12% of ultimate strain. Also the dimensions of the fibres are in a different range. PVA fibres available on the market have normally a diameter of 3-8 μm (Löfgren 2005). This gives the fibres a very high aspect ratio, which positively affects the efficiency of the fibre (Naaman 2003). Furthermore, PVA fibres bond well with the cement matrix as the fibre have a rough surface and the geometrical shape is not circular. PVA also allows hydrogen to form a bond with cement which creates an efficient composite (Zheng & Feldman 1995). According to the manufacturer of PVA fibres, NYCON (2015), this gives an improvement of the bond of up to three times greater compared to other types of fibre e.g. steel fibre. The strong bond have shown to make PVA fibres prone to fail in rupture, unlike most steel fibres (Bentur & Mindess 2007). Due to these properties of the PVA fibres they have a different purpose in the concrete matrix; the stiffer bond and relatively small size makes them more beneficial and efficient on the micro scale than e.g. end-hooked steel fibres. Thus the scale on which the PVA fibre is expedient is for suppressing the initiation and propagation of macro cracks by arresting the growth of micro cracks (Löfgren 2005).

Commonly the PVA fibre is used for controlling cracking from thermal loads and plastic shrinkage.

2.3 FRC in combination with conventional reinforcement

In most cases fibre concrete is combined with conventional reinforcement but still the full potential of the interaction is not utilized in practice (Bernardi et al. 2015). Further, through experiments, fibres have proven to enhance the ultimate performance of concrete structures with lower amounts of conventional reinforcement (Löfgren 2005). Fibres improve the post-cracking behaviour of the concrete matrix, which mainly improves the behaviour in SLS regarding crack widths, crack spacing and deflection (due to increased flexural stiffness). However, the ability to bridge cracks and improve the load capacity widely depends on the amount of fibres mixed into the concrete. Unfortunately, due to uncertainties in fibre distribution and fibre orientation it is hard to utilize the full capacity of the fibres in design. It is therefore very common

that conventional reinforcement is used for the ULS capacity (Bentur & Mindess 2007), which has a known placement in the structure and has a more efficient internal lever arm.

2.4 Corrosion of FRC

Corrosion of reinforcement bars in concrete structures is a major concern for their durability. Severe corrosion of the reinforcement will lead to lowered capacity of the structure with increased risk of failure but also an aesthetical degrading when cover spalling occurs and rust stains discolour the surface.

For uncracked concrete the concrete cover acts as a protective layer which enables a relative slow ingress of corrosion-inducing agents. As concrete is a brittle material and cracks are inevitable when in tension, cracks allow other types of mechanisms to more quickly reach the reinforcement through the concrete cover and initiate corrosion of the reinforcement bars. This leads then to a faster degradation of the structure compared to an uncracked structure (Berrocal 2015). The flow of water through a crack in concrete has been described by the expression presented by Edvardsen (Edvardsen 1999), see equation (1). The flow depends on geometrical parameters as well as the pressure situation, but the dominant factor here is the crack width, *w*. This implies that small changes to the crack width have large impact to the water flow. If the water flow is decreased the corrosion of reinforcement bars most likely will be less.

$$q_r = \frac{\xi \cdot \Delta p \cdot b \cdot w^3}{12 \cdot \eta \cdot d} \qquad (1)$$

where:

q_r = water flow of natural rough cracks [m^3]

w = crack width [m]

ξ = reduction factor compromising the roughness of cracks [-]

Δp = differential water pressure [Pa]

b = length of crack [m]

η = absolute viscosity [Pa*s]

d = flow path length of crack [m]

As mentioned before, FRC in cracking exhibits additional, smaller and more narrowly spaced cracks compared to conventionally reinforced concrete. While these features are beneficial with regard to corrosion of the reinforcement bars, it is unclear whether the fibres themselves impact the concrete matrix in a negative way with regard to corrosion (Berrocal 2015). Bentur and Mindess (Bentur & Mindess 2007) compiled research on corrosion of SFRC without conventional reinforcement. Most of their results showed that fibres have no or little impact on the durability of the concrete itself. Looking locally on the steel fibre it can be seen that due to the small diameter any corrosion will affect the failure mode of the SFRC, from fibre pull-out to fracture of the fibre (Kosa & Naaman 1990). However, in practice it has been seen that SFRC structures does not experience much impact of fibre corrosion. Even in highly corrosive environment it has been observed that corrosion of fibre close to the concrete surface does not lead to spalling (Bentur & Mindess 2007).

Due to a possible reduction of corrosion-induced damage stemming from the use of FRC, there is an interest to discretise the crack limiting effects of fibre-reinforcement in order to find new areas of application.

3 Crack Width Theory

This chapter aims to give a short overview on the subject of crack width and crack spacing in RC and FRC elements. Both plain concrete and FRC are included to show the theoretical effect fibres have on the crack width.

3.1 Crack width theory for plain concrete

There are different approaches to calculate crack widths and predict the cracking behaviour of reinforced concrete elements. The models used for calculations range from purely analytical to purely empirical.

According to Tammo (Tammo 2009) the design methods can be divided into two different major groups. The first group includes models which are purely empirical. This means that the models are based only on experimental data which have been compiled to describe the relation between different parameters and the crack width and crack spacing. The other group includes semi-empirical models. These are analytical/theoretical models which are then fine-tuned and modified after experimental testing.

The method in Eurocode that is used for detailed crack calculations is based on a semi-empirical model (Tammo 2009). The basis for this method is derived from the cracking behaviour of an axially loaded reinforced concrete prism.

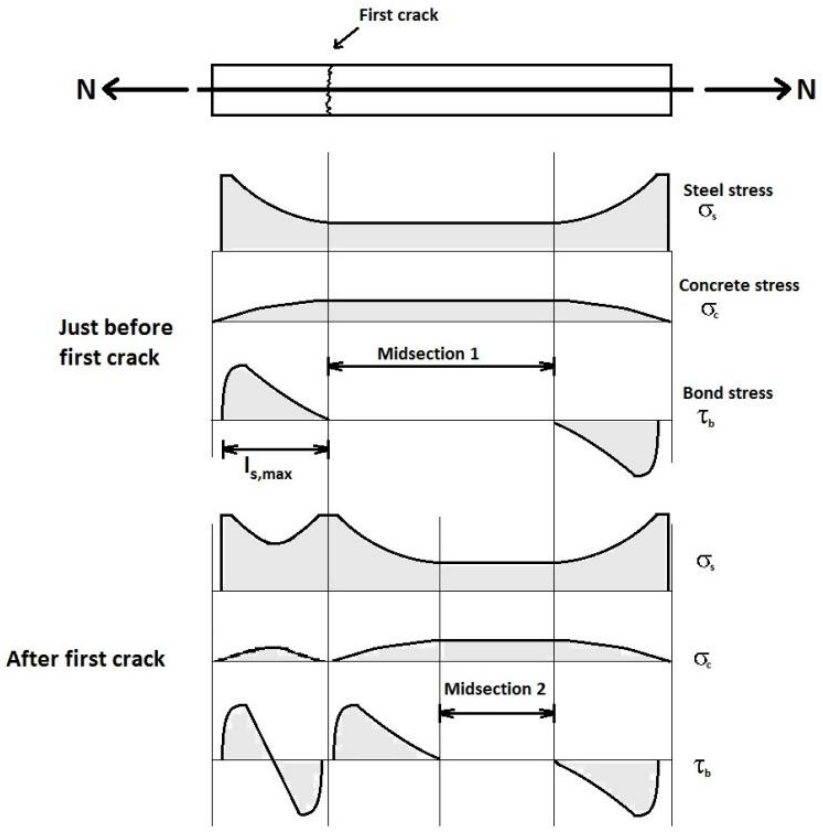

Figure 3.1. Stress distribution during cracking.

Consider the uncracked concrete section with an increasing axial force, *N*, acting on the concentric reinforcement bar. In the ends of the element the force is transferred from the bar into the concrete by bond stresses, τ_b. The length that is required to fully

transfer N into the concrete section is called the transmission length, l_s. Due to high bond stresses there will be small cracks near the reinforcement bar over a short length, Δl, in the end sections, which leads to a local bond failure where there is no stress transmission. In the transmission length the steel strain is higher than the concrete strain. As N increases the length needed to transfer the load into the concrete also increases. Eventually the axial force N reaches the cracking load, N_{cr}, of the cross section. When N_{cr} is reached the transmission length has reached its maximum length, $l_{s,max}$. The crack will not appear in the transmission length since the concrete stress there is lower than in the mid-section. Consequently, the first crack will appear in the locally weakest area somewhere in the midsection.

When the first crack appears two new end sections are created there which have their own transmission lengths, see Figure 3.1, where a new crack will not appear. Neither will there be a new crack forming in midsection 1, since the concrete stress will not reach the tensile stress due to insufficient transmission length. Hence, the subsequent crack will form in the new midsection (midsection 2). This process will continue until there is insufficient transmission length between each crack to reach f_{ct} in that concrete section, i.e. the cracking process has stopped. Consequently, the crack spacing will vary between $l_{s,max} + \Delta l$ and $2\times(l_{s,max} + \Delta l)$.

$$s_{r,max} = 2 \cdot s_{r,min} = 2 \cdot (\Delta l + l_{s,max}) \tag{2}$$

At this stage the average concrete strain between the cracks, ε_{cm}, is equal to:

$$\varepsilon_{cm} = \frac{f_{ct} \cdot (\frac{E_s}{E_c} + \frac{A_c}{A_s})}{E_s} \tag{3}$$

Any increase in load after the cracks have stabilised will only increase the stress in the reinforcement bar and increase the crack widths. The average strain in the steel, ε_{sm}, between the cracks after this stage is depending on steel stress, σ_s.

$$\varepsilon_{sm} = \frac{\sigma_s}{E_s} \tag{4}$$

The difference in strain between the concrete and steel over the crack distance is equal to the crack width.

$$w_k = s_{r,max} \cdot (\varepsilon_{sm} - \varepsilon_{cm}) \tag{5}$$

The load that has been transferred into the concrete section at cracking is equal to the mean bond stresses multiplied with the transmission surface, which is the transmission length multiplied with the circumference of the reinforcement bar, $\emptyset\times\pi$.

$$N_{cr} = A_c \cdot f_{ct} = \tau_{b,mean} \cdot l_{s,max} \cdot \emptyset \cdot \pi \tag{6}$$

$$l_{s,max} = \frac{f_{ct} \cdot \emptyset}{4 \cdot \tau_{b,mean} \cdot \rho} \tag{7}$$

The same basic relations are used for crack width calculations in Eurocode 2, but there are coefficients added to calibrate the model to conform to experimental studies. For instance, the maximum crack spacing is expressed the following way:

$$s_{r,max} = \underbrace{k_3 \cdot c}_{2 \cdot \Delta l} + \underbrace{k_1 \cdot k_2 \cdot k_4}_{\frac{f_{ct}}{4 \cdot \tau_{b,mean}}} \cdot \frac{\emptyset}{\rho} \qquad (8)$$

Where *c* is the concrete cover thickness and *k* are various calibration coefficients. The average strains are the same as in (3) and (4), but are expressed in a different way:

$$(\varepsilon_{sm} - \varepsilon_{cm}) = \frac{\sigma_s - k_t \cdot \frac{f_{ct,eff}}{\rho_{p,eff}} \cdot (1 + \alpha_e \cdot \rho_{p,eff})}{E_s} \qquad (9)$$

These relationships are derived from a uniaxially loaded concrete element, but that is not very applicable since few structural concrete components fit into that description. It is however possible to apply this theory to flexural elements and bending cracks as well. This is done by viewing the area around the reinforcement bars in the tension zone as an axially loaded element.

3.2 Crack width theory for FRC

The basic theory behind crack width calculations for FRC is the same as for plain concrete, which is described in section 3.1, with the difference being that the residual strength from the fibres is also taken into account. By adding the residual strength to equation (6) the relation in equation (10) can be formed, which is described by Löfgren (Löfgren 2007).

$$A_c \cdot f_{ct} = \tau_{b,mean} \cdot l_{s,max} \cdot \emptyset \cdot \pi + A_c \cdot f_{t,residual} \qquad (10)$$

By expanding equation (8), as similarly done for equation (6) in section 3.1, the following relation can be obtained for the maximum crack spacing in FRC elements with conventional reinforcement:

$$s_{r,max} = k_3 \cdot c + k_1 \cdot k_2 \cdot k_4 \cdot \left(1 - \frac{f_{t,residual}}{f_{ct}}\right) \cdot \frac{\emptyset}{\rho} \qquad (11)$$

This is also the basis for the equation given in the recently published Swedish standard SS812310:2014. For calculation of the average strain there are two options given. One of the options is to calculate a fictitious steel stress, $\sigma_{s,fict}$, which is the stress in the tension reinforcement bar in the cracked section but neglecting the residual capacity given by the fibres. In other words it is the steel stress that would have been present if there were no fibres present in the concrete. This method is the easiest to use for showing the effects of fibres on crack widths in RC structures.

$$(\varepsilon_{sm} - \varepsilon_{cm}) = \frac{(1 - k_f) \cdot \left(\sigma_{s.fict} - k_t \cdot \frac{f_{ct,eff}}{\rho_{s,eff}} \cdot (1 + \alpha_{ef} \cdot \rho_{s,eff})\right)}{E_s} \quad (12)$$

$$k_f = \frac{f_{ftd,R1}}{f_{ctm}} \leq 1.0 \quad (13)$$

Comparing the equations for plain concrete and FRC is can be seen that the difference is in the residual tensile strength. As long as there is any residual strength, k_f will be smaller than 1 and both the crack spacing and the average strain will be smaller compared to plain concrete, given the same load. Since the crack width equation (5) is still true for FRC, the crack width will be reduced as well.

3.3 Shape of crack profile for plain concrete

The theory behind crack width calculations mentioned in section 3.1 and 3.2 takes little to no consideration to the shape of the crack profile. For tensile elements, as described in Figure 3.1, it is assumed that the crack width at the concrete surface is the same as it is close to the reinforcement (Tammo 2009).

As mentioned in section 3.1, the crack width calculated from equation (5) for bending cracks is the crack width at the level of the reinforcement bar. In Model Code 2010 is assumed that the crack width follows the strain distribution of the tensile zone, i.e. varies linearly from the neutral axis to the maximum tensile fibre, see Figure 3.2. This variation is derived from geometrical principles of triangles and the assumption that the whole tensile zone is cracked. However, it is still assumed that the crack width is constant along the width (z-axis) of the beam, unless the spacing of the reinforcement bars is too big.

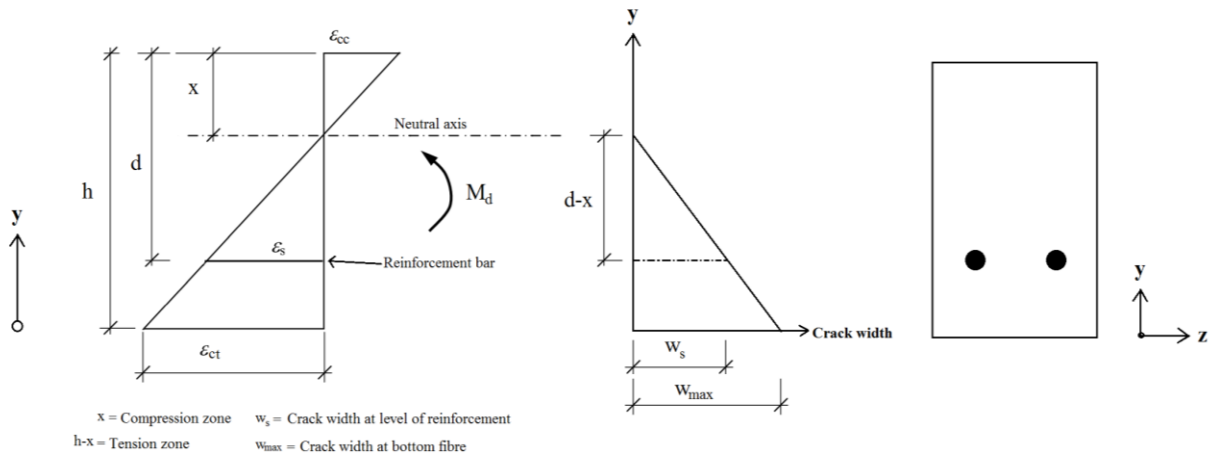

Figure 3.2. Assumed crack width profile according to Model Code 2010, vol 2.

For instance if w_s in Figure 3.2 is known through calculations, then the maximum surface crack width, w_{max}, according to Model Code 2010 is assumed to be:

$$w_{max} = w_k \cdot \frac{h - x}{d - x} \tag{14}$$

which is the geometrical relation described previously.

There are several studies that showed that cracks are actually smaller close to the reinforcement, $w_{rein,}$ than at the concrete surface, w_{surf}, see (Husain & Ferguson 1968), (Broms 1965), (Tammo 2009) and (Borosnyól & Snóbli 2010). Borosnyól and Snóbli (Borosnyól & Snóbli 2010) stated that other studies showed that the surface crack width can vary between 2 to 10 times the crack widths near the reinforcement. Their own test results from uniaxially loaded concrete prisms with varying concrete cover showed that the ratio w_{surf}/w_{rein} varies approximately from 3 to 10, depending on the thickness of the concrete cover. See Figure 3.3 for an example of how the measured crack width varied for one of their specimens.

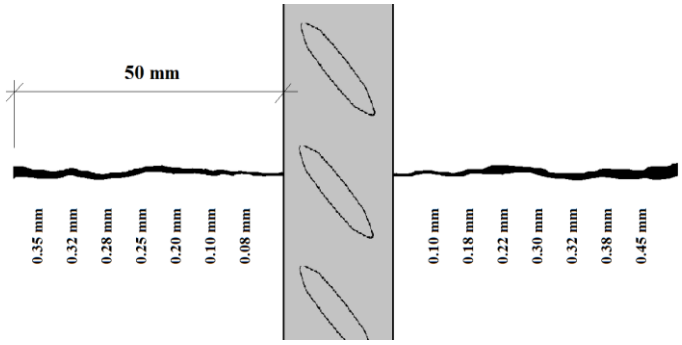

Figure 3.3 Variation of crack width for sample with 50 mm concrete cover (Borosnyól & Snóbli 2010).

Husain & Ferguson (1968) measured crack width profiles of a large amount of plain concrete elements loaded in bending. The testing showed that the crack profile variation is true also for flexural cracks. The crack widths were measured both in height (y-direction) and width (z-direction) which showed that the w_{surf}/w_{rein} ratio is larger than 1 in both directions, see Figure 3.4.

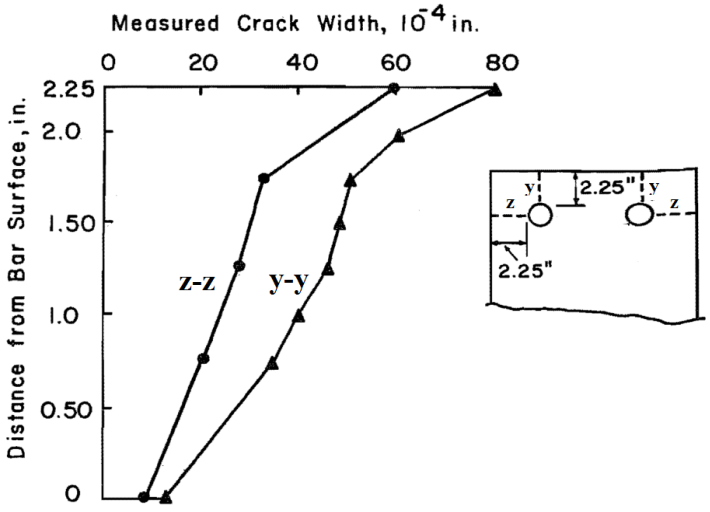

Figure 3.4. Crack width profile in z- and y-direction (Husain & Ferguson 1968).

Broms (Broms 1965) performed tests on tension members with one reinforcement bar and plain concrete. One of his findings was that the w_{surf}/w_{rein} ratio was dependent on the steel stress in the reinforcement bar. At very low steel stresses, the crack width at the concrete surface and reinforcement surface were the same, but this quickly changed, see Figure 3.5.

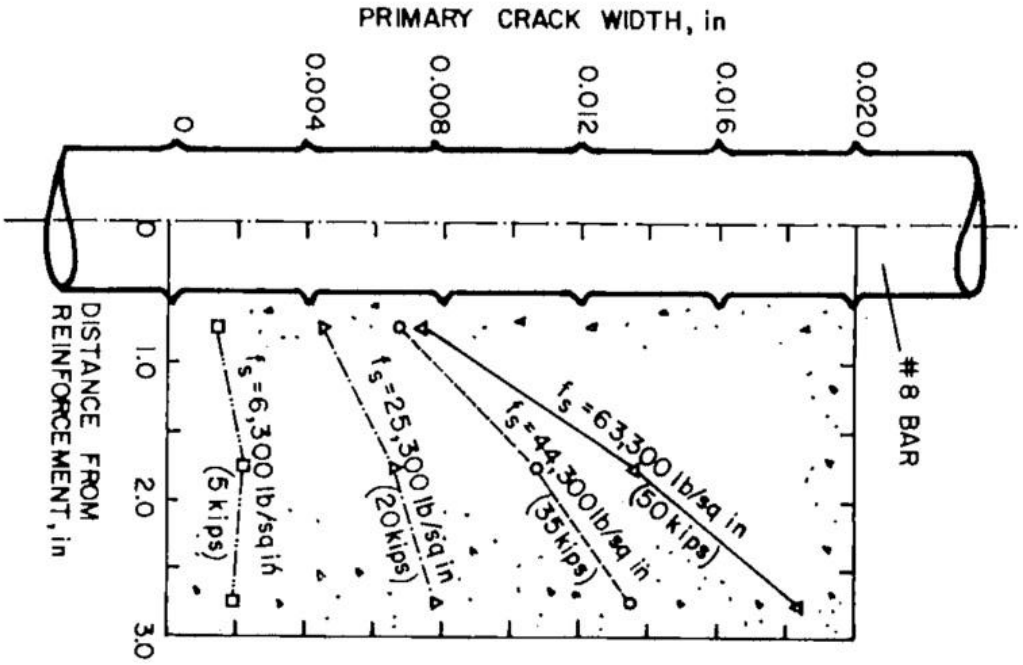

Figure 3.5. Crack width profile for different steel stresses (Broms 1965).

Test results from both axially loaded elements and flexural elements show that the crack width is not constant between the concrete surface and the reinforcement and that there is a variation in the profile that cannot be explained by geometrical causes. Tammo (Tammo 2009), Broms (Broms 1965) and Borosnyól & Snóbli (Borosnyól & Snóbli 2010) all explain the lower crack width at the bar with internal cracks propagating from the ribs of the reinforcement bar. These cracks arise due to high bond stresses close to the crack face of the main cracks, which are described briefly in section 3.1. The small internal cracks help to close the main crack close to the reinforcement.

3.4 Crack propagation

Cracking in concrete is a very complex process that depends on several factors. The process of crack propagation can be described in three steps as the concrete element is deformed, see Figure 3.6 (from Löfgren 2005); (1) the initiation of a crack starts when stresses are introduced into the matrix from an applied load. Some micro cracks have already been present before loading. These occur due to internal restraints during temperature changes and shrinkage. When the stress increases additional micro cracks start to form and grow, this continues until the tensile strength of the concrete is reached which is in step (2). In the second step the micro cracks have grown to propagate faster and forms into a larger macro crack. The curve going straight down from step (2) in the graph shows the relaxation of the concrete when a crack occurs. When the macro crack propagates there is some toughening mechanism that tries to stabilize the further propagation of the macro crack. Step (3) involves these mechanisms and after losing most of the stress built up in the matrix the crack stabilizes until failure.

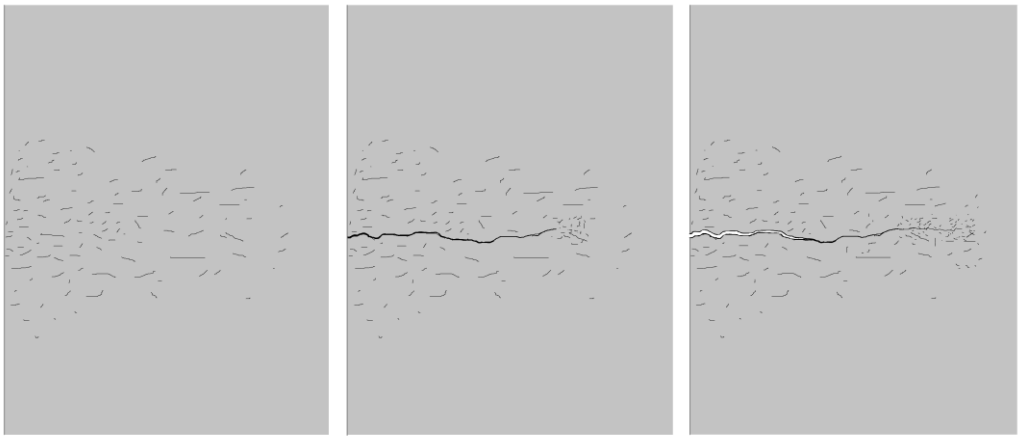

Figure 3.6 Schematic stress-crack opening for plain concrete based on Löfgren (2005).

Within the crack there are these mechanism previously mentioned. Crack bridging in terms of aggregate bridging is one of the main parameters for the toughness of the

concrete matrix. After reaching step (2) and to failure in Figure 3.6 the aggregate bridging is present, allowing some tensile stress to be distributed over the crack.

As previously mentioned, the effect of fibres on concrete properties mainly show in the post-cracking state, see Figure 3.7 (after step (2) until failure). The benefits come from the fibres ability to perform crack bridging. Depending on the fibre's efficiency, earlier presented in Figure 2.2, they allow higher stresses to be distributed over the crack when compared to plain concrete where the aggregate bridging is dominant stress carrier. As seen in the graph in Figure 3.7 the fibre-reinforced concrete can allow higher post-cracking strength, which takes place after the drop from step (2) to step (3). This is due to the necessary displacement to activate the steel fibres. Since the shown graph is a schematic one, different FRC will exhibit different behaviour.

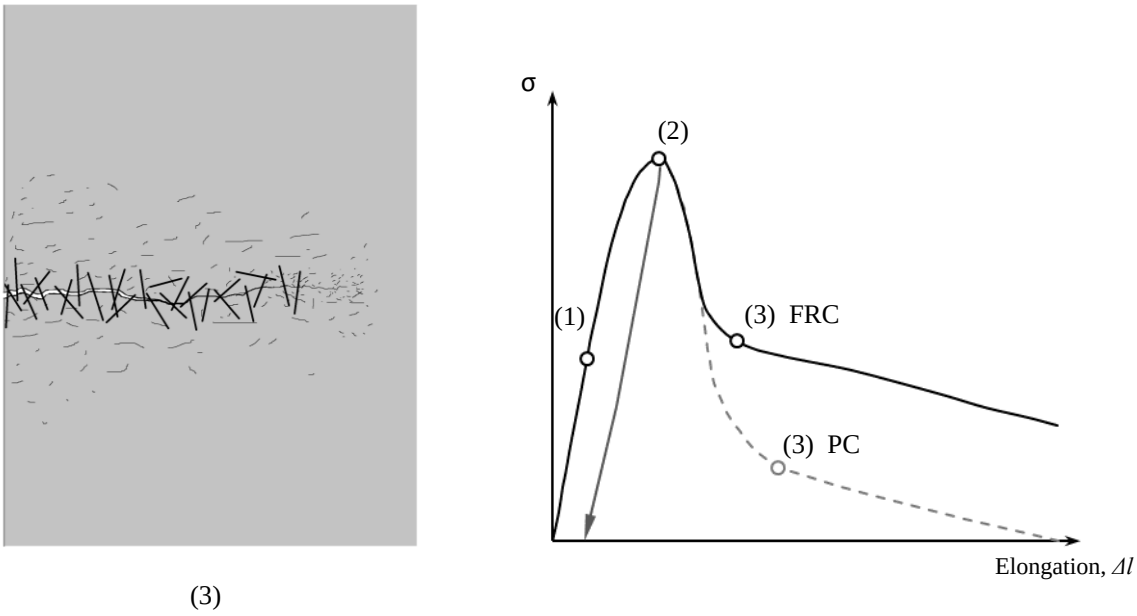

Figure 3.7 Fibre bridging in FRC based on Löfgren (2005).

4 Experimental Programme

The chapter first introduces the experimental programme in terms of types of testing and the experimental arrangement conducted in this thesis. Also the aim of the tests and how the tests were planned to be executed is described. Further, the specifics of the specimens are presented with the results from testing of mechanical properties. Finally, the procedure and preparation for the testing of the notched beams and a description of the results analysis are presented.

4.1 Overview

In order to verify the FE model there was a need for experimental crack widths data to use for comparison. As mentioned in section 3.3 there have been some previous investigations into the variation of the crack width between the concrete surface and the reinforcement. However, they only conducted experiments with plain concrete. Therefore further testing was needed to get the necessary information for the FE model and to properly investigate the effect of fibres on the crack profile.

Several tests were conducted during the project. The main experiments were the 3PBT that were carried out on modified RILEM beams (RILEM TC 162-TDF 2000). Testing was also done to verify and obtain the material properties of the specimens. See Table 4.1 for material testing scheme and Table 4.2 for the program for crack width testing conducted in this project. The material properties of the reinforcement were tested in previous work done by Berrocal (Berrocal 2015). Since material from the same manufacturing batch was used for the specimens in this project no additional testing and defining of the reinforcement material properties was deemed necessary.

Table 4.1. Number of specimens for material testing.

Test	*Type*	*Standard*	*Plain*	*SFRC*	*HyFRC*
Compressive strength	Cube	EN 12390-3:2002	4	3	4
Tensile split strength	Cube	EN 12390-6:2000	4	2	1
Flexural tensile strength	Beam	EN 14651:2005	-	4	4

Table 4.2. Number of tested beams for each mix and load case (specimen).

	Target crack width at notch	*Plain*	*SFRC*	*HyFRC*
Load case 0.5	0.5 mm	2 (PC1-PC2)	2 (SF1-SF2)	2 (Hy1-Hy2)
Load case 1	1 mm	2 (PC3-PC4)	2 (SF3-SF4)	2 (Hy3-Hy4)

4.2 Specimen specifications

In Table 4.3 the three different concrete recipes are specified with materials and amounts for 1 m^3. For the experimental work the recipes were scaled to fit the needed amount of concrete for each mix. Also it is of importance to notice that all three mixes are of self-compacting nature.

The full names of the abbreviated mixes are Plain Concrete (PC), Steel Fibre-reinforced Concrete (SFRC) and Hybrid Fibre-reinforced Concrete (HyFRC). Further on the mixes will be mentioned in short form.

Table 4.3. Description of concrete mixes used in testing

Mix	*PC*	*SFRC*	*HyFRC*
Concrete constituents (kg/m^3)			
Cement CEM I 42.5 N SR3 MH/LA (ANL Slite)	360	360	360
Limestone filler (Limus 40)	165	165	165
Fine aggregate (Sand 0/4)	776	767	768
Coarse aggregate (Stone 5/16)	840	833	831
Plasticiser (Glenium 51/18)	5.76	5.76	5.76
Air-entraining (MicroAir 105)	0.36	0.36	0.36
Amount of effective water	169	169	169
Fibres (Volume %)			
Steel fibres (Dramix 65/35-BN)	-	0.5%	0.5%
Synthetic fibres (PVA RSC 15x8)	-	-	0.15%

The fibres used were selected with consideration to be commonly used and to have different features. Here steel fibres were chosen as macro fibre-reinforcement and PVA fibres for micro scale. See Table 4.4 for mechanical and geometrical properties.

Table 4.4 Properties of the used fibres.

	Steel fibres Dramix 65/35-BN	*Synthetic fibres* PVA RSC 15x8
Length	35 mm	8 mm
Thickness	0.55 mm	0.038 mm
E-modulus	210 GPa	-
Tensile strength	1 345 MPa	1 400 MPa

4.3 Material testing

The compressive and split tests were done with a Toni Technik Model 2040 (max. 3000 kN) at the Department of Civil and Environmental Engineering, at Chalmers University of Technology. The 3PBT were performed at the same location.

4.3.1 Compressive strength

The compressive strength was tested on cubes with measurements 150x150x150 mm^3. The cubes were initially cured in water and then stored in dry conditions in room temperature before testing. The cubes for SFRC and plain concrete were tested at 28 days and the cubes for HyFRC were tested at 29 days.

The testing was conducted in accordance with EN 12390-3 and load speed was chosen to keep a stress increase of 0.6 MPa/s for all cubes. The values for compressive strength were adjusted from cube to cylindrical since the cylindrical values are used for the FEM. This was done using a conversion equation from Eurocode 2, see equation (15).

$$f_{c,cyl} = 0.85 \cdot f_{c,cube} - 1.6 \qquad (15)$$

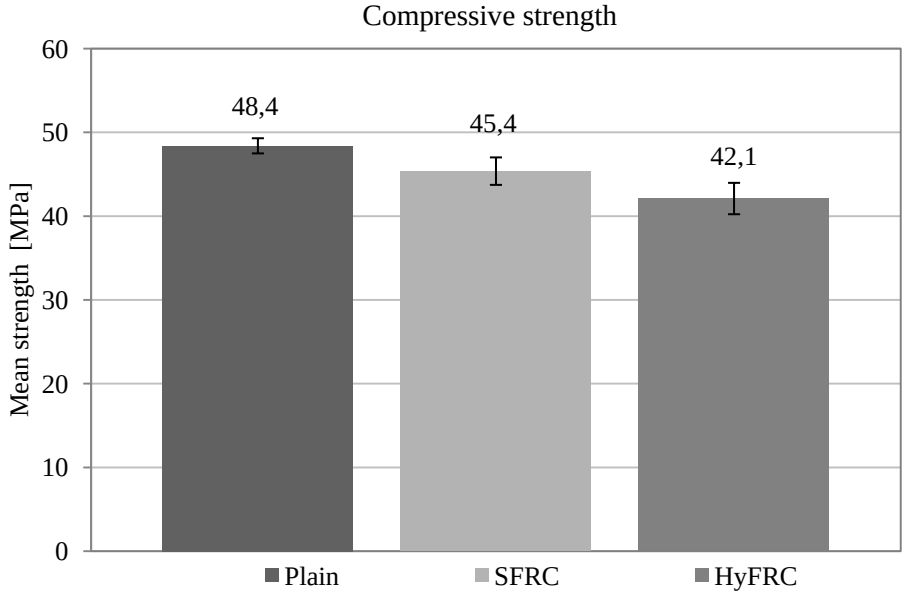

Figure 4.1 Compressive cylinder strength (calculated from cube test) with standard deviation.

Steel fibre dosages below 1% volume should generally not affect the properties of the concrete mix before the maximum stress is reached (Löfgren 2005). However, as can be seen in Figure 4.1 the results from the compressive tests show that the compressive strength is reduced when the fibre content is increased. It is possible that the reduction in compressive strength is due to increasing air content. Air bubbles were clearly visible on the sides of the specimens with fibres. For the plain concrete the air bubbles were substantially less occurring. The increased air content might be partly due to the

need of more stirring to properly distribute the fibres in the mix. Furthermore the fibres themselves can act as small whisks when they are moved around in the concrete, further increasing the air content.

4.3.2 Tensile strength

The tensile strength was tested on cubes with measurements 150x150x150 mm^3. The curing conditions and the age at testing for the split test cubes was the same as for the compressive testing in section 4.3.1.

The testing was conducted in accordance with EN 12390-6 and load speed was chosen to keep the stress increase to 0.05 MPa/s for all cubes. The testing jig for the split test can be seen in Figure 4.2.

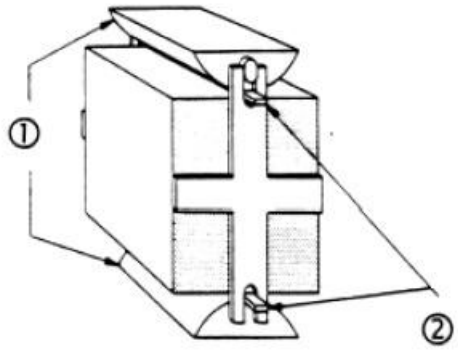

Key
1 Steel loading piece
2 Hardboard packing strips

Figure 4.2 Drawing of test setup for split test of concrete cube (BS EN 12390-6 2003)

The formula described in EN 12390-6 (BS EN 12390-6 2003) for evaluating the tensile splitting strength of the concrete can be used both for cylindrical specimens and prismatic specimens. However the standard says that it is likely that testing of prismatic specimens will yield approximately 10% higher results than cylindrical specimens. Therefore, the tensile strength derived from (16) was divided by 1.1. This means that the results presented in Figure 4.3 are calculated using (17).

$$f_{\mathrm{ct,sp}} = \frac{2 \cdot F}{\pi \cdot L \cdot d} \tag{16}$$

$$f_{\mathrm{ct,cyl}} = \frac{f_{\mathrm{ct,cube}}}{1.1} \tag{17}$$

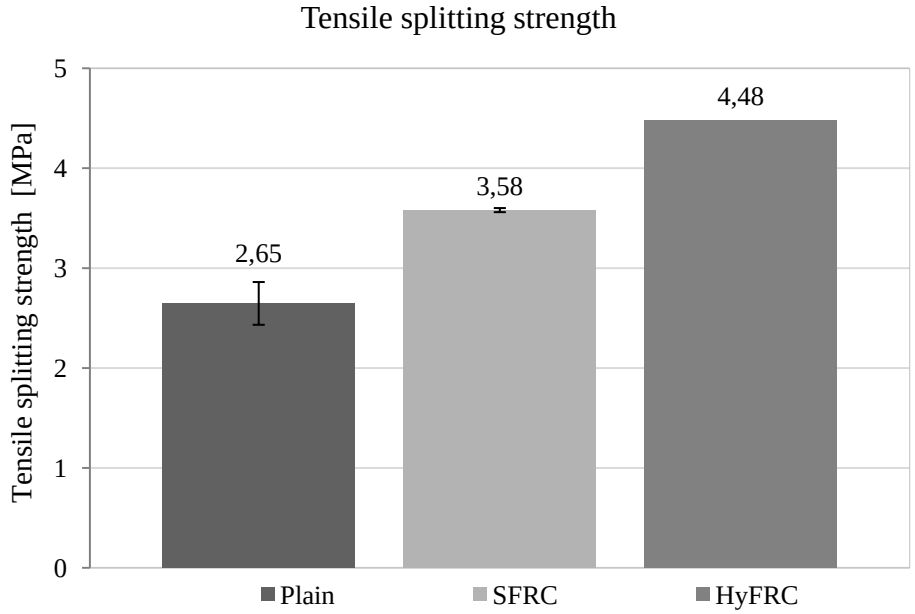

Figure 4.3 Tensile splitting strength with standard deviation, $f_{ct,sp,cyl}$

As can be seen in Figure 4.3 the tensile splitting strength increases significantly when fibres are added to the concrete mix. The split tests were mainly meant to determine the tensile splitting strength of the plain concrete. For SFRC and HyFRC, however, it only served as an indication of the strength since the test is not calibrated for fibre concrete and that the conversion factor for calculating the direct tensile strength in Eurocode 2 ($f_{ct} = 0.9 \cdot f_{ct,sp}$) is not directly applicable

4.3.3 Flexural tensile strength

The testing of the flexural tensile strength of the fibre mixes complied with EN 14651:2005 for most parts. Testing was done on beams with dimensions 550x150x150 mm^3 with a sawn 25 mm deep notch, as can be seen in Figure 4.4. Small deviation from the intended size of the beam as well as the notch were present but insignificant. During curing the beams were stored in water and the last days before testing in dry conditions at room temperature. The SFRC were tested at 62-63 days of age whereas for HyFRC 58-59 days.

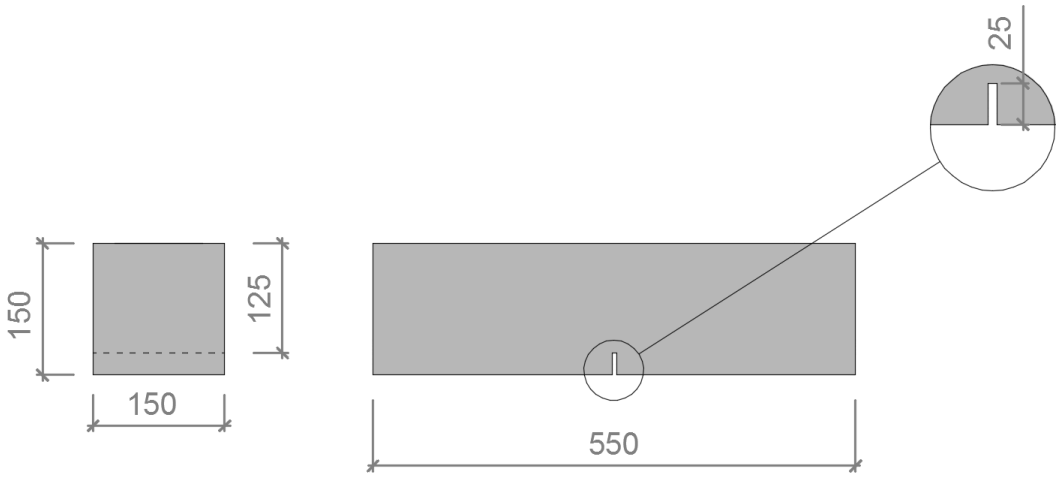

Figure 4.4 RILEM beam for flexural tensile strength.

For all the instances where the actual sample preparation or testing deviated from EN 14651 the actual conditions deviated in such a way that it was more similar to the way the beams with ribbed reinforcement were tested. For example, instead of rotating the beam 90° before making the notch the cut was made on the same surface as for the beams with ribbed reinforcement. In addition the rate of loading was the same for flexural tensile strength test and the crack width test. This is due to the shortcomings of the used test machine, for which it was not possible to directly decide a CMOD-controlled loading. According to EN 14651 the loading rate should be 0.05 mm/min up until CMOD = 0.1 mm is reached, after which the loading rate should be increased to 0.2 mm/min. These recommendations were not fulfilled during the flexural testing, instead the loading rate varied between 1.0 and 1.8 mm/min.

The results of the tests can be seen in Figure 4.6 and Figure 4.5. For both the SFRC and HyFRC mix there was one beam that had deviating results, therefore also an average without deviated value is presented. The tests show that the chosen fibre dosage gives a bending softening behaviour for both the SFRC and HyFRC mix. Furthermore, the residual flexural tensile strength was derived from the average without the deviating values (see Table 4.5). The flexural strength values were derived according to EN 14651. These values were however not used for FE modelling.

Table 4.5 Flexural tensile strength for SFRC and HyFRC.

	$f_{R,1}$ [MPa]	$f_{R,2}$ [MPa]	$f_{R,3}$ [MPa]
SFRC	5.0	4.4	3.8
HyFRC	6.0	4.9	3.8

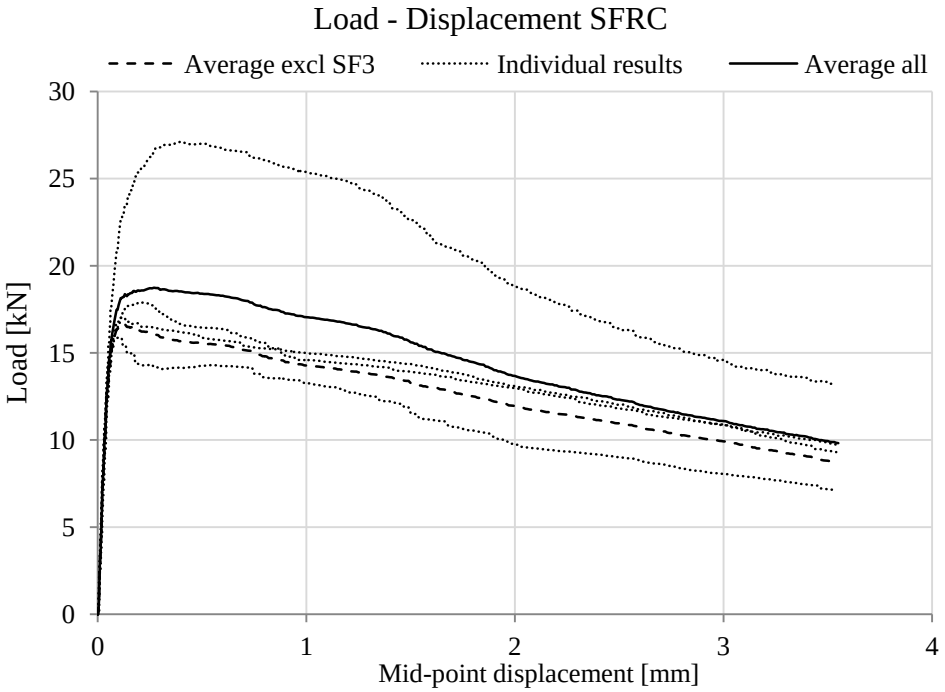

Figure 4.6 Load - Displacement diagram for SFRC beam.

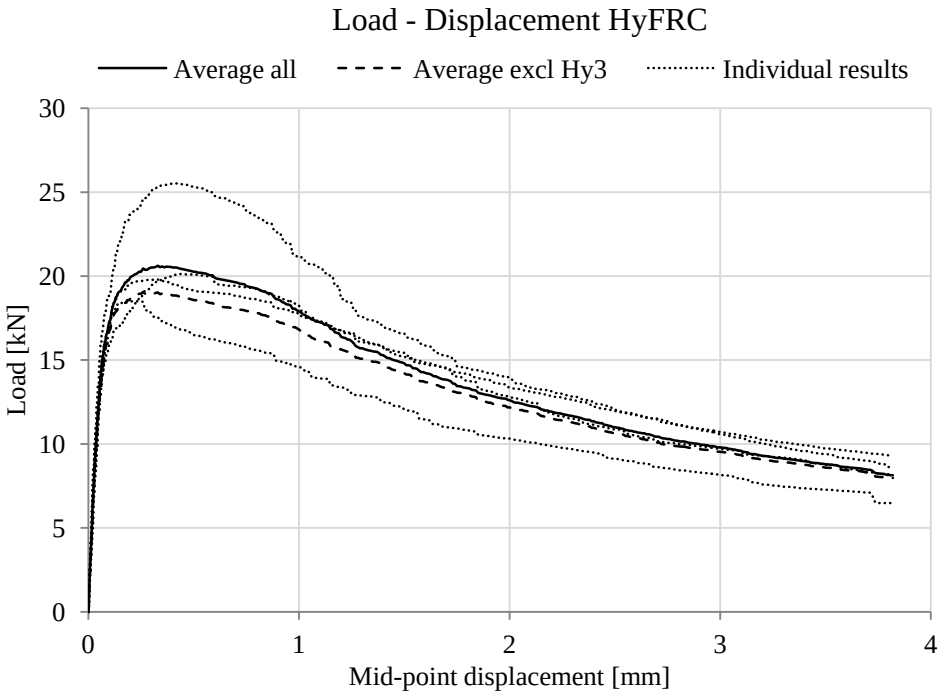

Figure 4.5 Load - Displacement diagram for HyFRC beam.

From the load-displacement curves obtained from testing the RILEM beams, an inverse analysis to derive input values for the finite element model was performed. This inverse analysis routine used in this project was developed by Lennart Østergaard (see also (Stang & Olesen 2000; Olesen 2001). The inverse analysis uses the experimental data in terms of load-displacement (mid-point displacement) from a beam test and by an iterative process finds a bi-linear stress-crack width curve (see Figure 4.7) by minimizing the difference between the experimental result and the model. This can be transformed into a stress-strain relation by converting the crack width into strain, using the characteristic length of the elements in the FE model (see equation (18)). The new relation can be used as input for the concrete tensile behaviour in the FE model. In Figure 4.7a schematic stress-crack width relation is shown with the defined parameters and the associated values are presented in Table 4.6.

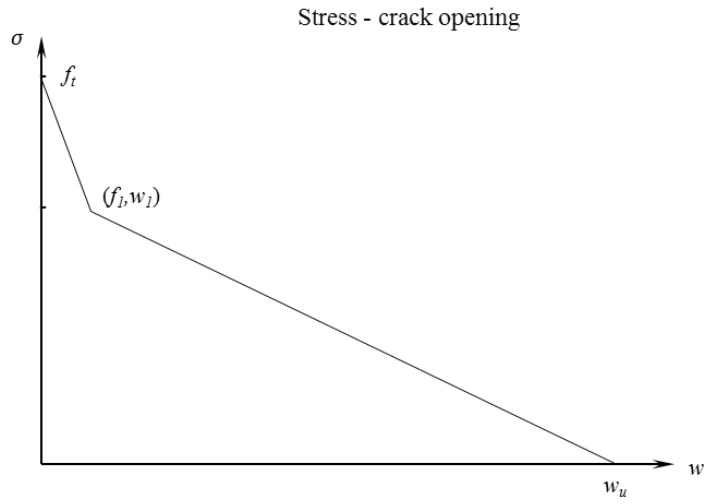

Figure 4.7 Stress-crack opening relation obtained from inverse analysis.

$$\varepsilon = w/l_{element} \qquad (18)$$

Table 4.6 Stress-strain values for fibre-reinforced concrete mixes, see Figure 4.7.

	f_t [MPa]	f_1 [MPa]	w_1 [mm]	w_u [mm]
SRFC	3.41	1.93	0.0409	4.20
HyFRC	4.25	2.34	0.0065	3.37

To check the accuracy of the inverse analysis the flexural tensile test was modelled and analysed in DIANA (read about the modelling process in chapter 5). In Figure 4.8 and Figure 4.9 the results of the numerical analyses are presented. As can be seen in both cases an overestimation of the flexural strength occurs. For the SFRC a comparison between cracking loads shows that FEM results in a 22% higher load capacity, and for HyFRC the same comparison gives 10%. However, the over-all behaviour corresponds reasonably well to the experimental average.

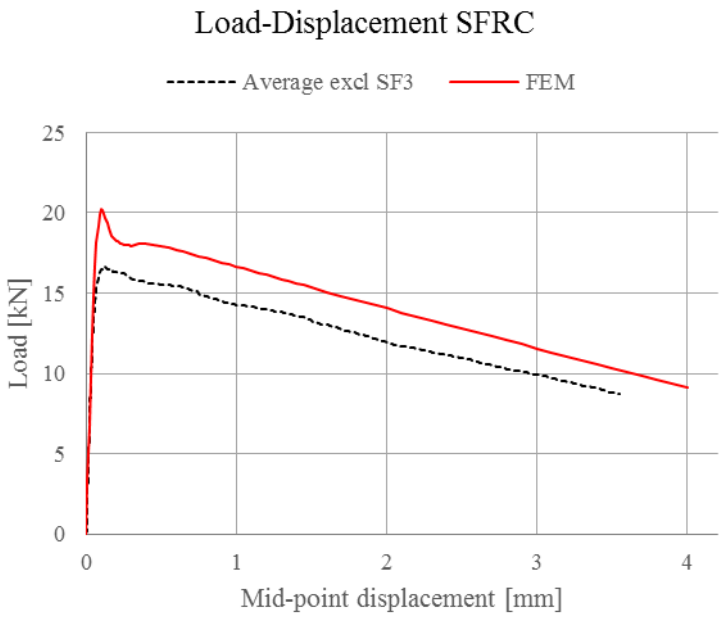

Figure 4.8 Results from numerical analysis for SFRC with material prop. from inverse analysis.

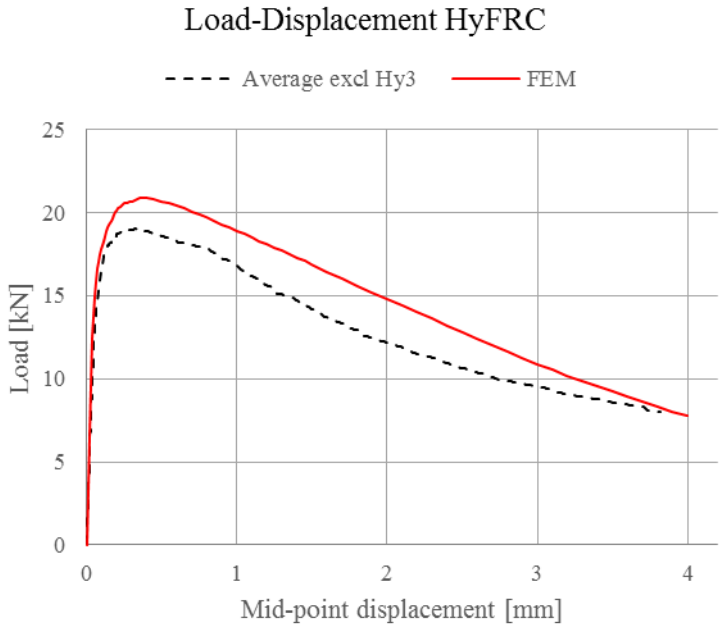

Figure 4.9 Results from numerical analysis for HyFRC with material prop. from inverse analysis.

4.3.4 Ribbed reinforcement bar

The properties of the reinforcement bars used in this thesis are presented in Table 4.7 and they were obtained from previous testing done by Berrocal (Berrocal 2015). The reinforcement bars had a diameter of 10 mm.

Table 4.7. Mechanical properties of reinforcement bar.

	Yield strength, f_y	*Tensile strength,* f_u	*Young's modulus*
Average	546 MPa	627 MPa	204 GPa
Standard deviation	11.9 MPa	10.2 MPa	13.5 GPa

4.4 Crack width testing

The procedure for cracking the beam and measuring the crack width consisted of: (i) preparation of the specimens before loading; (ii) loading; (iii) applying of epoxy resin in the crack; and (iv) unloading. Moreover, to obtain suitable specimens to analyse the crack width meant an extensive work had to be performed to cut out and process the pieces of interest.

4.4.1 Loading

The first step after preparing the beams with notches was to induce the crack that was later going to be measured. The notch that was located in the middle of the specimen will create a stress raiser in that section and will force the specimen to crack there.

The test setup is designed like a regular 3PBT test but is conducted with the beam upside down. This means that the notch is located on the top of the beam and that the ends of the beam are pressed down instead of the middle. See Figure 4.10 for a graphical explanation of the setup.

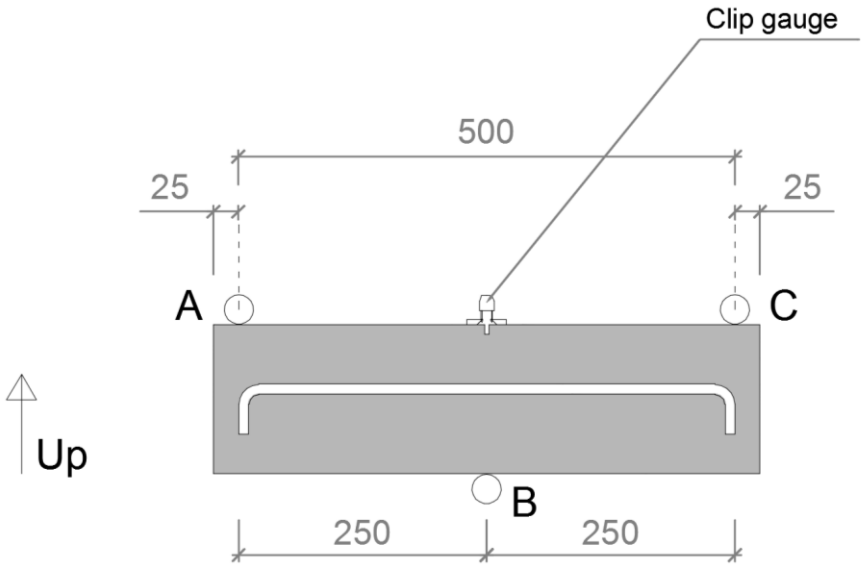

Figure 4.10 Test setup for crack width testing.

A clip gauge was mounted over the notch to measure the CMOD and a load cell was placed under the bottom roller bearing to measure the load. Measurements from both devices were collected and plotted against each other in a Load-CMOD curve. The purpose of these measuring devices were mainly to get a good approximation of when the desired crack width was reached and to get a rough comparison of the bending behaviour of the different beams. Further use of the Load-CMOD curve will be for comparing to corresponding FEA results.

When the target crack width had been reached the loading was halted and the crack was kept at a constant width by keeping the imposed deformation constant. A glue gun was used to cover the surface cracks on the beam to prepare for the pouring of epoxy. The purpose of the glue is to create a barrier to prevent the epoxy from leaking from the crack. When the glue had cooled and hardened, the notch was filled with epoxy (NM Injektering INP 003) that was mixed with fluorescent dye. Since the epoxy resin used had a low viscosity of 0.10 Pa*s, it flowed through and filled even the smaller cracks easily.

When the notch on the beam had been completely filled the beam was left loaded during the night. The epoxy was left to harden for minimum 16 hours before the beam was unloaded and dismounted from the testing rig. When unloaded the crack naturally tries to close due to residual stresses in the reinforcement bar and fibres when present. The purpose of the hardened epoxy was to keep the crack open even when not loaded in bending.

4.4.2 Cutting and preparation

To fully analyse the crack profile near the reinforcement bar it was necessary to be able to see the section at the reinforcement. The simplest way to achieve this was to split the concrete beam in smaller pieces and to make a cut along the reinforcement bar. A sketch of how the cuts were made can be seen in Figure 4.11.

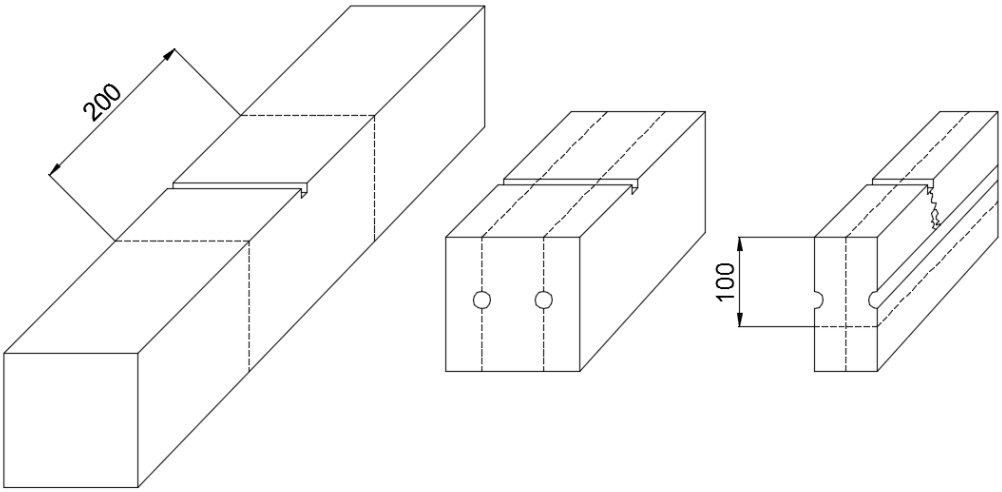

Figure 4.11 Cutting scheme for cracked beam.

The goal of the sample preparation was to get a smooth surface with all cracks filled with epoxy. Much of the bending crack was filled when the epoxy was poured into the notch, but there were many voids and smaller cracks that were not filled in this stage. In order to fill those as well, it was necessary to do a vacuum impregnation with fluorescent epoxy on the cut concrete section. However, after impregnation the surface must be shallowly grinded again to reveal the underlying surface and make it suitable for analysis. The precision work, including grinding and vacuum impregnation with epoxy of the samples, was conducted in the premises of CBI, a part of the SP Group, in Borås.

4.5 Crack width measurement

In order to establish the crack width profile for the specimen two different techniques were used. The first method was to digitally measure the crack width by image processing of the fluorescent pictures. This meant to automatically output the crack width profile, but it showed to have some drawbacks in terms of accuracy. The second method practised was to use computer software to manually measure the crack width and creating a profile.

4.5.1 Automatic measurement from fluorescent picture

After the final sample preparation was finished it was possible to analyse the specimens with a microscope. Two lamps with UV-emitting light bulbs were used to illuminate the specimens under the microscope. Due to the fluorescent properties of the epoxy, the crack became clearly visible in contrast to the surrounding concrete, see Figure 4.12 (a). Three pictures were taken of each specimen to cover the whole area. Afterwards the three separate pictures were merged into one to get a single picture over the whole sample surface. Showing the full sample surface made it possible to see a more complete image over the crack and the surrounding concrete.

The image processing script created in Matlab was written by Carlos G. Berrocal for the purpose to create output for this thesis. In short, the script converted the fluorescent image of the crack into a binary, black-and-white image, only picturing the crack of interest Figure 4.12 (b). In the next step the white pixels were counted and plotted and the crack width profile was then acquired. The plot shows the corresponding crack width in level with the pictures, see Figure 4.12 (c).

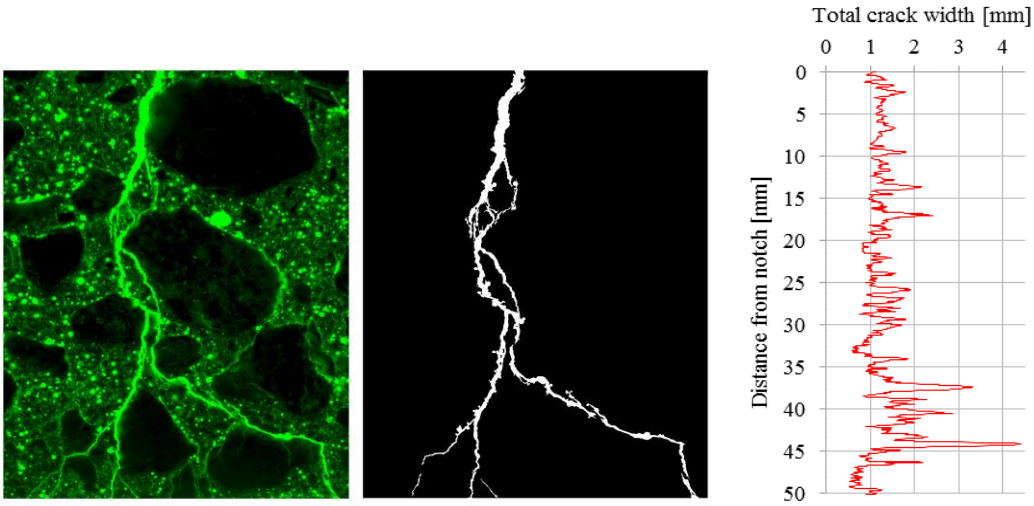

(a) (b) (c)

Figure 4.12 From fluorescent to black-and-white, with total crack width from automatic measurement script.

4.5.2 Manual measurement from regular picture

To be able to measure the crack widths manually the pictures had to be high resolution. That was achievable with a SteREO Discovery.V20 microscope with an AxioCamMR5 camera with the possibility to create panoramas with auto-alignment function. The software used to manage the images was AxioVision. A feature of the setup with microscope and software was scale information. The automatic scaling was checked using a ruler, no deviations could be observed. Each crack was documented by merging together 20-30 images (at 20x magnification) into one, using the available tool in AxioVision to measure at an interval of 2 mm and compiling the data in an Excel sheet to be able to plot the crack width profile. The crack could be measured with two different approaches; horizontally or perpendicular the crack direction. As can be seen in Figure 4.13 the crack width will differ significantly depending on which approach is chosen. For the results in this thesis the perpendicular approach was selected due to the horizontal approach did not show consistent crack widths when the crack changed direction to horizontal.

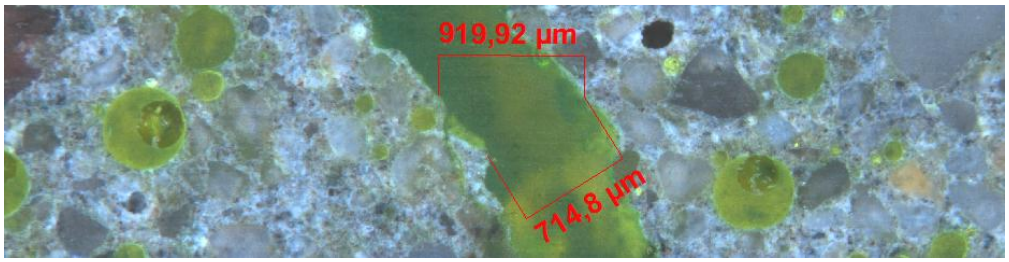

Figure 4.13 Showing the two approaches to measure the crack width.

5 Non-linear Finite Element Modelling

The purpose of modelling the beams with conventional reinforcement was to find if the behaviour of the beam could be recreated by using material input data from the experimental work. When implementing physical models which as far as possible represent the real beam behaviour, the numerical results of the models should be comparable to the ones acquired from testing the real beams. How the beam testing was performed can be found under section 4.4.

The chapter first introduces the reader to what finite element method is and the possibilities that comes with it. Main purpose of the chapter is to explain in a short manner how the model was created and what settings were adjusted to ensure the convergence of the analyses and to calibrate the model according to the experimental data.

5.1 General

The general approach to solve complicated mechanical problems today is by means the finite element method. This can be executed with models in 1D, 2D and 3D and solves numerically the differential equations which model the real problem (Ottosen & Petersson 1992). By dividing the geometry into finite elements a mesh is created. The mesh represents a structure divided into smaller elements, each of which describes mathematical relations to embody the structure.

Non-linear finite element modelling allows, as the name articulates, non-linear behaviour such as material properties, e.g. cracking in concrete. Adding non-linearity to the model increases the computational time as the equations get more complex. The non-linear model will give a more accurate result as the input now describes the real material behaviour better.

5.2 Finite Element Model

This section serves to introduce the finite element model (FE model) used for analysis in this thesis. The finite element 3D model is modelled as a half of the test beam due to non-linear FEM being very demanding with regards to computational power. Therefore it is of interest to simplify the geometry of the model using symmetry. In Figure 5.1 the test beam is pictured as a whole (a) and the final FE model (b). By using the symmetry line and boundary conditions thereafter when setting up the

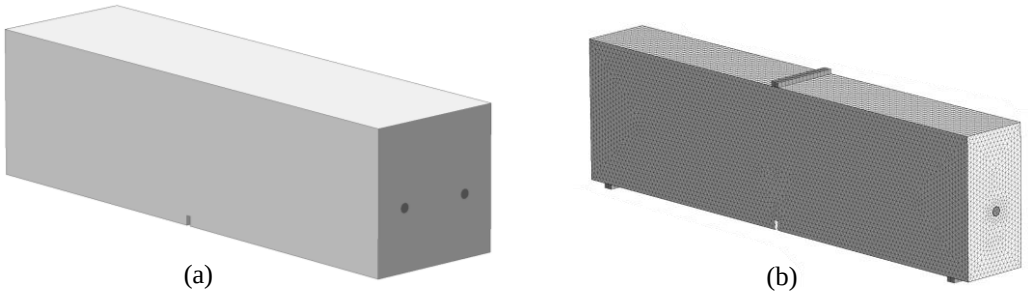

Figure 5.1 The 3D model; (a) test beam, (b) finite element model.

model, the size was reduced to half. This gave the model continuity of the mesh over the most interesting part of the beam, the middle where the crack will form, and decreased number of nodes and time to obtain results. In order to avoid stress concentrations at interaction points, steel plates were placed at supports and where the load was applied, these can also be seen in Figure 5.1 (b).

Used for non-linear finite element analysis was the commercial FE software DIANA (TNO DIANA 2014) with graphical interface software Midas FX+ 3.3.0 for pre/post-processing of the models and MeshEdit 9.5 for performing analyses. In the following section selected material properties assigned for the models are stated.

The DIANA model file and analysis file are presented in Appendix C.

5.3 Modelling choices

In order to model the beams there have been mainly three categories of parameters where input have been considered important, see Figure 5.2 where some examples of parameters are mentioned. Each category, representing a number of different input values, curves or models, will be described further below.

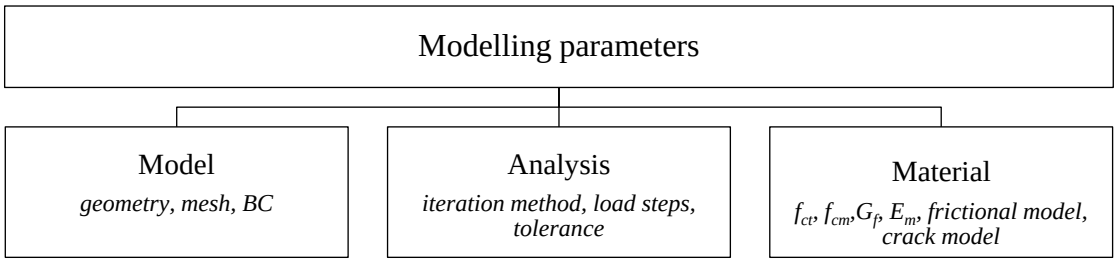

Figure 5.2 Overview of sample parameters changed for creating the FE models.

Section 5.4 explains the essentials of how the model has been done in FX+. Section 5.5 describes the physical properties that have been assigned to the model. Finally, section 5.6 serves to describe what choices have been made to perform a reliable analysis.

5.4 Model

Creating the finite element model resulted in a number of choices that had to be made in order to obtain a functional and as accurate performance as possible. This also comes with a number of simplifications compared to the real beams. The model was set up with the following specifications:

Geometry: the finite element model was modelled as half of the beam using the symmetry of the longitudinal centre plane. By reducing the size of the model, associated boundary conditions had to be introduced according basic mechanics. In Figure 5.3 the boundary conditions are shown for the FE model. Another tweaking of the geometry was to add steel plates at supports and loading point to distribute the load and avoid local stress peaks, where roller bearings were used in reality. The reinforcement bar was modelled as a straight bar without the bends that were in the real beams. These simplifications were argued since the area of interest would not get affected to a large extent.

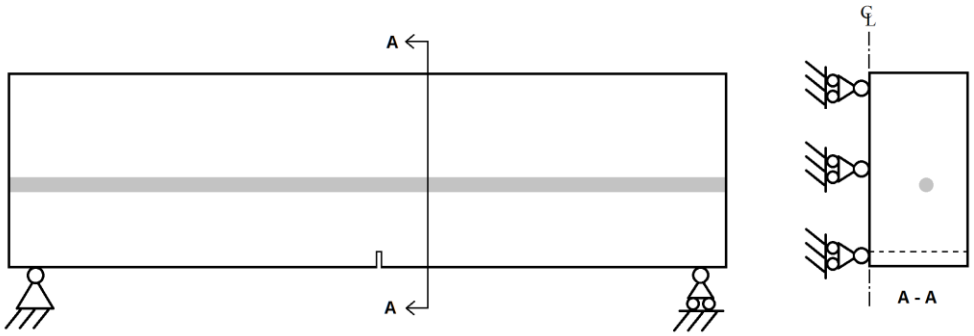

Figure 5.3 Boundary conditions for the FE model.

Mesh: during the thesis process different mesh sizes were used. A coarser mesh was applied at the beginning, which allowed shorter running time for the analysis. However, for the final model the mesh size was chosen to be 5 mm elements in order to picture the results more accurately and with higher definition.

Element type: for the finite element model four-node tetrahedron were used, see Figure 5.4 (in Diana named TE12L). By default is one integration point for the element chosen. The element type is compatible with 4 and 5 integration points. For the final element size it was decided that one integration point was sufficient to describe the structural behaviour due to the number of elements, also not to increase the computational time.

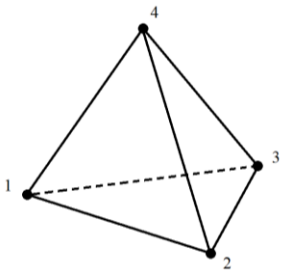

Figure 5.4 TE12L, element structure with four nodes.

Frictional model: to model the non-linear bond-slip behaviour which is present between the reinforcement bar and the concrete a frictional model developed by Lundgren (Lundgren 2005) and implemented in DIANA as a user-defined subroutine was adopted. By creating 2D interface elements (zero-thickness) at the surface of the reinforcement bar and prescribing the subroutine to the elements the bond-slip behaviour was modelled. Data input for the subroutine was tensile strength, compressive strength and elastic modulus for each concrete mix.

5.5 Material

For the model to have the same behaviour as the test beams, the input values for material properties are of great importance. Also the choice of material models affects the behaviour and result to a large extent. Values have been obtained by experimental work with two exceptions for the PC mix, using equations according to Eurocode 2

(2008) to derive the elastic modulus (19) and the fracture energy (20), both not possible to be obtained from the experimental work.

$$E_{cm} = 22 \cdot \left(\frac{f_{cm}}{10}\right)^{0.3} \qquad (19)$$

$$G_F = G_{Fo} \cdot \left(\frac{f_{cm}}{f_{cmo}}\right)^{0.7} \qquad (20)$$

$$f_{cmo} = 10\ MPa$$

The material models for concrete and the reinforcement bar are presented in Table 5.1. In Figure 5.5 the models are described in stress-strain relation. The material properties used for modelling each concrete mix are presented in Table 5.2–Table 5.4.

Table 5.1 Material models used in FE modelling.

	PC	*SFRC*	*HyFRC*
Tensile model	Hordijk	User-defined	User-defined
Compression model	Ideal	Ideal	Ideal
Steel model	Ideal	Ideal	Ideal

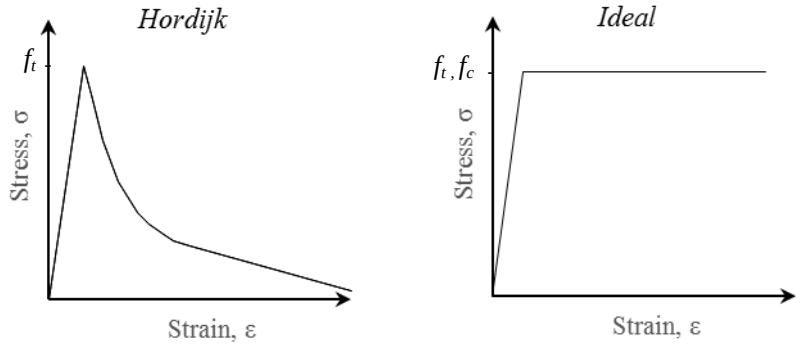

Figure 5.5 Material models for concrete and steel; Hordijk, Ideal.

Table 5.2 Input parameters for PC.

Plain Concrete	*value*	*unit*
Young's modulus concrete	35 300	MPa
Compressive strength	48.4	MPa
Tensile strength	3.0	MPa
Fracture energy	90.5	Nm/m^2
Frictional model	see (Lundgren 2005)	

Table 5.3 Input parameters for SFRC.

SRFC	*value*	*unit*
Young's modulus concrete	34 640	MPa
Compressive strength	45.4	MPa
Tensile strength	3.41	MPa
Frictional model	see (Lundgren 2005)	

Table 5.4 Input parameters for HyFRC.

HyFRC	*value*	*unit*
Young's modulus concrete	33 860	MPa
Compressive strength	42.1	MPa
Tensile strength	4.25	MPa
Frictional model	see (Lundgren 2005)	

Table 5.5 Steel properties of the reinforcement bar.

Reinforcement bar	*value*	*unit*
Young's modulus	204 000	MPa
Yield stress	547	MPa
Cross-sectional area	78	mm^2

5.6 Analysis

In order to obtain results from the model the analysis procedure have to be adjusted to the type of loading situation. Step size as well as convergence norm need to be considered. Below in Table 5.6 it is stated the choices that have been applied to the models used in this thesis. The total load value is considered to give results comparable to the full range of the experimental results. Step size was at first set to automatic, it means MeshEdit would change step size if convergence was not reached. However, this gave no effect so a discrete step size was instead chosen.

The iterative process used to solve the equations was the Newton-Raphson method. It uses the stiffness of the structure to find the solution and by updating the stiffness matrix in each iteration, it normally reaches convergence after just a few iterations. To reach convergence the model was checked to a displacement norm and a force norm. Tolerance for these norms was set to half default value and if convergence was not reach within 30 iterations the analysis was terminated.

Table 5.6 Analysis procedure and limitations.

Displacement controlled analysis	
Load	1.2 mm
Explicit step size (number of steps)	0.01 (120)
Iteration method	Newton-Raphson, tangential
Convergence norm	displacement “OR” force
Tolerance (default)	0.005 (0.01)
No convergence	terminate iteration after 30 iterations

To be able to run the analyses with the user-defined subroutine for bond-slip behaviour they had to be run on a computer cluster. The cluster used for this thesis was Chalmers Centre for Computational Science and Engineering, C3SE.

From running the analysis several results can be collected. In this thesis the selected output was 3D Element Strain, 3D Element Stress, 3D Element Crack Pattern, Reactions and Displacement. These values made it possible to check the overall behaviour of the model, in order to establish a trustworthy result.

5.7 Crack model

Modelling cracking behaviour in non-linear FE analysis can be done with two different approaches, smeared or discrete crack approach. The main difference between the two is how the cracks are represented in the model. For the discrete approach the geometry of the crack has to be known while for smeared it does not.

5.7.1 Smeared crack approach

The smeared crack model introduce the effects of cracks by making changes to the coefficients of the material stiffness matrix, not changing the geometry or the mesh (Selby 1993). Compared to the discrete approach it is a more efficient and less time consuming method to model cracking behaviour. Therefore, it is the most commonly used and recommended approach for the analysis of reinforced concrete structures (TNO DIANA 2014).

For the smeared crack approach there is two main models. Firstly there is the Total Strain crack model which allows only one stress-strain relation for the material in tension and one in compression (TNO DIANA 2014). When used it should be stated if the propagation of the crack should be Rotating (allows the crack to change direction as it propagates), Fixed (continuous direction) or Rotating-Fixed (behaviour switches from rotating to fixed at specified strain value). Secondly there is the Multi-directional Fixed crack model which allows multiple cracks to occur at the same time. In this thesis the smeared crack approach with Total Strain Rotating crack model is used for the non-linear FE analysis.

5.7.2 Discrete crack approach

As introduced above the discrete crack approach needs a geometrically pre-defined crack in the mesh. The crack is normally modelled as interface elements which model the cracking behaviour (Löfgren 2005).

5.8 Validation

To validate the finite element model it was evaluated in terms of the structural behaviour. By checking the criteria, presented in Figure 5.6 below, after running each analysis the results could be considered as representative for the real beams.

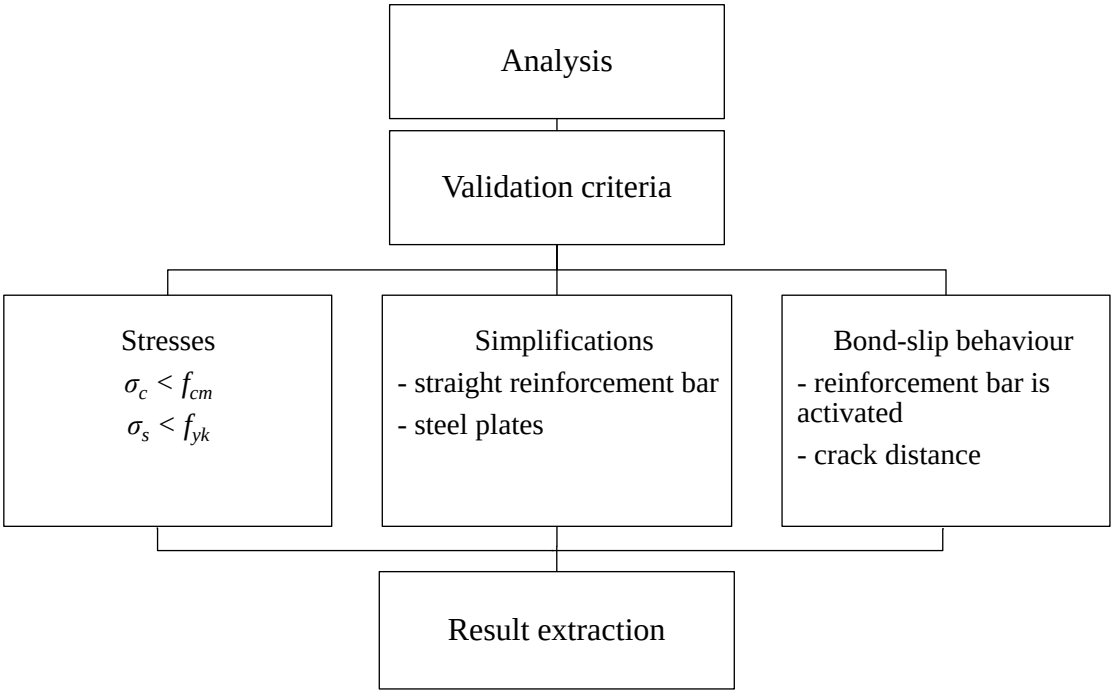

Figure 5.6 Validation process.

The stresses in the model had to be checked against the limit values to assure compressive failure or yielding of the full rebar cross-section did not occurred. The simplifications made to define the finite element model also had to be checked. Since the reinforcement bend was modelled to a straight bar it was of interest to check that the bond to the concrete was not affected at the location of the bend seen in section 4.4. Also the effect of the added steel plates was checked by making sure the plates did not deform abnormally. Last was to see how the frictional model had affected the bond-slip. By looking at the crack distance and distribution of stresses along the reinforcement bar the interaction could be approved as reasonable.

6 Results and Discussion

The thesis had mainly two focus areas. Firstly, experimentally investigating the influence of fibres on the crack width profile and morphology. Secondly, the numerical analyses using DIANA, with the aim to reproduce the behaviour of the tested beams. In this chapter the results will be presented and discussed in terms of what factors might have had an impact on the results.

6.1 Crack width profile

Initially, the automatic method described in section 4.5.1 was used to measure the crack width, but it was quickly noticed that the method yielded bad results with the used picture resolution. Firstly, there was a slight bleeding effect from the light emitting from the fluorescent epoxy which created a transition zone where the colour of the crack gradually faded into the colour of the surrounding concrete. The used edge detection algorithm could not properly find where in this transition zone the actual crack edge was located. If a higher threshold was used for the crack colour it was possible to significantly reduce the effect of the bleed but the algorithm could not find the smaller cracks instead. This problem could potentially be less severe if a higher resolution would have been used taking the fluorescent picture. Secondly, the voids due to air bubbles were also filled with epoxy. When the crack propagated through a void, the void became part of the crack and it was not possible for the algorithm to differentiate between the crack and the void. While the method was time efficient in terms of obtaining crack width data it was unreliable and had to be verified with manual measurements.

The final crack width values between the concrete surface and the reinforcement bar was obtained from the specimens using the manual measurement technique described in 4.5.2. In total, 24 slices were measured with one main crack per slice. Unless something else is specified in relation to a diagram, one data point is the total crack width at a certain distance from the notch from one slice. Total crack width means that the crack width of each individual crack has been summed in case the main bending crack split into several smaller cracks at a certain level. The distance between the notch and the reinforcement is approximately 50 mm and the measuring interval was approximately 2 mm. The diagrams in this section show the crack width between the notch and a distance of approximately 0 – 2 mm from the surface of the reinforcement.

In some areas there were large bubbles or other irregularities that made it impossble to measure the crack width. Either the width was measured before and after the irregularity or there were no measurement taken in that interval, depending on the size of the irregularity. Considering the roughness of the crack surface, the writhing propagation direction, etc, there is a large scatter in measurements on the same depths and even on the same beam.

During the 3PBT of the modified RILEM beams with conventional reinforcement the goal was to get a surface crack at the notch of 0.5 mm and 1 mm. This was done mainly through monotoring the CMOD value. Due to high updating frequency in the CMOD measuring equipment and a quick response in the load testing machine it was possible to get approximately the same CMOD values for the different mixes. It is also worth noting that the load required to reach the CMOD values are higher for

SFRC and HyFRC, see Table 6.1. In other words, at the same load the CMOD and crack width at the notch would be smaller for SFRC and HyFRC. It was noticed that the CMOD continued to increase slightly during a period after the loading stopped. This was probably due to creep since the load decreased as well. The maximum CMOD registered during the epoxy resing hardening process can be found in Appendix D.

Table 6.1. Maximum load for modified RILEM beam and corresponding CMOD for all mixes and load cases. Average values.

	Load case 0.5			*Load case 1*		
	PC	*SFRC*	*HyFRC*	*PC*	*SFRC*	*HyFRC*
CMOD [mm]	0.74	0.74	0.76	1.23	1.22	1.22
LOAD [kN]	39.6	58.2	53.1	48.7	63.0	62.2

In this section data points from several slices, beams and/or mixes will be presented in the same diagram. Presentation of the results from each individual slice is presented in Appendix A.

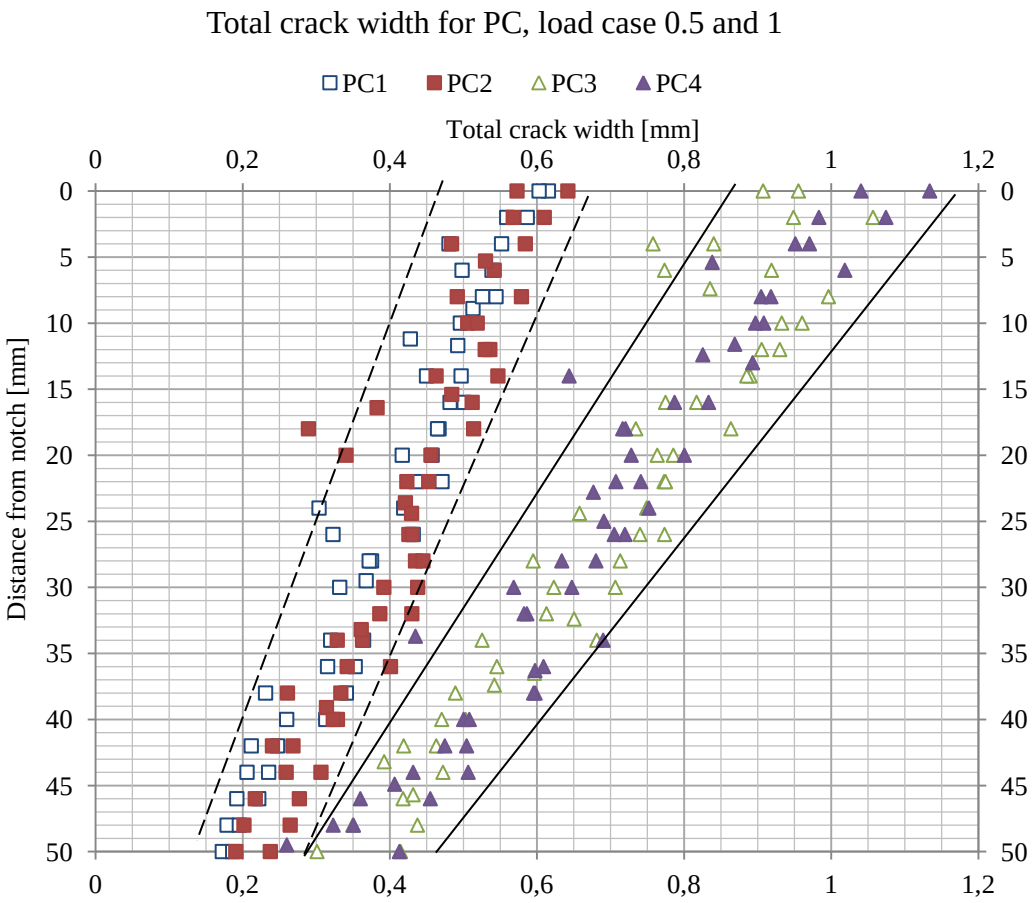

Figure 6.1. Crack widths for PC concrete with 0.5 mm and 1 mm surface crack width.

Looking at Figure 6.1 it is possible to see that there is a clear trend to the data points. The crack width profiles for the PC mix show a linear behaviour, even though there is some scatter and some data points which deviate from the rest. The crack width close to the reinforcement is considerably smaller than at the notch. The ratio between the notch crack and the reinforcement crack is approximately 3 for the smaller crack and closer to 2.5 for the larger crack.

Due to the scatter of the data points for the two crack sizes, the profile curves can almost be described as a crack band, for which most of the data points are located within.

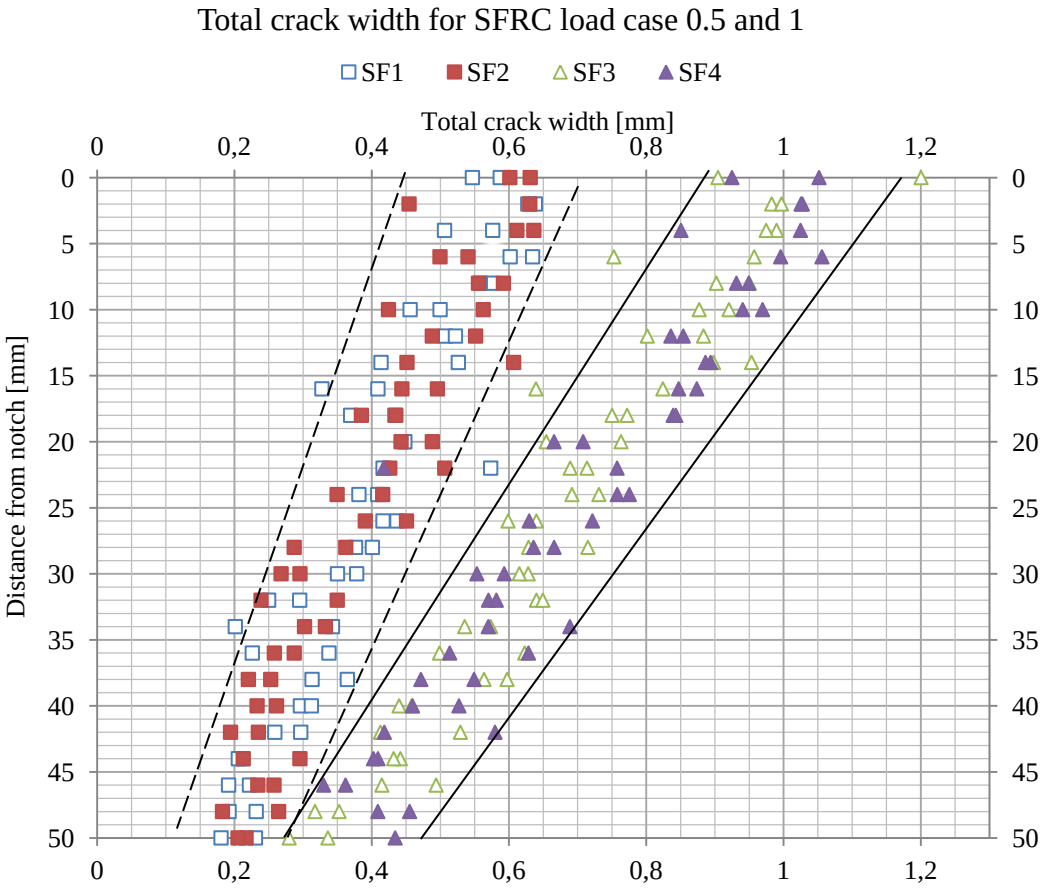

Figure 6.2. Crack widths for SFRC with 0.5 mm and 1 mm surface crack width.

The crack width measurements for SFRC samples also show a linear trend of the crack width profile. However, for the smaller crack there are some tendancies for the curve to become steeper close to the reinforcement. This behaviour is not clearly visible for the larger crack, which instead has a linear trend for the whole profile. From these results alone it does not seem like the addition of 0.5 volume % of end-hooked steel fibres have any discernable effect on the total crack width profile, especially not for the larger crack width.

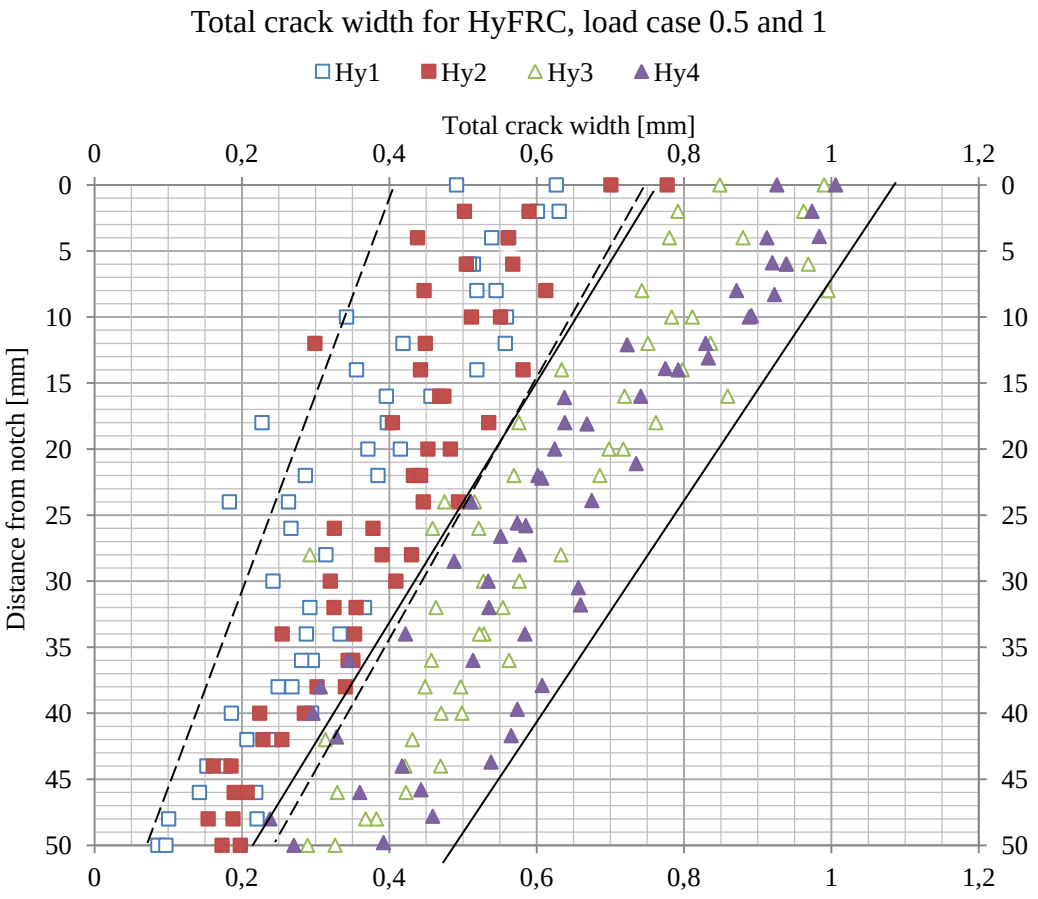

Figure 6.3. Crack widths for HyFRC with 0.5 mm and 1 mm surface crack width.

The results for the HyFRC mix shown in Figure 6.3 show a trend similiar to the PC and SFRC mix, but the trend is not as clear due to the large increase in scatter of the data points. The crack bands become so wide that they overlap each other in the middle. It is unclear if this scatter is due to the addition of 0.15 volume % of PVA fibres or a more uneven fibre distribution. Cracks which have a large variation in its propagation direction tends to also give varying crack width measurements when the perpendicular width is measured. Adding PVA fibres gave a more varying crack pattern, as will be discussed in section 6.2. Therefore it is possible that the higher crack width scatter for HyFRC is due to a higher variation in the crack propagation direction.

Summarizing the plotted data points in Figure 6.1, Figure 6.2 and Figure 6.3 shows the overall trends of the crack width profiles and clearly shows the range of the scatter. Unfortunately, the scatter and the small difference in values between the concrete mixes makes it hard to compare the results from the different mixes in a clear way if the data points are shown in the same diagram. A way of presenting the overall crack width behaviour is by comparing the fitted trend lines of the data points from each mix and load case. Another way is by calculating the average crack width at each depth for each mix and load case and comparing those values. Each presentation method has its own benefits and drawbacks. It is therefore necessary to present the data in several ways and use the information that each method gives together to give a clearer picture of what the results actually indicates.

Below, the trend lines and average crack widths for each mix will be compared. Each trend line and average is based on all the data points from one concrete mix and load case, i.e. 4 values on each distance from the notch.

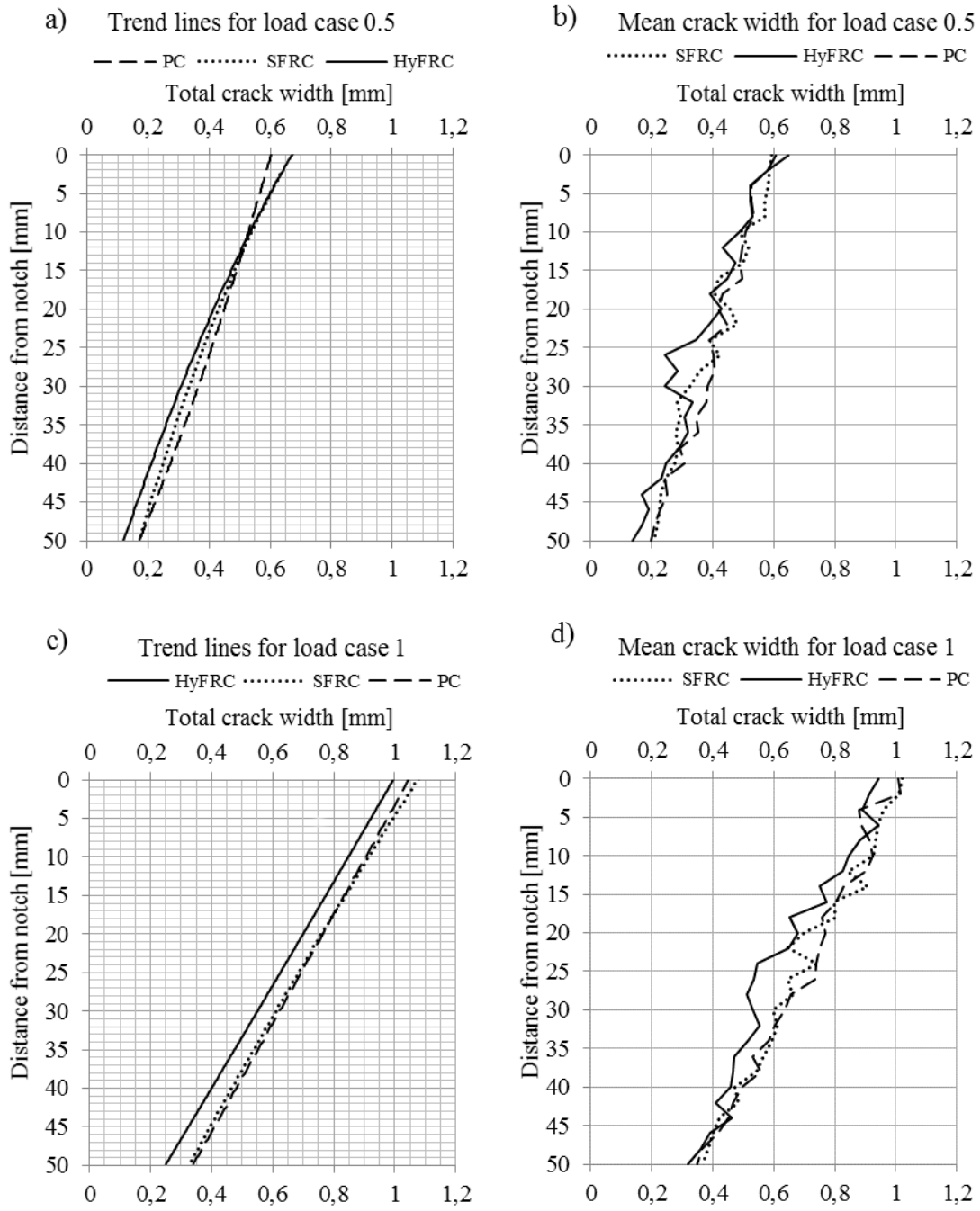

Figure 6.4. Comparison of trend lines and mean crack widths for all samples.

As mentioned earlier the crack bands from PC, SFRC and HyFRC all seem to point towards an overall linear trend of the crack width profile. The trend lines in Figure 6.4 a) and c) are 2nd order polynomial lines which gave a slightly better fit than a linear line. However, a linear trend line would have been almost as good for showing the overall trend because the polynomial line is almost linear in a), and for c) it is almost impossible to see that they are not linear.

The trend line for HyFRC for the large crack in c) has the same slope as the lines for PC and SFRC, only that it is moved a bit to the left. This suggests that the crack width for HyFRC is smaller over the whole distance between the notch and the reinforcement. However, the average crack width line shows that the HyFRC line is similar to the other two, both at the notch and close to the reinforcement, which makes the trend line a bit misleading. It seems strange that the addition of as little as 0.15% volume of PVA fibres would reduce the crack width all over the large crack, c), when this effect cannot be seen in the smaller crack, a). In addition there is no apparent effect of the steel fibres, considering that the lines for PC and SFRC are following each other both in a) and b). It would seem reasonable that the macro steel fibres would have a greater effect on large cracks than the micro PVA fibres, not the other way around. Therefore it seems unlikely that the trend line for HyFRC is a completely correct representation of HyFRC behaviour. The slope of the HyFRC curve seems reasonable, assuming that the micro PVA fibres are almost ineffective for larger crack widths, but not the displacement to the left.

The curves for SFRC and PC are very similar for the small crack as well. The trend line for HyFRC starts to deviate from the PC and SFRC curves closer to the reinforcement bar. Between the distances 0 mm to 8 mm from the reinforcement bar the mean total crack width for the HyFRC mix is notably smaller than the PC and SFRC mixes. Considering the properties of micro PVA fibres it would seem reasonable that it is in these conditions that they have an effect.

In Table 6.2 it is possible to see the mean crack widths at the notch and at the reinforcement for the two load cases. The mean crack widths for SFRC and HyFRC are also compared to PC with a ratio, w_{SFRC}/w_{PC} and w_{HyFRC}/w_{PC}. From these values it is clearer that the addition of PVA fibres has its largest effect close to the reinforcement for load case 0.5.

Table 6.2. Mean crack widths at reinforcement and notch for load case 0.5 and 1, ratio of PC crack width in parenthesis.

	Load case 0.5				*Load case 1*			
[mm] [-]	Reinforcement		Notch		Reinforcement		Notch	
PC	0.197	(1)	0.608	(1)	0.347	(1)	1.01	(1)
SFRC	0.208	(1.06)	0.591	(0.97)	0.365	(1.05)	1.02	(1.01)
HyFRC	0.138	(0.70)	0.649	(1.07)	0.319	(0.92)	0.943	(0.93)

From the results of the comparison it does not seem like the end-hooked macro steel fibres had any effect on the total crack width profile for either the small or the large crack. The micro PVA did not seem to have any effect on the large crack either, but it does seem to have an effect on the smaller cracks close to the reinforcement for load case 0.5 mm. While the effect of micro PVA seems supportable it is important to take the large scatter into consideration. The results should be viewed as an indicator, but they are not conclusive.

As can be seen in Figure 6.1, Figure 6.2 and Figure 6.3 the scatter is large, which is not neglectable. The trend of the crack width curves goes in a way that is more

reasonable considering fibre bridging. Even though the behaviour is not easily discernable due to the scatter, the measurements still show that the average total crack width is getting smaller close to the reinforcement with a increasing fibre dosage.

6.2 Crack pattern and effective crack width

Total crack width is one of the more easily quantifiable measurements for describing a crack, but it is not the only one. Another way to describe a crack is the crack morphology or crack pattern. The crack pattern is a more visual representation of the crack. Information regarding which direction the crack propagates, if it splits into several cracks, etc., are all things that can help to understand the cracking behaviour. On the other hand it is hard to quantify this information in order to make objective comparisons.

After looking at all the 24 cracks a trend could be distinguished (see Appendix E for pictures of all cracks). For all the PC samples the bending crack propagated as a single large crack for most of the distance from the notch to the reinforcement. If the main crack split into several cracks at any point it was either over short distances or it was at the last millimetres close to the reinforcement, see Figure 6.5 a). For SFRC and HyFRC it was common that the bending crack split into two smaller cracks which propagated towards the reinforcement on their own. This behaviour was considerably more common for HyFRC and there was also a higher tendency for the smaller cracks to split into several even smaller cracks, see Figure 6.5 b). In fact all the 8 cracks for the HyFRC showed this behaviour to some extent.

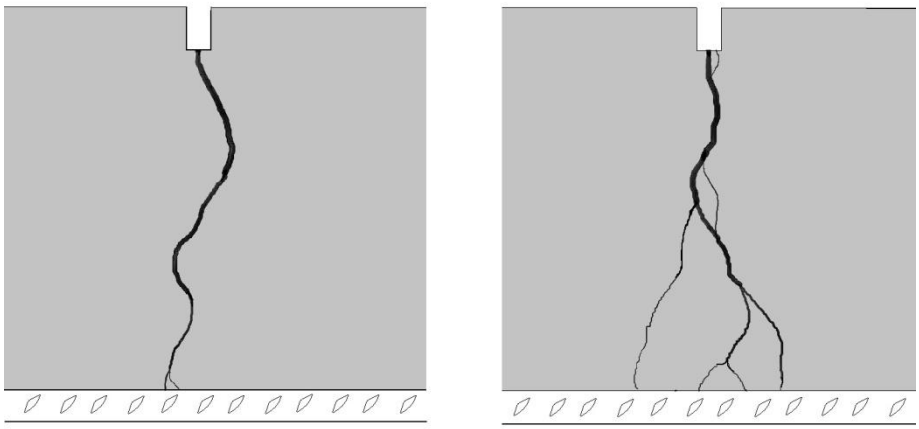

a) PC b) HyFRC

Figure 6.5 Comparison of common crack pattern of PC and HyFRC.

Fibre bridging affects the macro cracking behaviour by decreasing the crack spacing and crack widths. It would seem that they have a similar effect on the crack between the concrete surface and the reinforcement bar.

Even if the sum of several small cracks close to the reinforcement for HyFRC is the same as one large crack for PC, it can still make a difference. Several smaller cracks can in fact be beneficial with regard to corrosion of the rebar. As mentioned earlier in section 2.4 the corrosion rate increases with larger cracks since the flow of corrosive fluids increase. The equation that describes the flow rate is actually dependant on the

crack width to the power of three, w^3. Consequently the flow through two small cracks is lower than one large, given that the total crack width is the same. To illustrate which effect this has on the measured crack width, an effective crack width, w_{eff}, was calculated for each slice. The effective crack width represents the crack width that has the same flow as the sum of all the small cracks and is calculated using equation (21). The results are plotted in Figure 6.6 below. The effective crack width for each individual specimen can be seen in Appendix B.

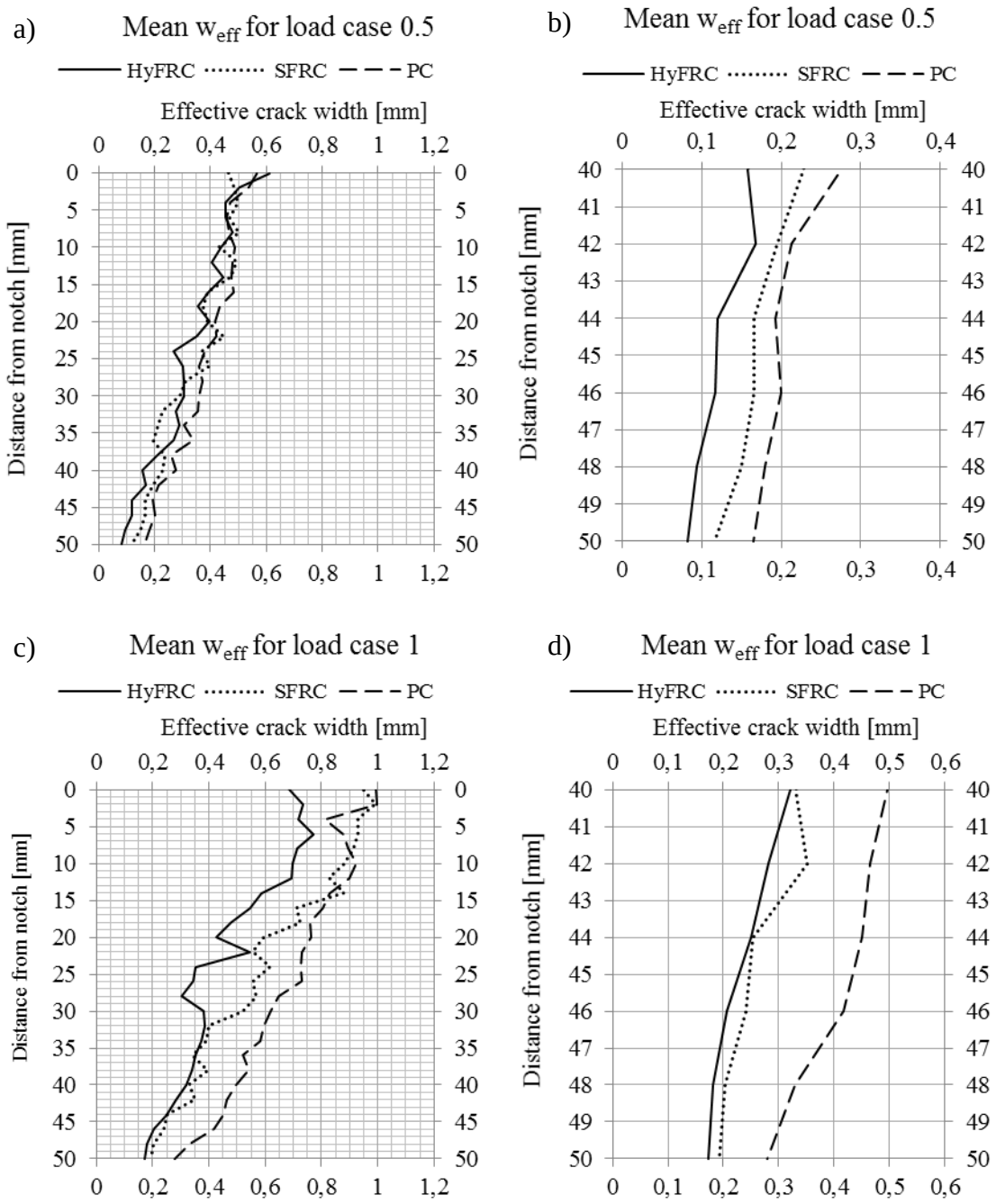

Figure 6.6 Mean effective crack width over whole distance [a) & c)] and over the 10mm closest to the reinforcement [b) & d)].

$$w_{eff} = \sqrt[3]{\sum_{i=1}^{n} w_i^3} \qquad (21)$$

From the diagrams it can be seen that the average effective crack width behaves in a different way than the regular average total crack width. Looking at c) in Figure 6.6 the difference of the effective crack width of PC compared to SFRC and HyFRC is clear. As mentioned before the crack pattern for the HyFRC mix more frequently consisted of several smaller cracks over the whole distance, between the notch and the reinforcement. This behaviour is represented in c) by the substantially smaller effective crack width over the whole area, compared to PC. In addition the SFRC line deviates more from the PC line closer to the reinforcement, which indicates a higher amount of smaller cracks for the SFRC as well. In the previous section it was shown that the total crack width profiles for SFRC and PC was very similar, which is not the case for the effective crack width profile.

Another way of showing the effect of several smaller cracks is by calculating the ratio between the effective crack width and the regular total crack width. Calculating the ratio, see Table 6.3, close to the reinforcement bar for each mix and load case it can be seen that the effective crack width method has a higher impact on SFRC and HyFRC compared to PC.

Table 6.3 Ratio between mean effective crack width and mean total crack width at 50 mm from the notch, w_{eff}/w.

Load case	*PC*	*SFRC*	*HyFRC*
0.5	0.84	0.56	0.60
1	0.80	0.53	0.54

There was still a considerable scatter for the crack widths when using effective crack width as well. When the main crack branches into several evenly sized cracks it reduces the effective crack width considerably in that area. Since the crack branching is irregular and does not occur at the same distance from the notch for all specimens, it increases the scatter.

6.3 Numerical analyses

The results from the finite element modelling are presented as plots of the Load-CMOD relation. These graphs (Figure 6.7- Figure 6.9) show that the behaviour of the specimens has been possible to model to a large extent. However, the main purpose to plot these graphs was to see how the numerical model was able to use the input values acquired from experimental work. From all three different concrete mixes different disagreements were observed, but some similarities could be established from the results.

Plain

For the plain concrete, see Figure 6.7, it can be seen that the initiation of the crack is suspended to a higher load compared to the experimentally tested beams. However, the shape of the curve and behaviour of the finite element model seemed to correlate well except for the dislocation of the curve. What also can be seen is that the FE model does not change stiffness like the test beams did at CMOD ~ 0.6 mm, indicating that the FE model was not cracking in the same manner as the test beams.

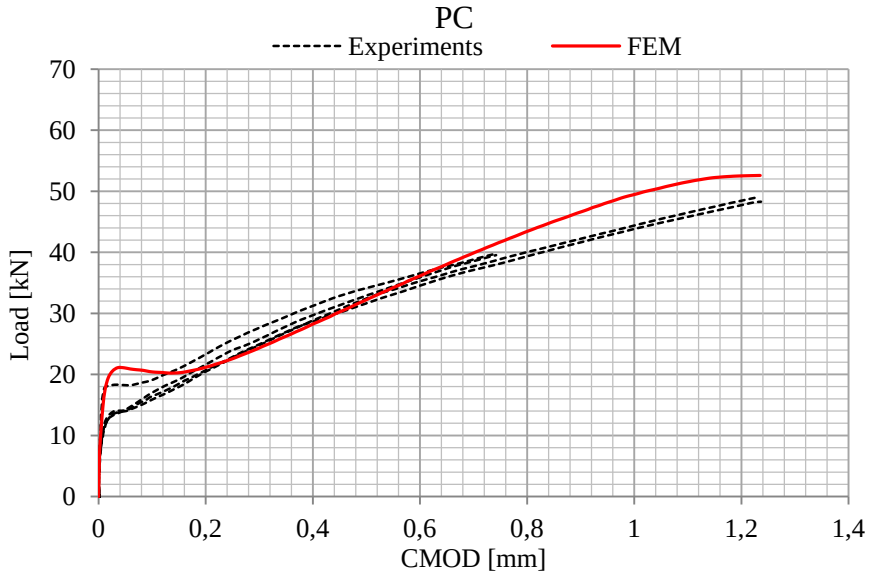

Figure 6.7 Results from numerical analyses for plain concrete mix.

SFRC

The FEA results show for the SFRC (see Figure 6.8) that cracking starts at higher load and thereafter a less stiff and almost linear behaviour can be observed, compared to the tested beams, which lose stiffness gradually after cracking. However, for the FE curve at its highest load it flattens out the last load steps which were a behaviour that could not be seen in the experiments.

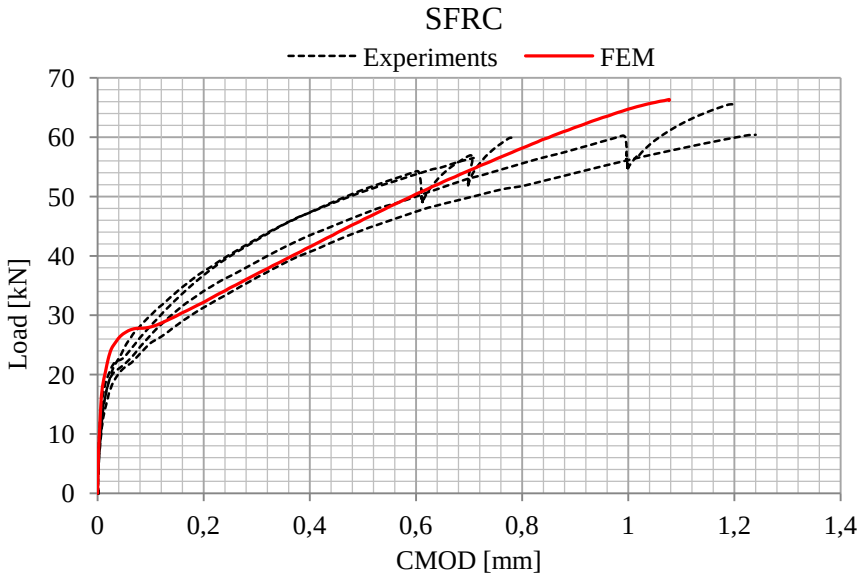

Figure 6.8 Results from numerical analyses for SFRC mix.

HyFRC

The FE results for the HyFRC appear to have the best fit to the experimental result curves. However, the cracking load was over-estimated also in this result. The stiffness of the FE result is slightly higher through-out the post-cracking behaviour but the progressive decrease of stiffness is a behaviour shared by the tested beams.

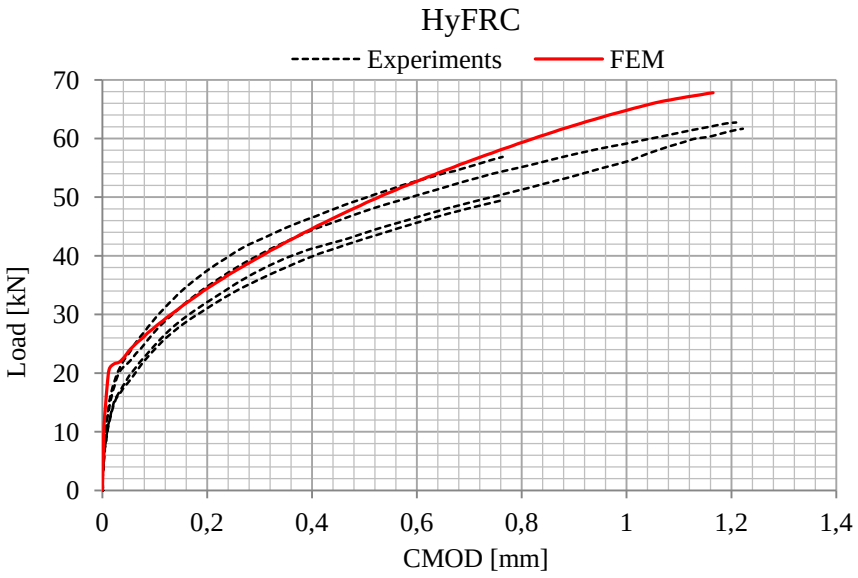

Figure 6.9 Results from numerical analyses for HyFRC mix.

In general for the FE results it was observed that the analyses conducted with the FE model resulted in a higher cracking load and over-all a stiffer behaviour. From the results of the RILEM beam FEA, presented in section 4.3.3, it could be established that the flexural strength had been overestimated from performing the inverse analyses. Thus, the stiffer behaviour of the FE models with FRC can most likely depend on this higher capacity added. Since no convergence study was performed in terms of load step and element size it is unknown if this had any effect on the result. Also it can be argued that the input values had an effect on the structural behaviour of the FE models. As previously described some input data was obtained through experimental testing while a few were derived from standards resulting in a more general representation of the real beams instead of the material specifics actually present.

Below, the FEA-results are presented (Figure 6.10 - Figure 6.18), illustrating the concrete strain and crack pattern in the plane of the reinforcement bar to show how the main crack propagated through the beam. The crack strain shows which elements reached a crack width > 0.1 mm, where the strain was converted to crack width using equation (18) in section 4.3.3. However, it does not show much difference between the three concrete mixes, except for that it is visible that the strain is higher above the reinforcement bar in the plain concrete compared to the two FRC mixes. When studying the crack pattern it is evident that the material input had a large impact on the cracking behaviour, in other words also the structural behaviour. Cracked elements are indicated by blue colour while uncracked elements are grey. The main crack is visible as the cluster of elements cracked in the middle, even though it is concentrated to the centre elements. Further the effect from the reinforcement bar can

be seen as cracked elements forming along the bar as a cone. For SFRC and HyFRC the secondary cracks start to form when reaching CMOD ~ 1 mm, but since it is not visible in the concrete strain the size is small enough to be negligible.

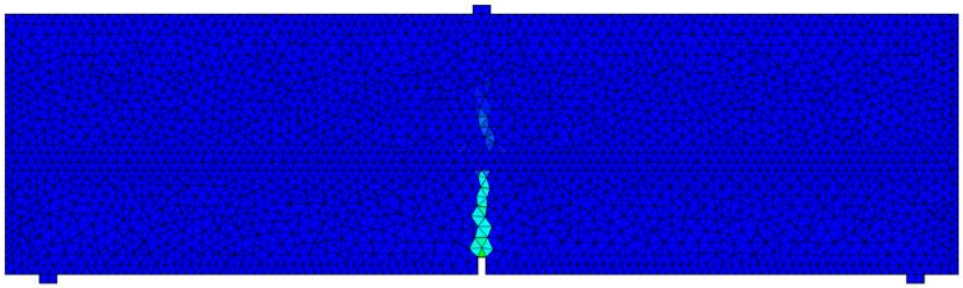

Figure 6.10 Concrete strain, PC, CMOD = 0.558 mm

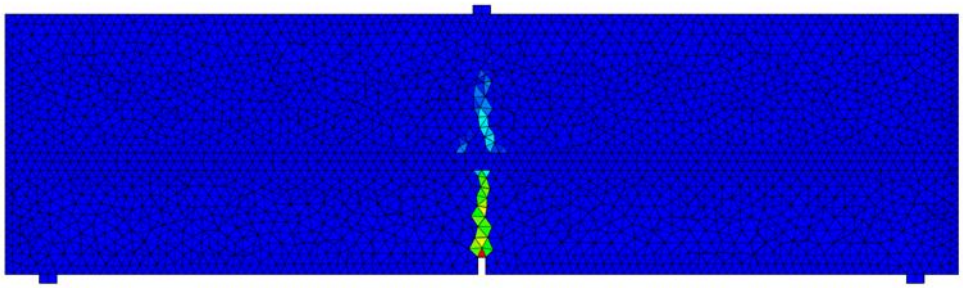

Figure 6.11 Concrete strain, PC, CMOD = 1.07 mm

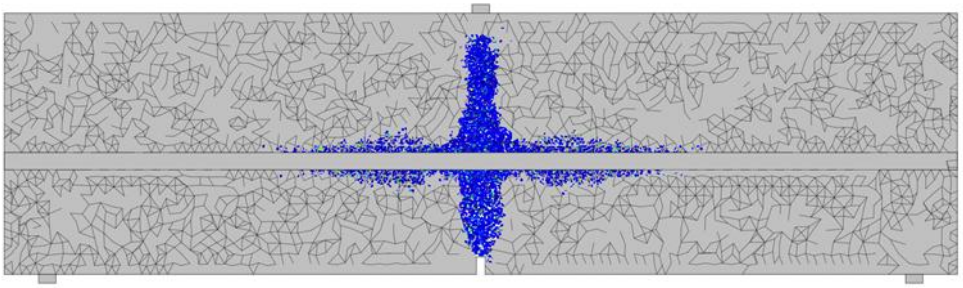

Figure 6.12 Crack pattern, PC, CMOD = 0.558 mm

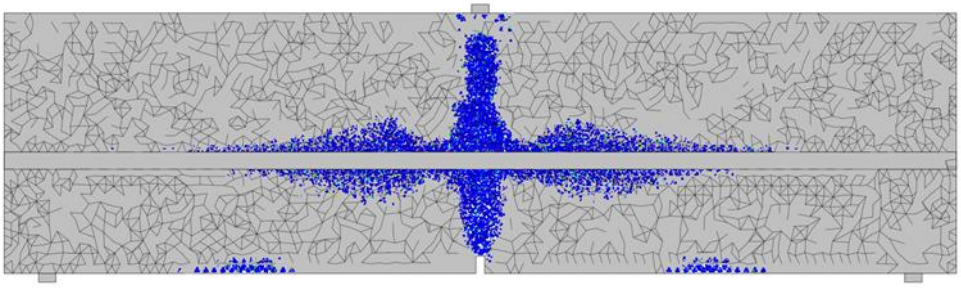

Figure 6.13 Crack pattern, PC, CMOD = 1.07 mm

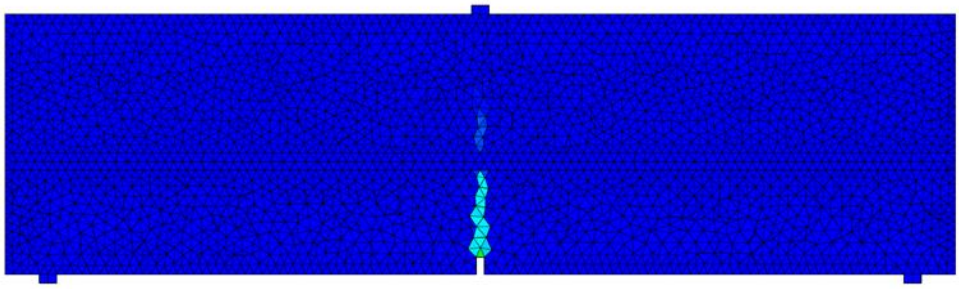

Figure 6.14 Concrete strain, SFRC, CMOD = 0.552 mm

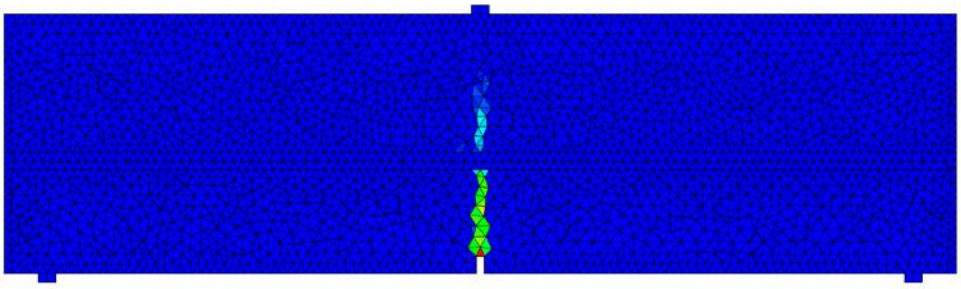

Figure 6.17 Concrete strain, SFRC, CMOD = 1.08 mm

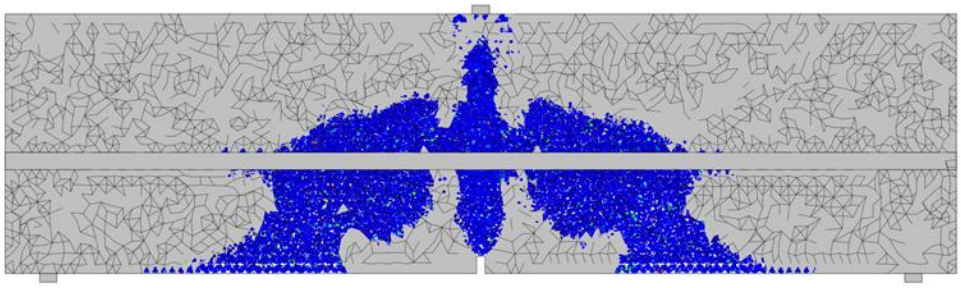

Figure 6.16 Crack pattern, SFRC, CMOD = 0.552 mm

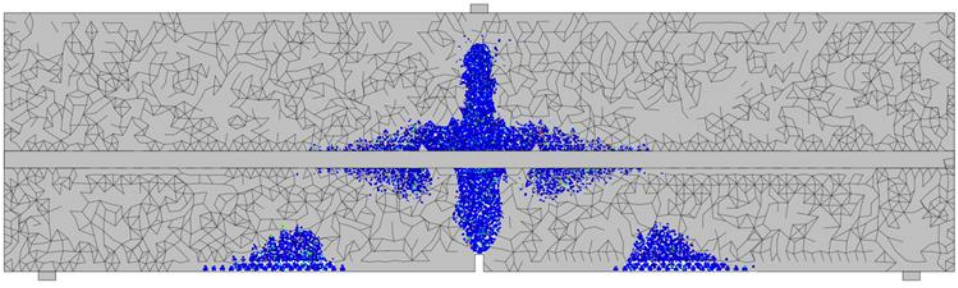

Figure 6.15 Crack pattern, SFRC, CMOD = 1.08 mm

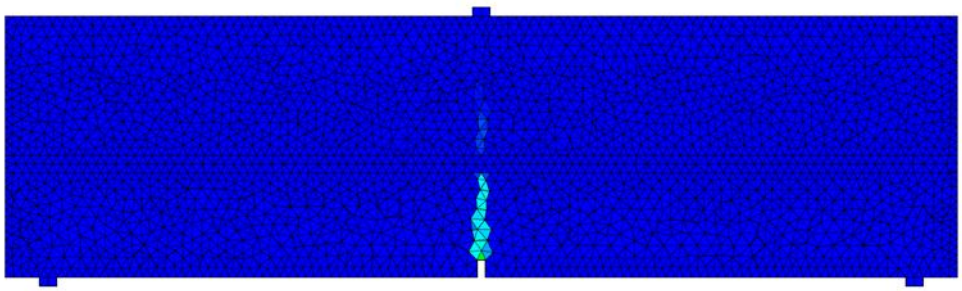

Figure 6.21 Concrete strain, HyFRC, CMOD = 0.552 mm

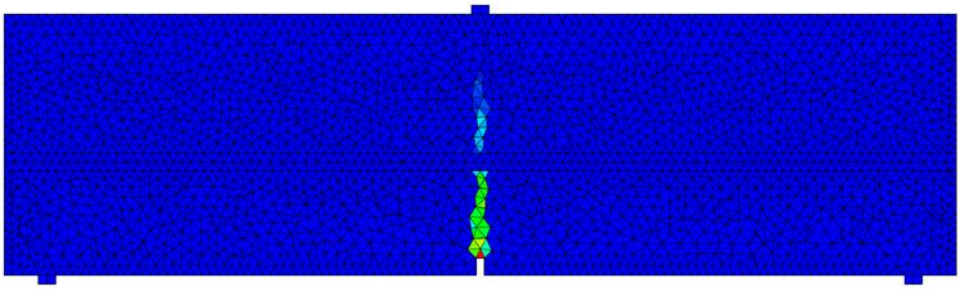

Figure 6.20 Concrete strain, HyFRC, CMOD = 1.07 mm

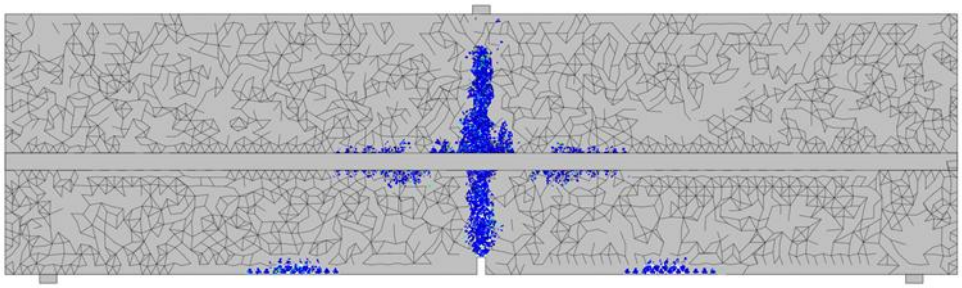

Figure 6.19 Crack pattern, HyFRC, CMOD = 0.552 mm

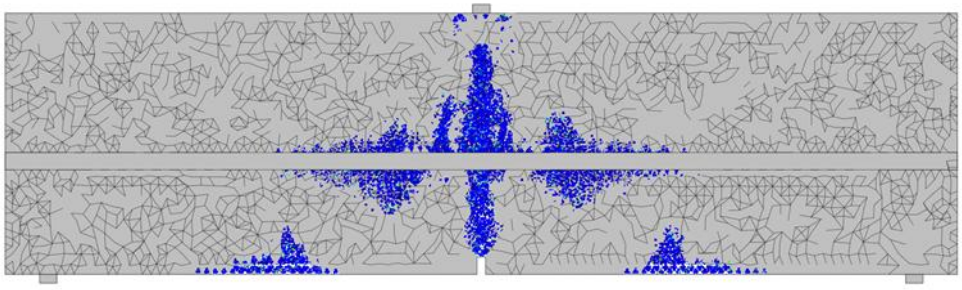

Figure 6.18 Crack pattern, HyFRC, CMOD = 1.07 mm

Crack width profiles from numerical analyses

From the numerical analyses the crack width in the plane of the reinforcement bar was extracted. The results are presented in Figure 6.22, comparing the trend line of the manually measured crack widths with the values from the FE model. In addition the comparison between the three FE results are plotted, where the last value is interpolated.

For the plots of FE results compared with experiments is it evident that finite element analysis does not give the correct crack width profile according to the values obtained from the experiments. However, it can be seen in Figure 6.22 d) that the properties of the FRC mixes had a small impact on the crack width compared with the plain concrete. The difference is not great, the effect of fibres only reduced the crack width with 5-7% of the plain concrete at the most impacted level.

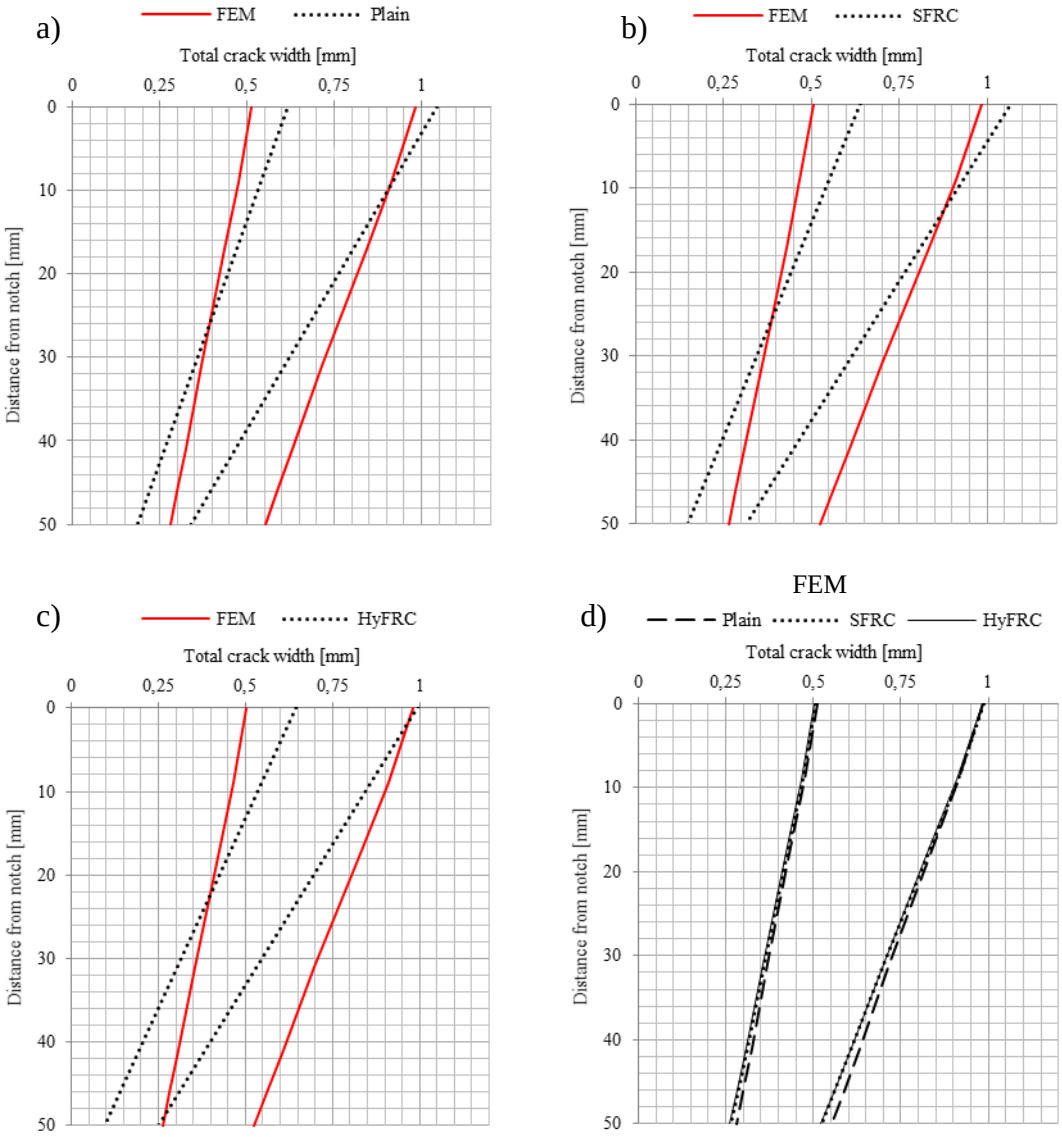

Figure 6.22 Crack width comparison of results from FEA and experiments.

7 Conclusions and Suggestions for Further Research

This thesis aimed at assessing the effect fibres have on the crack width profile, crack morphology and if finite element modelling can predict the change in behaviour compared to plain concrete. It can be established that the results have brought some new insights in terms of observed trends.

7.1 General conclusions

Modified RILEM beams were loaded in bending and the cracks were filled with fluorescent epoxy. Slices were cut from the beams and the crack widths were measured manually with digital image analysis software. This approach made it possible to study the crack morphology and how the crack width varied between the concrete surface and the reinforcement bar.

Two crack width parameters were defined for comparison of the crack width profile: (1) the total crack width, which is the sum of the individual crack widths when crack branching had occurred; and (2) the effective crack width which represents the crack width that has the same flow as the sum of all the small cracks.

The crack width measurements of SFRC showed that the used macro steel fibres had no clear effect on the total crack width profile, compared to plain concrete. For HyFRC a trend of smaller total crack widths close to the reinforcement was seen for the case of ~0.6 mm surface crack width, but not for the case of ~1 mm surface crack width, indicating a potential effect of micro PVA fibres on small cracks. However, a large scatter was observed for all mixes which increased with increasing fibre content and made any observed effect of fibres uncertain. It was therefore unclear if the small deviation in crack width profile of HyFRC for smaller cracks was due to the PVA fibres or a larger scatter. In any case, it is clear that the used fibre dosage did not have a significant effect of the total crack width profile. However, SFRC and HyFRC specimens required significantly higher loads to reach the same desired crack width at the notch, compared to plain concrete. This is in line with the current understanding of the behaviour of FRC, which is described earlier in this thesis.

While it is still unclear which effect fibres had on the total crack width profile it is clear that the addition of even small amounts of fibres changed the crack pattern. Both visual inspections and effective crack width calculations showed that the fibres made it more common for the main bending crack to branch out into several smaller cracks during its propagation towards the reinforcement bar. This was more evident for HyFRC than for SFRC, suggesting that an addition of micro PVA fibres could be more beneficial for this behaviour compared to using only end-hooked macro steel fibres. Several smaller cracks might reduce the flow of corrosive substances through the cracks for FRC, which in turn could slow down the corrosion process of conventional reinforcement.

Results from the finite element modelling showed that the crack width profile from experiments could not be obtained by numerical analysis using the presented model. The shape of the crack width profiles was linear for both FE and experiments, but the FE results overestimated the crack width at the reinforcement for cracks with identical surface crack. Furthermore, it can be said that FE analysis can be used to a large extent to model the structural behaviour of a flexural FRC element with conventional reinforcement, when experimentally obtained material properties are used. When

using the stress-crack opening relation obtained from inverse analysis of results from 3PBT, the capacity of the beams was overestimated with the used FE model. Hence it is important that the tensile curve is verified and calibrated with a FE model of the test setup used to obtain the input data for the inverse analysis.

The main conclusions can be summarized with the following points:

- The used fibre dosages had no clear effect on the total crack width profile, but it significantly increased the load required to achieve the same crack width at the notch compared to plain concrete.
- Adding fibres to the concrete resulted in a higher tendency for crack branching which decreased the effective crack width close to the reinforcement bar. For SFRC and HyFRC the effective crack width was 40-45% smaller than the total crack width, compared to 15-20% for plain concrete.
- The results for the presented FE analyses showed an acceptable coherence with the structural behaviour of the tested beams, but the total crack width profile could not be reproduced.

The study, consisting of experimental and modelling work, can add to the discussion whether FRC can enhance the structural behaviour of concrete structures and increase the resistance to corrosion of conventional reinforcement.

7.2 Suggestions for future research

From the conclusions of the work that have been performed in this thesis it can be said that fibres show a tendency to influence the crack pattern and crack morphology that can be beneficial for concrete structures. However, there are some knowledge gaps that through further investigations could be filled. Here is a list of suggestions for future research:

- Specimens in this thesis were cast with relatively small fibre dosages and only two types of fibres. To fully investigate the effect fibres have on the crack width profile and morphology more variation is needed. For instance higher fibre content, other fibre materials and fibre anchorage types. It could then be established whether fibres in fact can have a quantifiable effect on the total crack width profile and if its effect on crack pattern and crack morphology is true for other fibre combinations than the ones used in this thesis.
- The modified RILEM beams in this thesis were cracked to relatively large crack widths at the notch. It would therefore be of interest if the same tendencies that were observed here can be seen for specimen cracked to a smaller crack width as well. This could be more relevant to the serviceability limit state of concrete structures.
- Several parameters can affect the results of the finite element analysis. For example the bond slip model and the tensile curve. To get a better understanding of how large effect certain parameters have on the results a parameter study would be needed. The conclusions from the parameter study could then be used to potentially develop a FE model that properly predicts the crack width profile shown in this thesis.
- An interesting conclusion of this thesis is that fibres had a clear effect on the crack pattern and crack morphology, which could be seen by the main crack branching into several smaller cracks. This could be beneficial with regards to

chloride ingress and carbonation. However, further analysis of the flow of liquids through the cracks presented in this thesis is needed to understand which effect this behaviour would actually have.

8 References

Bentur, A. & Mindess, S., 2007. *Cementitious Composites* Second edi., Abingdon, Oxon: Taylor & Francis.

Bernardi, P. et al., 2015. Experimental and numerical study on cracking process in RC and R / FRC ties. *Materials and Structures*, pp.1–17.

Berrocal, C.G., 2015. *Chloride Induced Corrosion of Steel Bars in Fibre Reinforced Concrete*. Chalmers University of Technology.

Borosnyól, a & Snóbli, I., 2010. Crack width variation within the concrete cover of reinforced concrete members. *Materials Technology*, 6(3), pp.70–74.

Broms, B.B., 1965. Crack width and crack spacing in reinforced concrete members. *American Concrete Institute -- Journal*, 62(10), pp.1237–1256.

BS EN 12390-6, 2003. BRITISH STANDARD EN 12390-6.

DAfStbUA SFB N 0146, 2005. *DAfStb-Richtlinie Stahlfaserbeton*, Ergänzung zu DIN 1045, Teile 1 bis 4 (07/2001): Deutscher Ausschluss fur Stahlbeton (DAfStb).

Edvardsen, C., 1999. Water permeability and autogenous healing of cracks in concrete. *ACI Materials Journal*, 96(4), pp.448–454.

EN 14651, 2005. EUROPEAN STANDARD EN 14651:2005. , pp.1–17.

Eurocode 2, 2008. *SS-EN 1992-1-1:2005 Eurocode 2: Design of concrete structures* 1st ed., Stockholm: SIS Förlag AB.

Husain, S.I. & Ferguson, P.M., 1968. *Flexural Crack Width At the Bars in Reinforced Concrete Beams*, Austin, Texas.

Jansson, A., 2011. *Effects of Steel Fibres on Cracking in Reinforced Concrete*. Chalmers University of Technology.

Kosa, K. & Naaman, A.E., 1990. Corrosion of Steel Fiber Reinforced Concrete. *ACI Materials Journal*, 87(1).

Lundgren, K., 2005. Bond between ribbed bars and concrete. Part 1: Modified model. *Magazine of Concrete Research*, 57(7), pp.371–382.

Löfgren, I., 2007. Calculation of crack width and crack spacing. In *Fibre reinforced concrete*. Trondheim: Nordic Mini-seminar.

Löfgren, I., 2005. *Fibre-reinforced Concrete for Industrial Construction - a fracture mechanics approach to material testing and structural analysis*. Göteborg: Chalmers University of Technology.

Model Code, 2010. *CEB-FIP, Bulletin 56, FIB 2010, First Complete Draft, Vol. 2*, International Federation for Structural Concrete (fib).

Naaman, A.E., 2003. Engineered Steel Fibers with Optimal Properties for Reinforcement of Cement Composites. *Journal of Advanced Concrete Technology*, 1(3), pp.241–252.

NYCON, 2015. NYCON-PVA RSC15 Physical Properties. Available at: www.nycon.com.

Olesen, J.F., 2001. Fictitious crack propagation in fibre reinforced concrete beams. *Journal of Engineering Mechanics*, 127(3), pp.272–280.

Ottosen, N.S. & Petersson, H., 1992. *Introduction to the finite element method*, New York: Prentice Hall.

Di Prisco, M., Colombo, M. & Dozio, D., 2013. Fibre-reinforced concrete in fib Model Code 2010: principles, models and test validation. *Structural Concrete*, 14(4), pp.342–361.

RILEM TC 162-TDF, 2000. Test and design methods for steel fibre reinforced concrete L. Vandewalle, ed. *Materials and Structures*, Vol. 33, pp.75–81.

Selby, R.G., 1993. *Three-dimensional constitutive relations for reinforced concrete*. University of Toronto.

Stang, H. & Olesen, J.F., 2000. A Fracture Mechanics Based Design Approach to FRC. *"Proc. , 5th RILEM Symp. on Fiber-Reinforced Concretes (FRCs)", BEFIB 2000*, pp.315–324.

Swedish Standards Institute, 2014. SS 812310:2014 Fibre Concrete - Design of Fibre Concrete Structures.

Tammo, K., 2009. *A NEW APPROACH TO CRACK CONTROL FOR REINFORCED CONCRETE An investigation of crack widths close to the reinforcement and the correlation to service life*. Lund University.

TNO DIANA, 2014. DIANA - Finite Element Analysis, User's Manual Release 9.6. Available at: tnodiana.com.

Zheng, Z. & Feldman, D., 1995. Synthetic fibre-reinforced concrete. *Progress in Polymer Science*, 20(94), pp.185–210.

APPENDIX A

Total crack width measurements

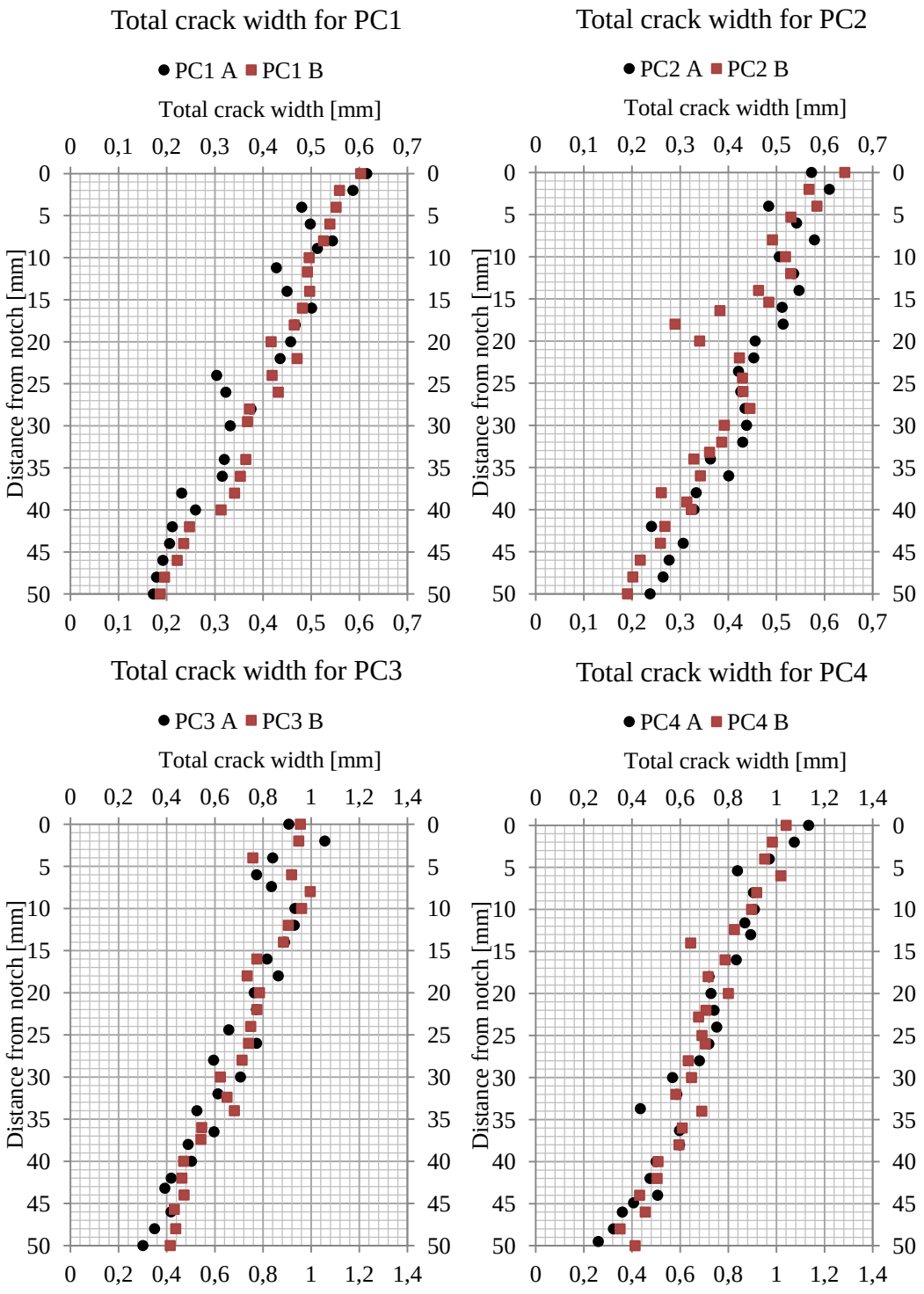
Total crack width for PC1
PC1 A
PC1 B
Total crack width [mm]
Distance from notch [mm]
Total crack width for PC2
PC2 A
PC2 B
Total crack width [mm]
Distance from notch [mm]
Total crack width for PC3
PC3 A
PC3 B
Total crack width [mm]
Distance from notch [mm]
Total crack width for PC4
PC4 A
PC4 B
Total crack width [mm]
Distance from notch [mm]

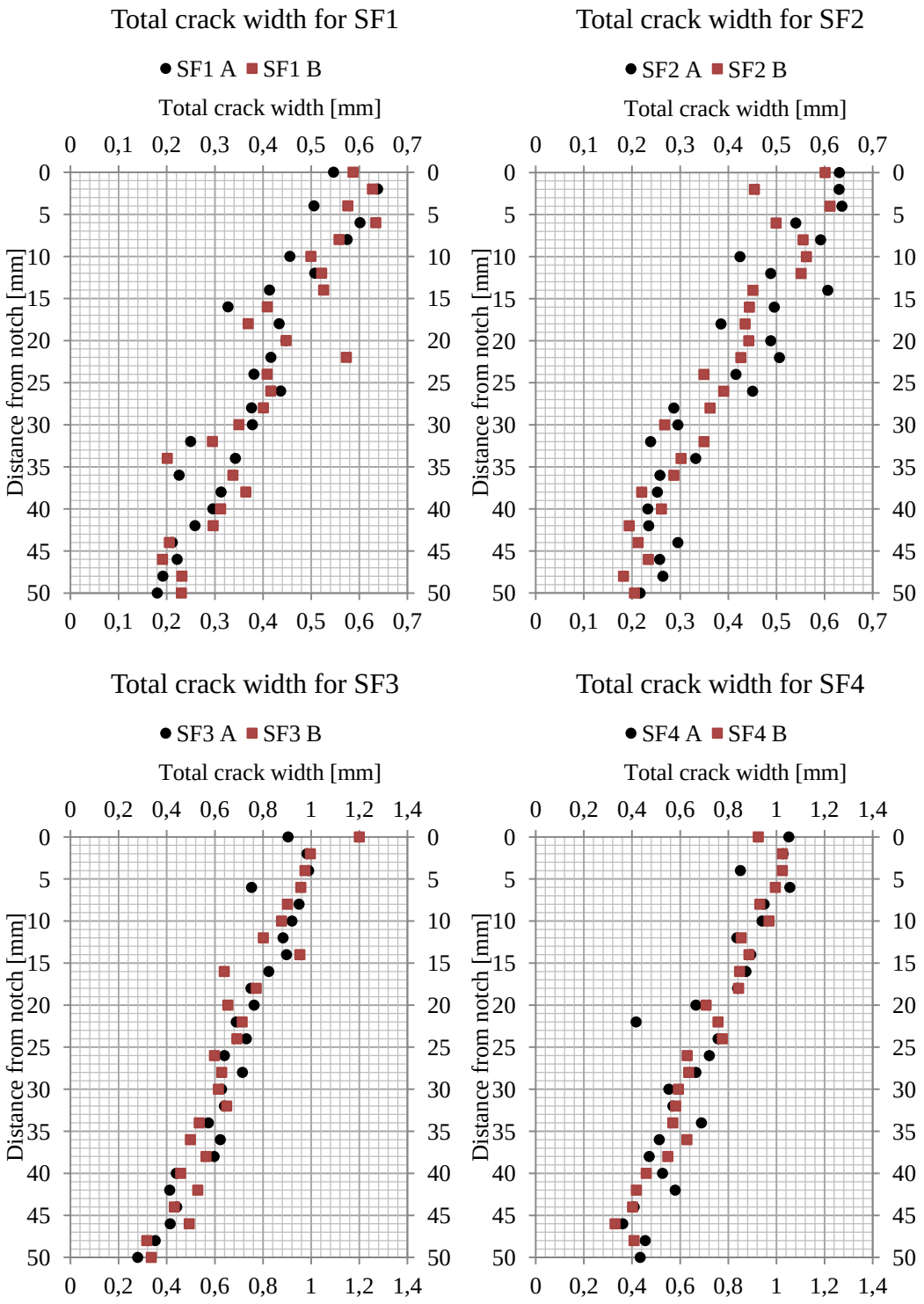
Total crack width for SF1
SF1 A
SF1 B
Total crack width [mm]
0 0,1 0,2 0,3 0,4 0,5 0,6 0,7
Distance from notch [mm]
0 5 10 15 20 25 30 35 40 45 50
Total crack width for SF2
SF2 A
SF2 B
Total crack width [mm]
0 0,1 0,2 0,3 0,4 0,5 0,6 0,7
Distance from notch [mm]
0 5 10 15 20 25 30 35 40 45 50
Total crack width for SF3
SF3 A
SF3 B
Total crack width [mm]
0 0,2 0,4 0,6 0,8 1 1,2 1,4
Distance from notch [mm]
0 5 10 15 20 25 30 35 40 45 50
Total crack width for SF4
SF4 A
SF4 B
Total crack width [mm]
0 0,2 0,4 0,6 0,8 1 1,2 1,4
Distance from notch [mm]
0 5 10 15 20 25 30 35 40 45 50

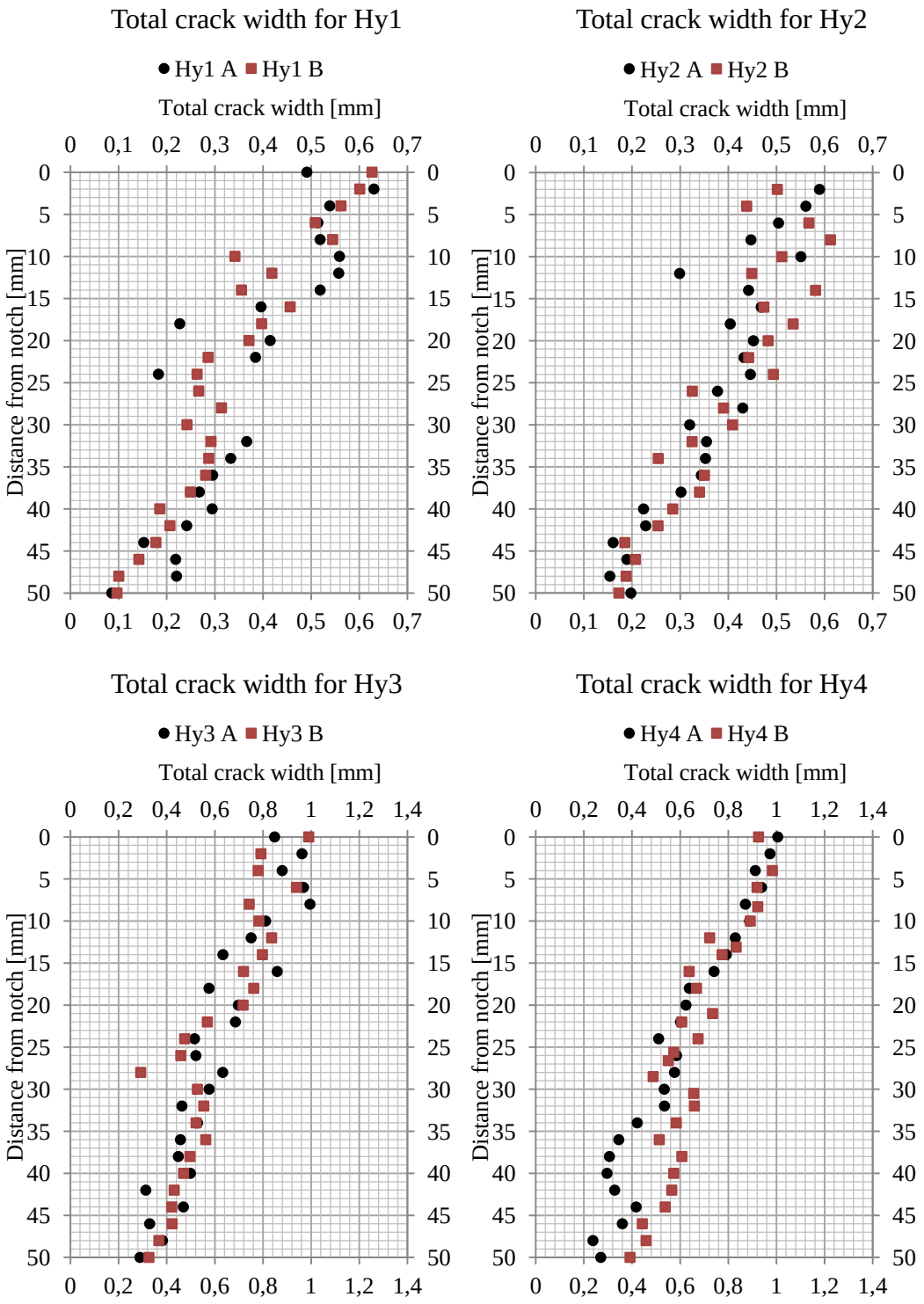
Total crack width for Hy1
Hy1 A
Hy1 B
Total crack width [mm]
Distance from notch [mm]
Total crack width for Hy2
Hy2 A
Hy2 B
Total crack width [mm]
Distance from notch [mm]
Total crack width for Hy3
Hy3 A
Hy3 B
Total crack width [mm]
Distance from notch [mm]
Total crack width for Hy4
Hy4 A
Hy4 B
Total crack width [mm]
Distance from notch [mm]

APPENDIX B

Effective crack width

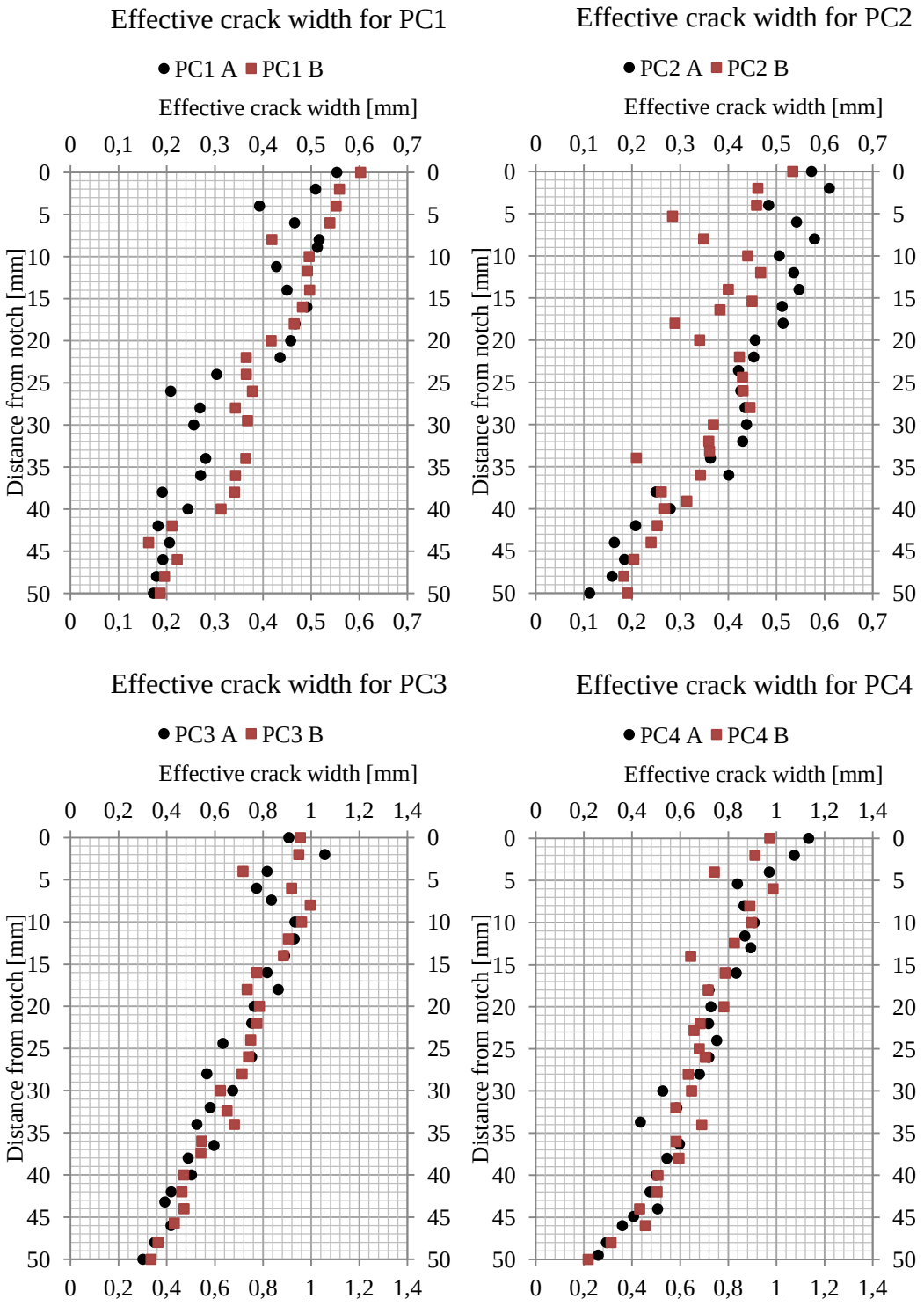
Effective crack width for PC1
PC1 A
PC1 B
Effective crack width [mm]
Distance from notch [mm]
Effective crack width for PC2
PC2 A
PC2 B
Effective crack width [mm]
Distance from notch [mm]
Effective crack width for PC3
PC3 A
PC3 B
Effective crack width [mm]
Distance from notch [mm]
Effective crack width for PC4
PC4 A
PC4 B
Effective crack width [mm]
Distance from notch [mm]

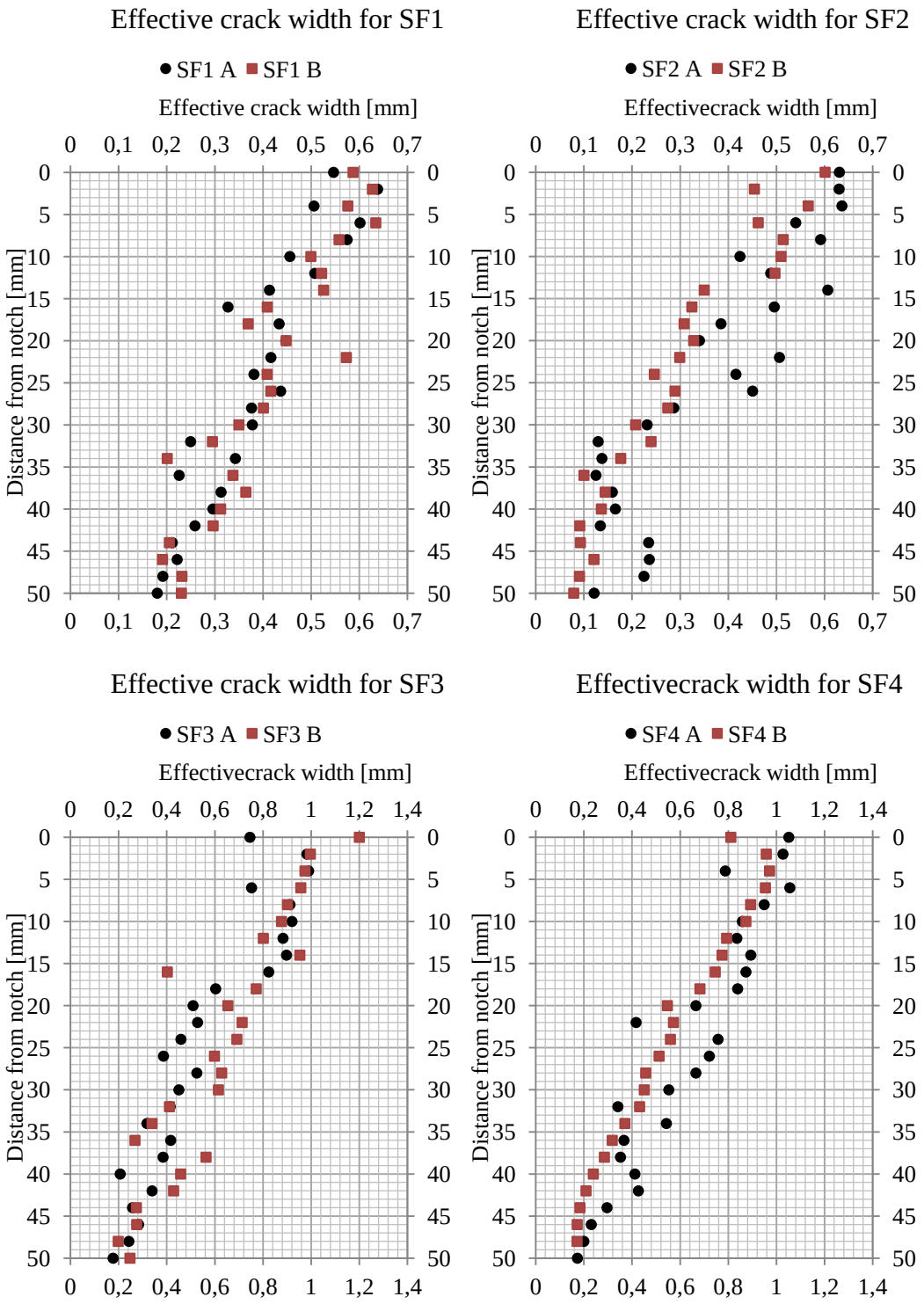
Effective crack width for SF1
SF1 A
SF1 B
Effective crack width [mm]
Distance from notch [mm]
Effective crack width for SF2
SF2 A
SF2 B
Effectivecrack width [mm]
Distance from notch [mm]
Effective crack width for SF3
SF3 A
SF3 B
Effectivecrack width [mm]
Distance from notch [mm]
Effectivecrack width for SF4
SF4 A
SF4 B
Effectivecrack width [mm]
Distance from notch [mm]

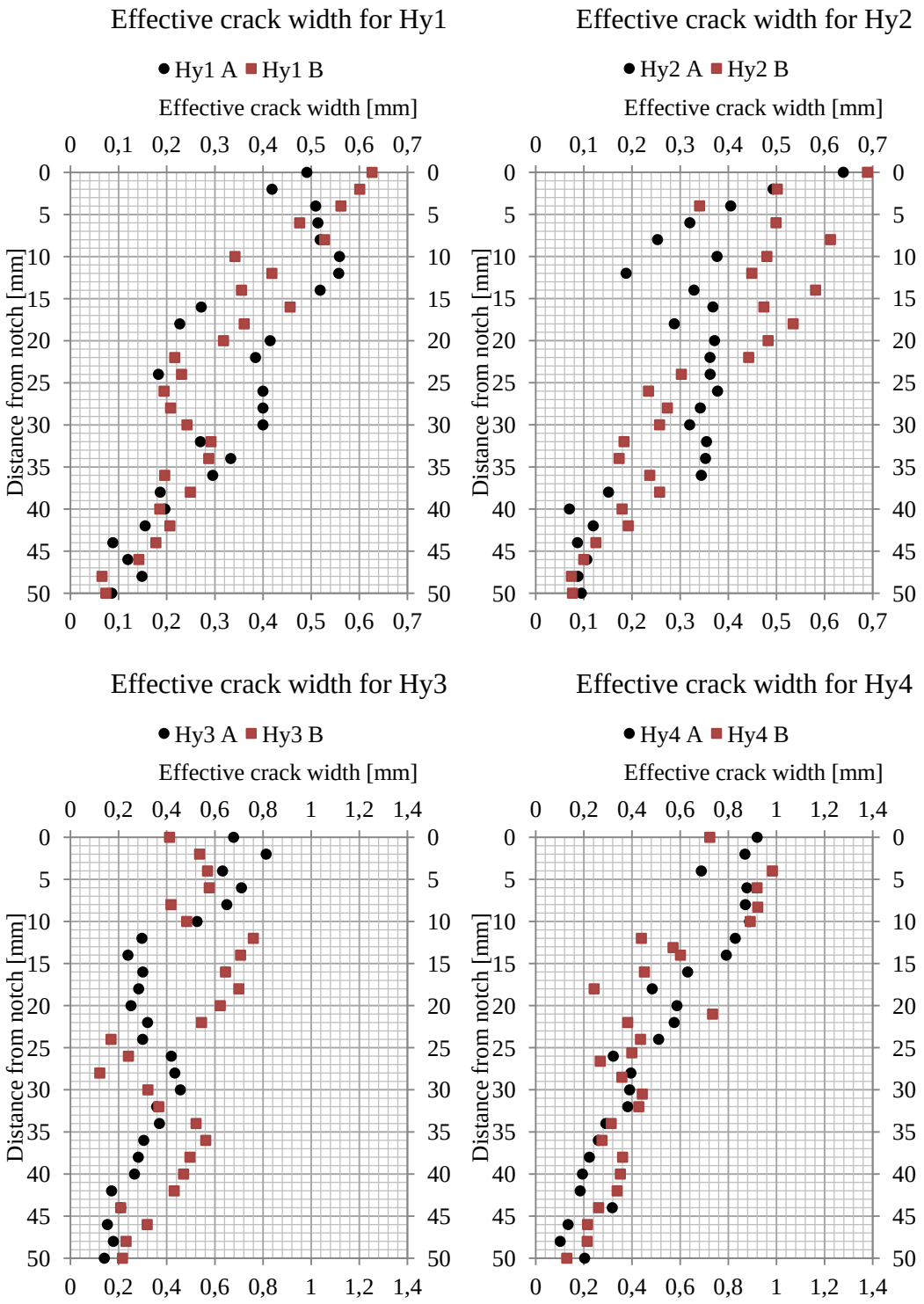
Effective crack width for Hy1
Hy1 A
Hy1 B
Effective crack width [mm]
Distance from notch [mm]
Effective crack width for Hy2
Hy2 A
Hy2 B
Effective crack width [mm]
Distance from notch [mm]
Effective crack width for Hy3
Hy3 A
Hy3 B
Effective crack width [mm]
Distance from notch [mm]
Effective crack width for Hy4
Hy4 A
Hy4 B
Effective crack width [mm]
Distance from notch [mm]

APPENDIX C

DIANA files (.dcf & .dat)

NON-LINEAR ANALYSIS – .dcf file

```
*FILOS
 INITIA
*INPUT
*FORTRAN
  USE "usrifc.so"
*NONLIN LABEL="Structural nonlinear"
  BEGIN EXECUT
    BEGIN LOAD
      LOADNR 1
      STEPS EXPLIC SIZES 0.0100000(120)
    END LOAD
    BEGIN ITERAT
      MAXITE 50
      METHOD NEWTON
      BEGIN CONVER
        FORCE TOLCON 0.005
        DISPLA TOLCON 0.005
        ENERGY OFF
      END CONVER
    END ITERAT
  END EXECUT
  SOLVE AUTOMA
  BEGIN OUTPUT
    TEXT "Output"
    FXPLUS
    BINARY
    SELECT STEPS ALL /
    DISPLA TOTAL TRANSL GLOBAL
    STRAIN CRACK GREEN
    STRAIN TOTAL GREEN GLOBAL
    STRESS TOTAL CAUCHY GLOBAL
    FORCE REACTI TRANSL GLOBAL
  END OUTPUT
*END
```

PC – .dat file

```
: Diana Datafile written by Diana 9.5
Translated from FX+ for DIANA neutral file (version 1.2.0).

'UNITS'
LENGTH M
FORCE N
TEMPER CELSIU

'DIRECTIONS'
   1   1.00000E+00   0.00000E+00   0.00000E+00
   2   0.00000E+00   1.00000E+00   0.00000E+00
   3   0.00000E+00   0.00000E+00   1.00000E+00

'MODEL'
GRAVDI 3
GRAVAC  -9.81000E+00

'COORDINATES'
    1   2.72500E-01   0.00000E+00   7.50000E-02
            ... (rows deleted)...
49707   2.97273E-02  -5.00000E-03   6.50000E-02

'MATERI'
   1 NAME   "CONCRETE"
     MCNAME CONCR
     MATMDL TSCR
     ASPECT
     POISON   2.00000E-01
     YOUNG    3.53000E+10
     DENSIT   2.40000E+03
     TOTCRK ROTATE
     TENCRV HORDYK
     REDCRV NONE
     POIRED NONE
     TENSTR   3.00000E+06
     GF1      0.90450E+02
     COMCRV CONSTA
     COMSTR   4.84000E+07
```

```
   2 NAME   "REINFORCEMENT STEEL"
     MCNAME MCSTEL
     MATMDL TRESCA
     ASPECT
     POISON   3.00000E-01
     YOUNG    2.04000E+11
     DENSIT   7.85000E+03
     YIELD  VMISES
     TRESSH NONE
     YLDVAL   5.464000E+08
   3 NAME   "FRICTIONAL MODEL"
:fcyl=     4.84E+01     MPa        fct.m=    3    MPa
:r=        5.00E+00     mm         x=        0    mikrometer
     DSTIF            1.17373E+13        1.2355E+12
     USRIFC        BOTH
     USRVAL          0        0.4        0.05        4.00E-03
                     0.00E+00               4.838E+07               1
3000000
                     1.35E-04        4.838E+07        0.86        300
                     2.80E-04        4.823E+07        0.78        0
                     4.11E-04        4.799E+07        0.72        0
                     6.21E-04        4.664E+07        0.65        0
                     8.30E-04        4.543E+07        0.59        0
                     1.07E-03        4.209E+07        0.56        0
                     1.51E-03        3.662E+07        0.52        0
                     1.90E-03        3.406E+07        0.52        0
                     2.60E-03        3.106E+07        0.52        0
                     4.71E-03        2.617E+07        0.52        0
                     1.21E-02        3.270E+07        0.52        0
                     1.50E+20        0.000E+00        0.52        0
               0 0
               1E6 0
               14E9 2.0                 5.00E-03        0E-6 7.0
     USRSTA   0.0   0.0   0.0   0.0   0.0   0.0   0.0           1.17E+13
0.0 0.0 0.0 0.0 0.0 0.0 0.0 0.0 0.0 0.0
     USRIND  0 13 2
   4 NAME   "STEEL PLATES"
     YOUNG    2.10000E+11
     POISON   2.00000E-01

'GEOMET'
```

```
   1 NAME   "INTstre_3-7"
     XAXIS    0.00000E+00  -3.54000E-03   1.46400E-03
   2 NAME   "INTstre_4-8"
     XAXIS    0.00000E+00  -1.46000E-03   3.53600E-03
   3 NAME   "INTstre_1-5"
     XAXIS    0.00000E+00  -1.46000E-03  -3.54000E-03
   4 NAME   "INTstre_2-6"
     XAXIS    0.00000E+00  -3.54000E-03  -1.46000E-03
   5 NAME   "steel_plate"
   6 NAME   "concrete"
   7 NAME   "steel"

'DATA'
   1 NAME   "concrete"
   2 NAME   "steel"
   7 NAME   "steel_plate"
   3 NAME   "INTstre_1-5"
   4 NAME   "INTstre_2-6"
   5 NAME   "INTstre_3-7"
   6 NAME   "INTstre_4-8"

'ELEMENTS'
CONNECT
253976 T18IF 48678 49032 48808 8814 12497 12279
            ... (rows deleted)...
255915 TP18L 275 329 330 49678 49703 49695
     1 TE12L  29127 22157 21535 28171
            ... (rows deleted)...
253975 TE12L 48624 12946 12947 12267
MATERI
/ 1-251401 / 1
/ 251402-253975 / 2
/ 253976-255735 / 3
/ 255736-255915 / 4
DATA
/ 1-251401 / 1
/ 251402-253975 / 2
/ 255736-255915 / 7
/ 253980 ... (rows deleted)... 255734 / 3
/ 253981 ... (rows deleted)... 255301 / 4
```

```
/ 253976 ... (rows deleted)... 255303 / 5
/ 253977 ... (rows deleted)... 255735 / 6
GEOMET
/ 253976 ... (rows deleted)... 255303 / 1
/ 253977 ... (rows deleted)... 255735 / 2
/ 253980 ... (rows deleted)... 255734 / 3
/ 253981 ... (rows deleted)... 255301 / 4
/ 255736-255915 / 5
/ 1-251401 / 6
/ 251402-253975 / 7

'LOADS'
CASE 1
NAME "Displacement"
DEFORM
49564 TR 2  -1.00000E-03
        ... (rows deleted)...
49608 TR 2  -1.00000E-03

'GROUPS'
ELEMEN
 127 "Concrete Solid Mesh" / 1-251401 /
 128 "Rebar Solid Mesh" / 251402-253975 /
 130 "1-5" / 253980 ... (rows deleted)... 255734 /
 131 "2-6" / 253981 ... (rows deleted)... 255301 /
 132 "3-7" / 253976 ... (rows deleted)... 255303 /
 133 "4-8" / 253977 ... (rows deleted)... 255735 /
 134 "Top Steel Plate" / 255736-255795 /
 135 "Support Steel Plates" / 255796-255915 /

'SUPPOR'
NAME "Supports"
/ 49661 ... (rows deleted)... 49705 / TR 1
/ 49661 ... (rows deleted)... 49655 / TR 2
NAME "Symmetry"
/ 1 ... (rows deleted)... 49596 / TR 3
NAME "L_Displacement"
/ 49564 ... (rows deleted)... 49608 / TR 2
'END'
```

```
: Diana Datafile written by Diana 9.5
Translated from FX+ for DIANA neutral file (version 1.2.0).

'UNITS'
LENGTH M
FORCE N
TEMPER CELSIU

'DIRECTIONS'
   1   1.00000E+00   0.00000E+00   0.00000E+00
   2   0.00000E+00   1.00000E+00   0.00000E+00
   3   0.00000E+00   0.00000E+00   1.00000E+00

'MODEL'
GRAVDI 3
GRAVAC  -9.81000E+00

'COORDINATES'
    1   2.72500E-01   0.00000E+00   7.50000E-02
            ... (rows deleted)...
49707   2.97273E-02  -5.00000E-03   6.50000E-02

'MATERI'
   1 NAME   "CONCRETE"
     MCNAME CONCR
     MATMDL TSCR
     ASPECT
     POISON   2.00000E-01
     YOUNG    3.46400E+10
     DENSIT   2.40000E+03
     TOTCRK ROTATE
     TENCRV MULTLN
     TENPAR   0  0  3.4082E+06  9.83891E-05  1.927269982E+06  0.008276814
1.019460784E+06 0.400098389 0 0.840110157
     COMCRV CONSTA
     COMSTR   4.600000E+07
   2 NAME   "REINFORCEMENT STEEL"
     MCNAME MCSTEL
```

```
     MATMDL TRESCA
     ASPECT
     POISON   3.00000E-01
     YOUNG    2.04000E+11
     DENSIT   7.85000E+03
     YIELD  VMISES
     TRESSH NONE
     YLDVAL   5.464000E+08
   3 NAME   "FRICTIONAL MODEL"
:fcyl=     4.54E+01    MPa        fct.m     3.41   MPa
:r=        5.00E+00    mm         x=        0      mikrometer
     DSTIF            1.15178E+13        1.2124E+12
     USRIFC        BOTH
     USRVAL          0        0.4        0.05        4.00E-03
                     0.00E+00        4.541E+07        1           0
                     1.35E-04        4.541E+07        0.86        0
                     2.80E-04        4.527E+07        0.78        0
                     4.11E-04        4.504E+07        0.72        0
                     6.21E-04        4.377E+07        0.65        0
                     8.30E-04        4.264E+07        0.59        0
                     1.07E-03        3.950E+07        0.56        0
                     1.51E-03        3.437E+07        0.52        0
                     1.90E-03        3.197E+07        0.52        0
                     2.60E-03        2.915E+07        0.52        0
                     4.71E-03        2.456E+07        0.52        0
                     1.21E-02        3.069E+07        0.52        0
                     1.50E+20        0.000E+00        0.52        0
               0 0
               1E6 0
               14E9 2.0                  5.00E-03        0E-6 7.0
     USRSTA   0.0   0.0   0.0   0.0   0.0   0.0   0.0          1.15E+13
0.0 0.0 0.0 0.0 0.0 0.0 0.0 0.0 0.0 0.0
     USRIND  0 13 2
   4 NAME   "STEEL PLATES"
     YOUNG    2.10000E+11
     POISON   2.00000E-01

'GEOMET'
   1 NAME   "INTstre_3-7"
     XAXIS    0.00000E+00  -3.54000E-03   1.46400E-03
   2 NAME   "INTstre_4-8"
```

```
     XAXIS    0.00000E+00  -1.46000E-03   3.53600E-03
   3 NAME   "INTstre_1-5"
     XAXIS    0.00000E+00  -1.46000E-03  -3.54000E-03
   4 NAME   "INTstre_2-6"
     XAXIS    0.00000E+00  -3.54000E-03  -1.46000E-03
   5 NAME   "steel_plate"
   6 NAME   "concrete"
   7 NAME   "steel"

'DATA'
   1 NAME   "concrete"
   2 NAME   "steel"
   7 NAME   "steel_plate"
   3 NAME   "INTstre_1-5"
   4 NAME   "INTstre_2-6"
   5 NAME   "INTstre_3-7"
   6 NAME   "INTstre_4-8"

'ELEMENTS'
CONNECT
253976 T18IF 48678 49032 48808 8814 12497 12279
           ... (rows deleted)...
255915 TP18L 275 329 330 49678 49703 49695
     1 TE12L  29127 22157 21535 28171
           ... (rows deleted)...
253975 TE12L 48624 12946 12947 12267
MATERI
/ 1-251401 / 1
/ 251402-253975 / 2
/ 253976-255735 / 3
/ 255736-255915 / 4
DATA
/ 1-251401 / 1
/ 251402-253975 / 2
/ 255736-255915 / 7
/ 253980 ... (rows deleted)... 255734 / 3
/ 253981 ... (rows deleted)... 255301 / 4
/ 253976 ... (rows deleted)... 255303 / 5
/ 253977 ... (rows deleted)... 255735 / 6
GEOMET
```

```
/ 253976 ... (rows deleted)... 255303 / 1
/ 253977 ... (rows deleted)... 255735 / 2
/ 253980 ... (rows deleted)... 255734 / 3
/ 253981 ... (rows deleted)... 255301 / 4
/ 255736-255915 / 5
/ 1-251401 / 6
/ 251402-253975 / 7

'LOADS'
CASE 1
NAME "Displacement"
DEFORM
49564 TR 2  -1.00000E-03
        ... (rows deleted)...
49608 TR 2  -1.00000E-03

'GROUPS'
ELEMEN
 127 "Concrete Solid Mesh" / 1-251401 /
 128 "Rebar Solid Mesh" / 251402-253975 /
 130 "1-5" / 253980 ... (rows deleted)... 255734 /
 131 "2-6" / 253981 ... (rows deleted)... 255301 /
 132 "3-7" / 253976 ... (rows deleted)... 255303 /
 133 "4-8" / 253977 ... (rows deleted)... 255735 /
 134 "Top Steel Plate" / 255736-255795 /
 135 "Support Steel Plates" / 255796-255915 /

'SUPPOR'
NAME "Supports"
/ 49661 ... (rows deleted)... 49705 / TR 1
/ 49661 ... (rows deleted)... 49655 / TR 2
NAME "Symmetry"
/ 1 ... (rows deleted)... 49596 / TR 3
NAME "L_Displacement"
/ 49564 ... (rows deleted)... 49608 / TR 2
'END'
```

```
: Diana Datafile written by Diana 9.5
Translated from FX+ for DIANA neutral file (version 1.2.0).

'UNITS'
LENGTH M
FORCE N
TEMPER CELSIU

'DIRECTIONS'
   1   1.00000E+00   0.00000E+00   0.00000E+00
   2   0.00000E+00   1.00000E+00   0.00000E+00
   3   0.00000E+00   0.00000E+00   1.00000E+00

'MODEL'
GRAVDI 3
GRAVAC  -9.81000E+00

'COORDINATES'
    1   2.72500E-01   0.00000E+00   7.50000E-02
            ... (rows deleted)...
49707   2.97273E-02  -5.00000E-03   6.50000E-02

'MATERI'
   1 NAME   "CONCRETE"
     MCNAME CONCR
     MATMDL TSCR
     ASPECT
     POISON   2.00000E-01
     YOUNG    3.38600E+10
     DENSIT   2.40000E+03
     TOTCRK ROTATE
     TENCRV MULTLN
     TENPAR   0  0  4.2476E+06  0.000125446  2.33996136E+06  0.001420924
0.954563148E+06 0.400125446 0 0.674839705
     COMCRV CONSTA
     COMSTR   4.210000E+07
   2 NAME   "REINFORCEMENT STEEL"
     MCNAME MCSTEL
```

```
     MATMDL TRESCA
     ASPECT
     POISON   3.00000E-01
     YOUNG    2.04000E+11
     DENSIT   7.85000E+03
     YIELD  VMISES
     TRESSH NONE
     YLDVAL   5.464000E+08
   3 NAME   "FRICTIONAL MODEL"
:fcyl=     4.21E+01   MPa       fct.m=  4.25   MPa
:r=        5.00E+00   mm        x=      0      mikrometer
     DSTIF            1.12585E+13        1.1851E+12
     USRIFC        BOTH
     USRVAL          0        0.4        0.05        4.00E-03
                     0.00E+00        4.209E+07        1           0
                     1.35E-04        4.209E+07        0.86        0
                     2.80E-04        4.196E+07        0.78        0
                     4.11E-04        4.175E+07        0.72        0
                     6.21E-04        4.057E+07        0.65        0
                     8.30E-04        3.952E+07        0.59        0
                     1.07E-03        3.662E+07        0.56        0
                     1.51E-03        3.186E+07        0.52        0
                     1.90E-03        2.963E+07        0.52        0
                     2.60E-03        2.702E+07        0.52        0
                     4.71E-03        2.277E+07        0.52        0
                     1.21E-02        2.845E+07        0.52        0
                     1.50E+20        0.000E+00        0.52        0
                0 0
                1E6 0
                14E9 2.0                  5.00E-03        0E-6 7.0
     USRSTA   0.0   0.0   0.0   0.0   0.0   0.0   0.0          1.13E+13
0.0 0.0 0.0 0.0 0.0 0.0 0.0 0.0 0.0 0.0
     USRIND  0 13 2
   4 NAME   "STEEL PLATES"
     YOUNG    2.10000E+11
     POISON   2.00000E-01

'GEOMET'
   1 NAME   "INTstre_3-7"
     XAXIS    0.00000E+00  -3.54000E-03   1.46400E-03
   2 NAME   "INTstre_4-8"
```

```
     XAXIS    0.00000E+00  -1.46000E-03   3.53600E-03
   3 NAME   "INTstre_1-5"
     XAXIS    0.00000E+00  -1.46000E-03  -3.54000E-03
   4 NAME   "INTstre_2-6"
     XAXIS    0.00000E+00  -3.54000E-03  -1.46000E-03
   5 NAME   "steel_plate"
   6 NAME   "concrete"
   7 NAME   "steel"

'DATA'
   1 NAME   "concrete"
   2 NAME   "steel"
   7 NAME   "steel_plate"
   3 NAME   "INTstre_1-5"
   4 NAME   "INTstre_2-6"
   5 NAME   "INTstre_3-7"
   6 NAME   "INTstre_4-8"

'ELEMENTS'
CONNECT
253976 T18IF 48678 49032 48808 8814 12497 12279
           ... (rows deleted)...
255915 TP18L 275 329 330 49678 49703 49695
     1 TE12L  29127 22157 21535 28171
           ... (rows deleted)...
253975 TE12L 48624 12946 12947 12267
MATERI
/ 1-251401 / 1
/ 251402-253975 / 2
/ 253976-255735 / 3
/ 255736-255915 / 4
DATA
/ 1-251401 / 1
/ 251402-253975 / 2
/ 255736-255915 / 7
/ 253980 ... (rows deleted)... 255734 / 3
/ 253981 ... (rows deleted)... 255301 / 4
/ 253976 ... (rows deleted)... 255303 / 5
/ 253977 ... (rows deleted)... 255735 / 6
GEOMET
```

```
/ 253976 ... (rows deleted)... 255303 / 1
/ 253977 ... (rows deleted)... 255735 / 2
/ 253980 ... (rows deleted)... 255734 / 3
/ 253981 ... (rows deleted)... 255301 / 4
/ 255736-255915 / 5
/ 1-251401 / 6
/ 251402-253975 / 7

'LOADS'
CASE 1
NAME "Displacement"
DEFORM
49564 TR 2  -1.00000E-03
        ... (rows deleted)...
49608 TR 2  -1.00000E-03

'GROUPS'
ELEMEN
 127 "Concrete Solid Mesh" / 1-251401 /
 128 "Rebar Solid Mesh" / 251402-253975 /
 130 "1-5" / 253980 ... (rows deleted)... 255734 /
 131 "2-6" / 253981 ... (rows deleted)... 255301 /
 132 "3-7" / 253976 ... (rows deleted)... 255303 /
 133 "4-8" / 253977 ... (rows deleted)... 255735 /
 134 "Top Steel Plate" / 255736-255795 /
 135 "Support Steel Plates" / 255796-255915 /

'SUPPOR'
NAME "Supports"
/ 49661 ... (rows deleted)... 49705 / TR 1
/ 49661 ... (rows deleted)... 49655 / TR 2
NAME "Symmetry"
/ 1 ... (rows deleted)... 49596 / TR 3
NAME "L_Displacement"
/ 49564 ... (rows deleted)... 49608 / TR 2
'END'
```

APPENDIX D

Maximum CMOD during curing of epoxy

Table D.1. Maximum CMOD reached during curing of epoxy for all tested beams.

Specimen	*PC1*	*PC2*	*PC3*	*PC4*
CMOD [mm]	0.77	0.75	1.25	1.25

Specimen	*SF1*	*SF2*	*SF3*	*SF4*
CMOD [mm]	0.78	0.74	1.21	1.26

Specimen	*Hy1*	*Hy2*	*Hy3*	*Hy4*
CMOD [mm]	0.78	0.8	1.25	1.24

APPENDIX E

Pictures of fluorescent crack pattern

PLAIN CONCRETE

PC1A

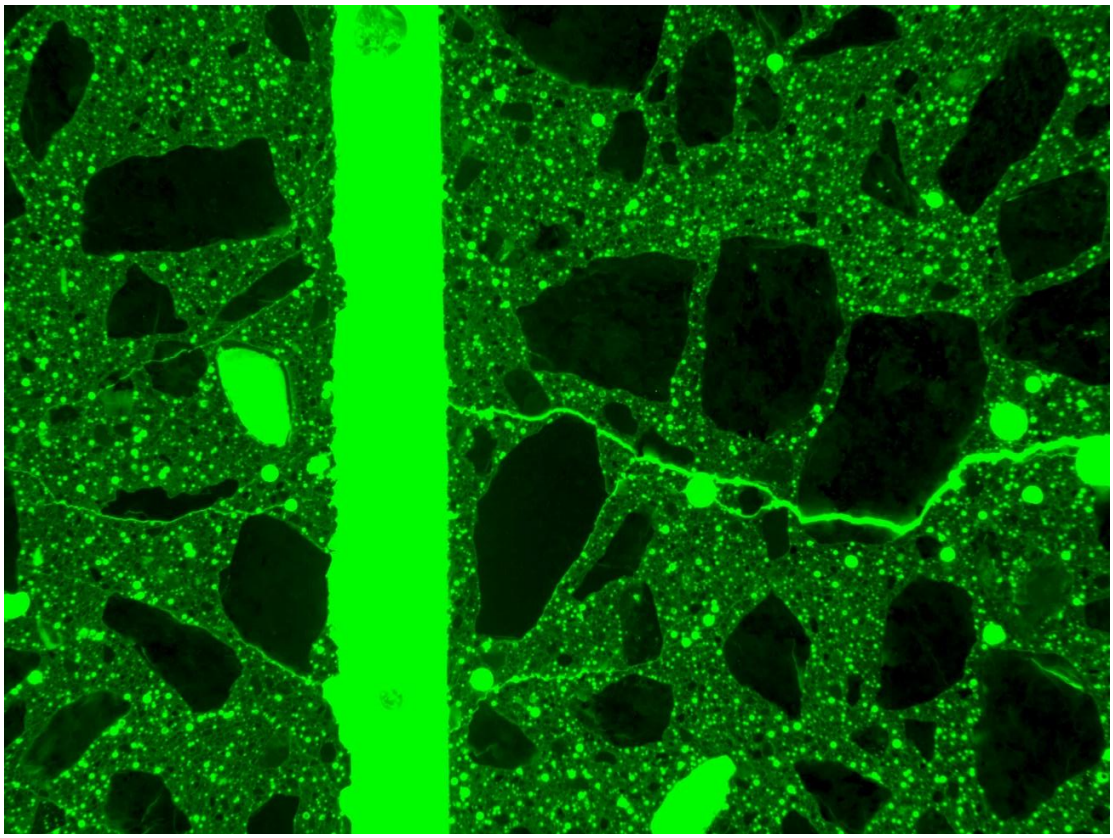

PC1B

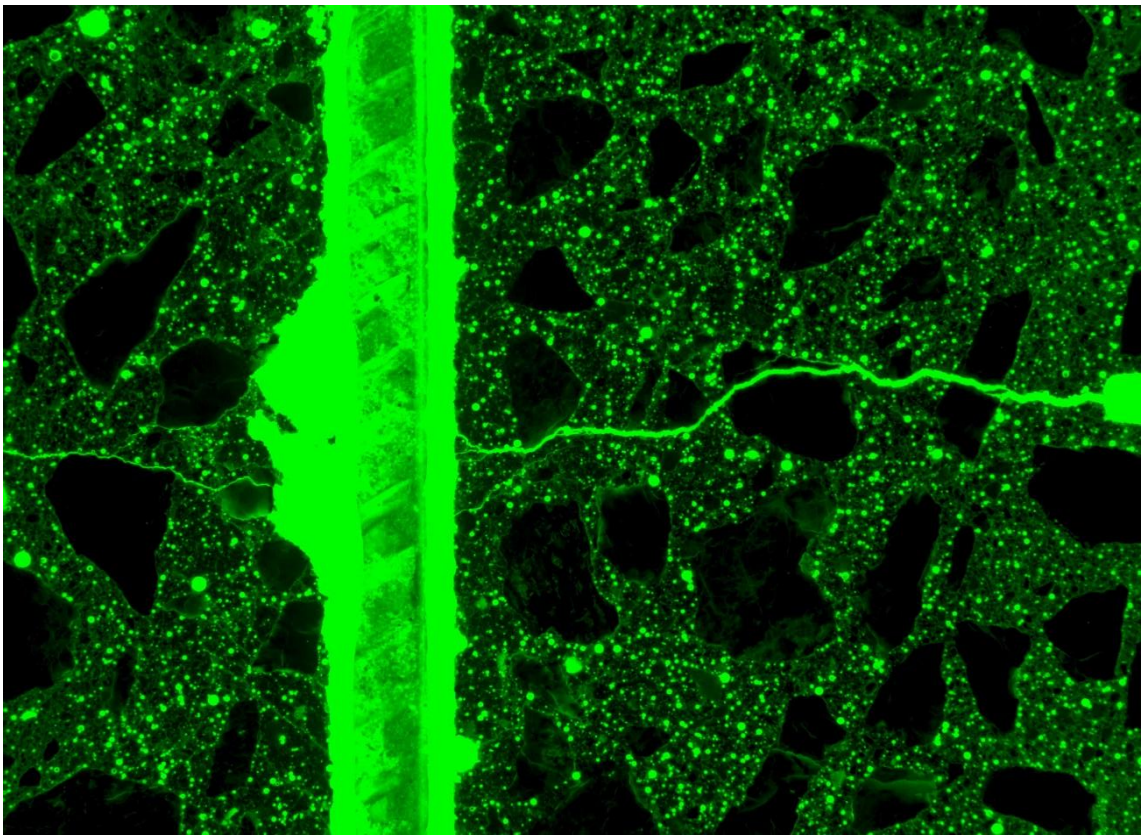

PC2A

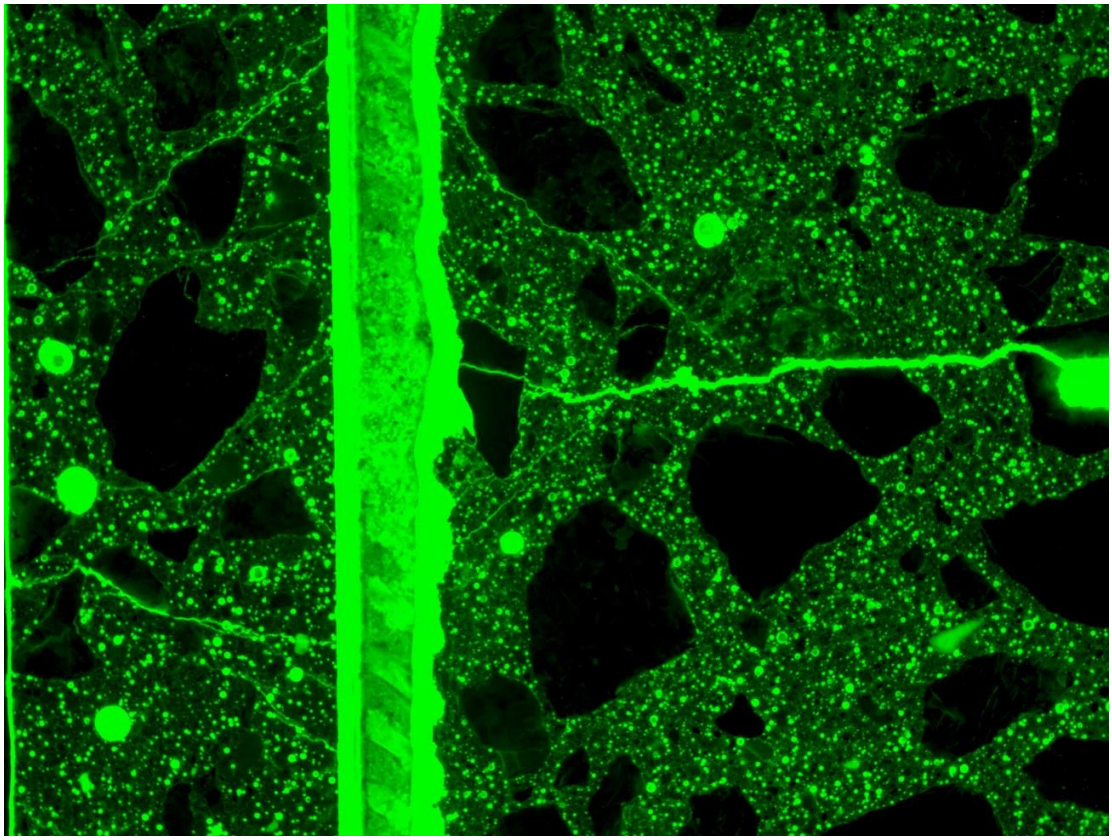

PC2B

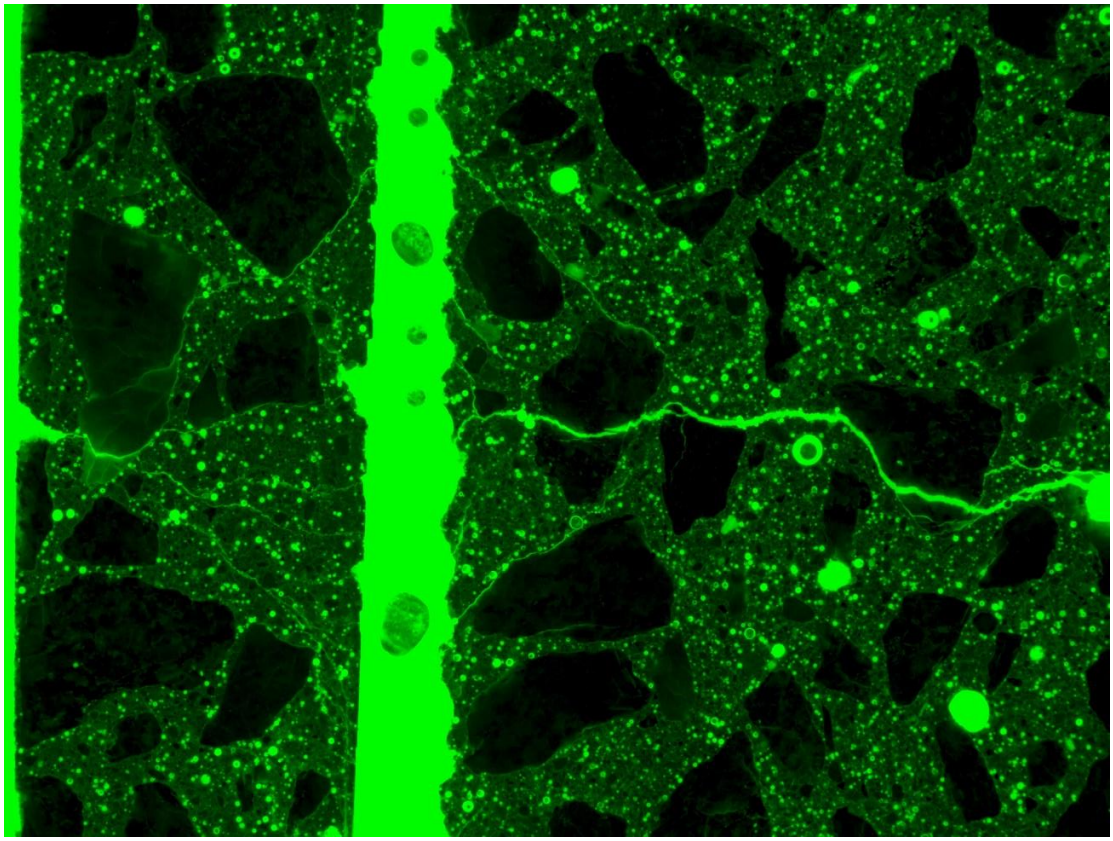

PC3A

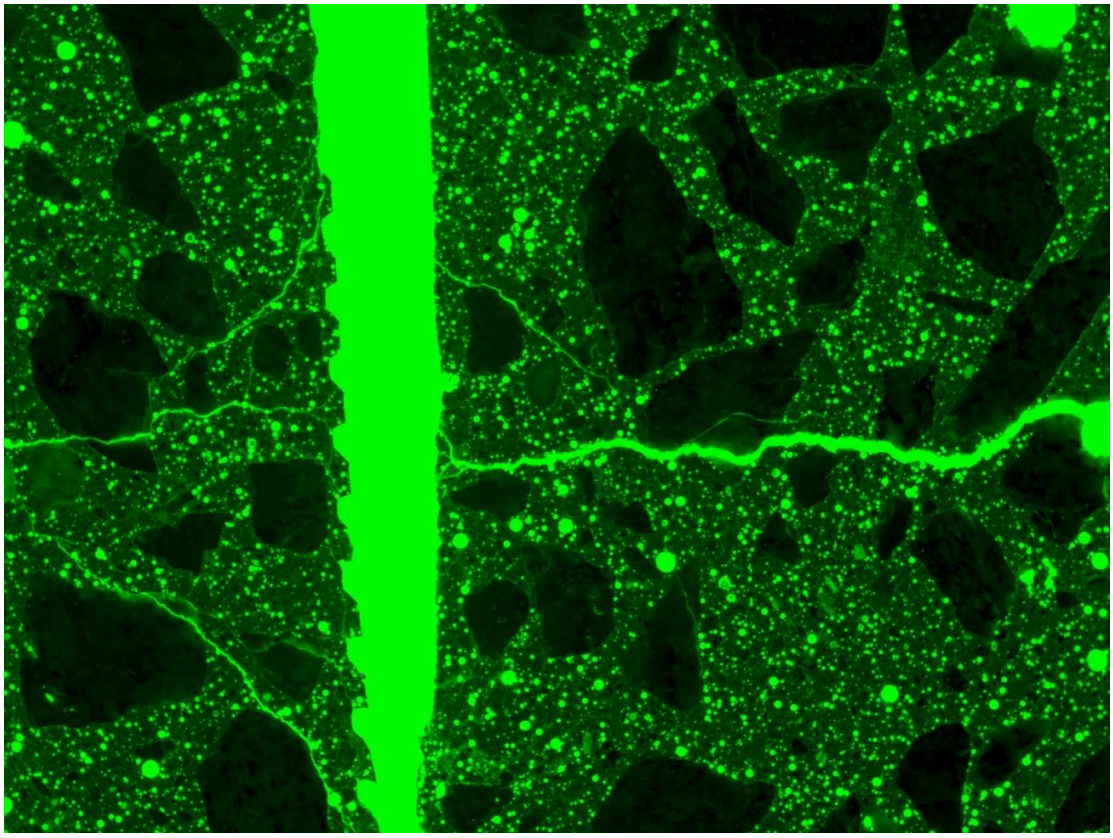

PC3B

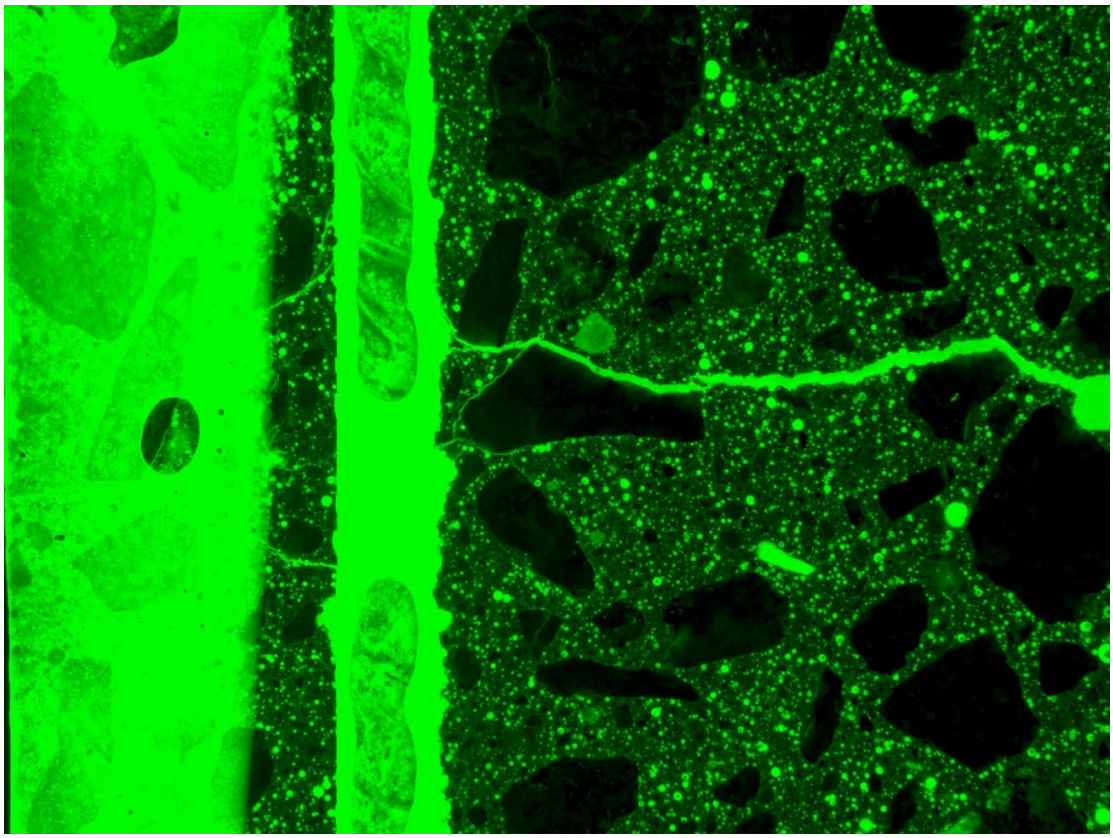

PC4A

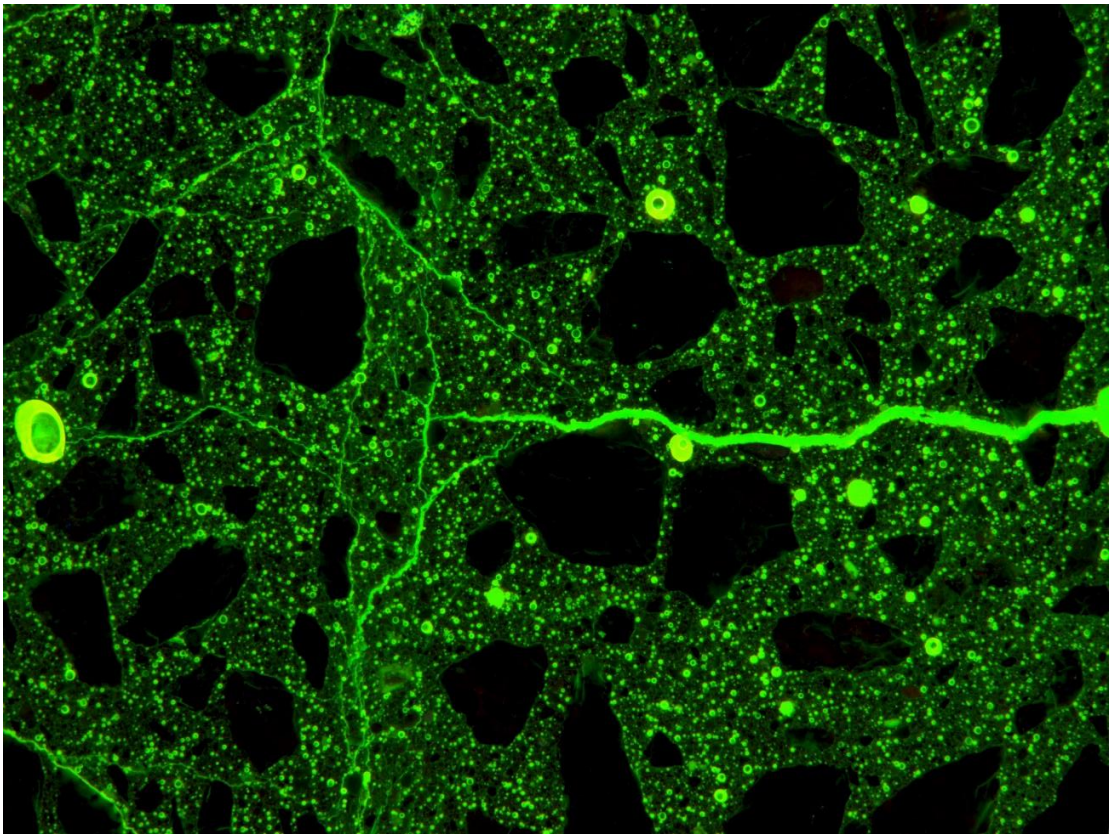

PC4B

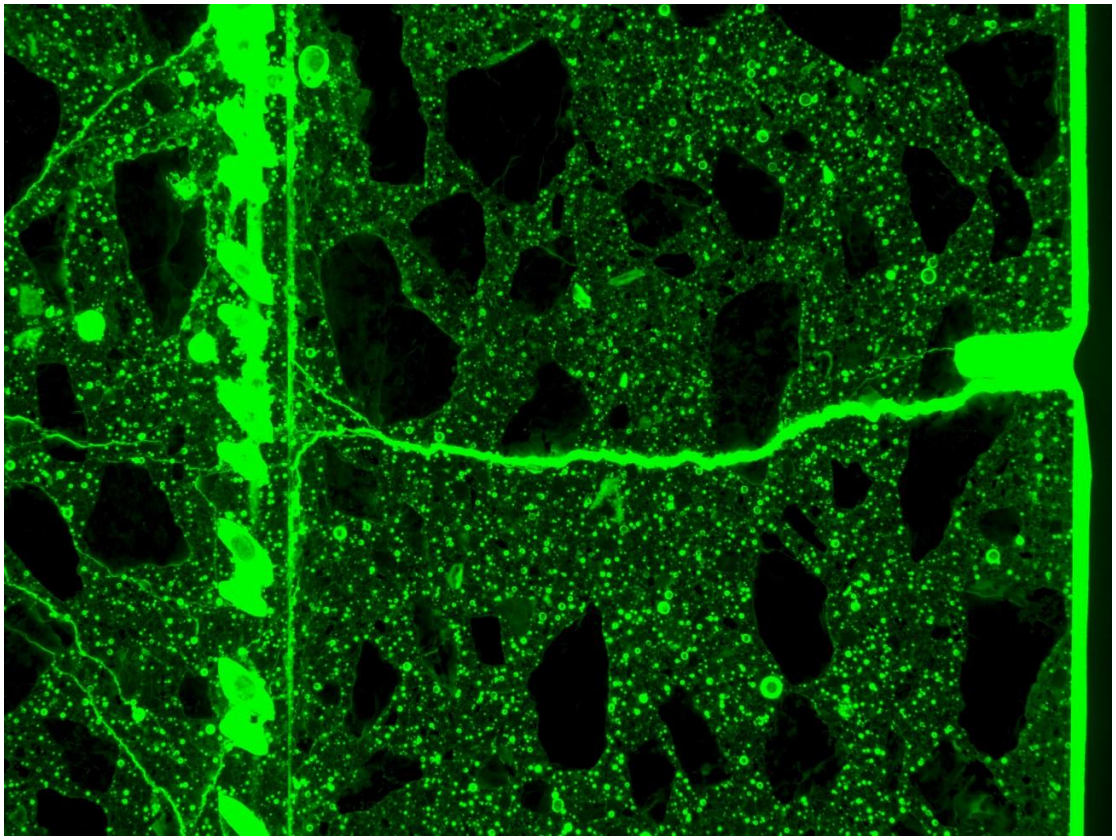

SFRC

SF1A

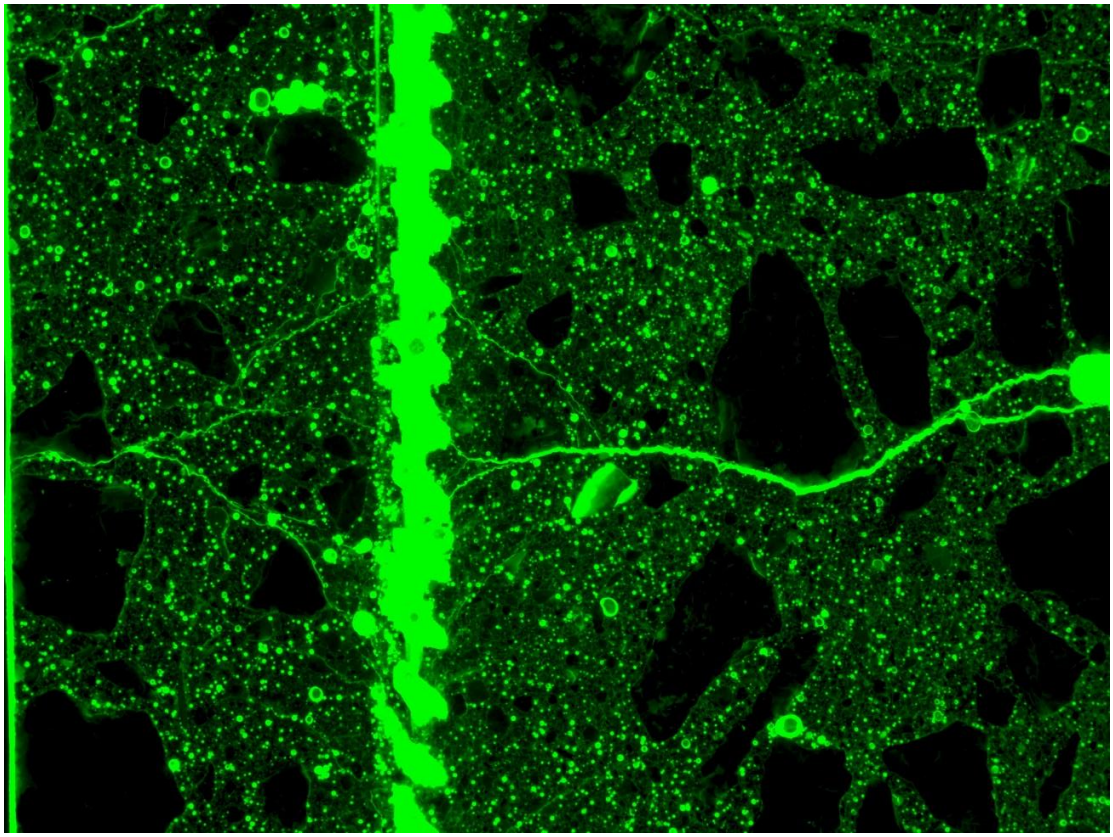

SF1B

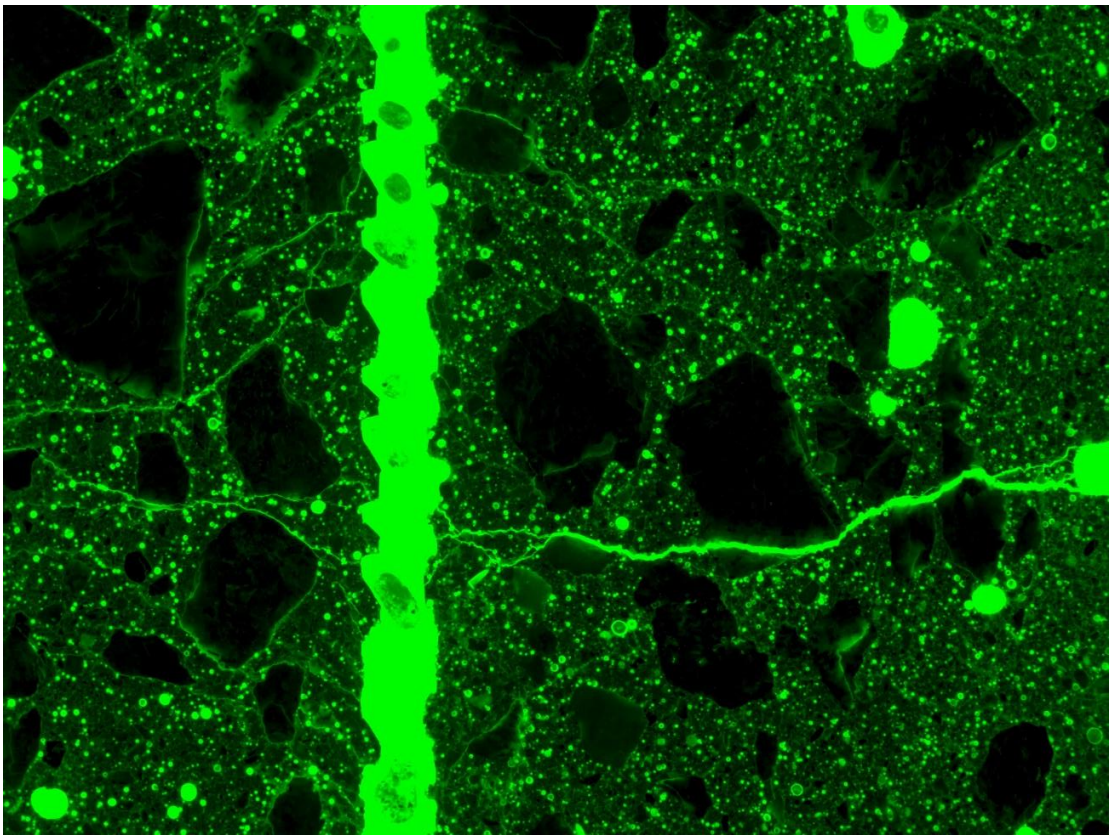

SF2A

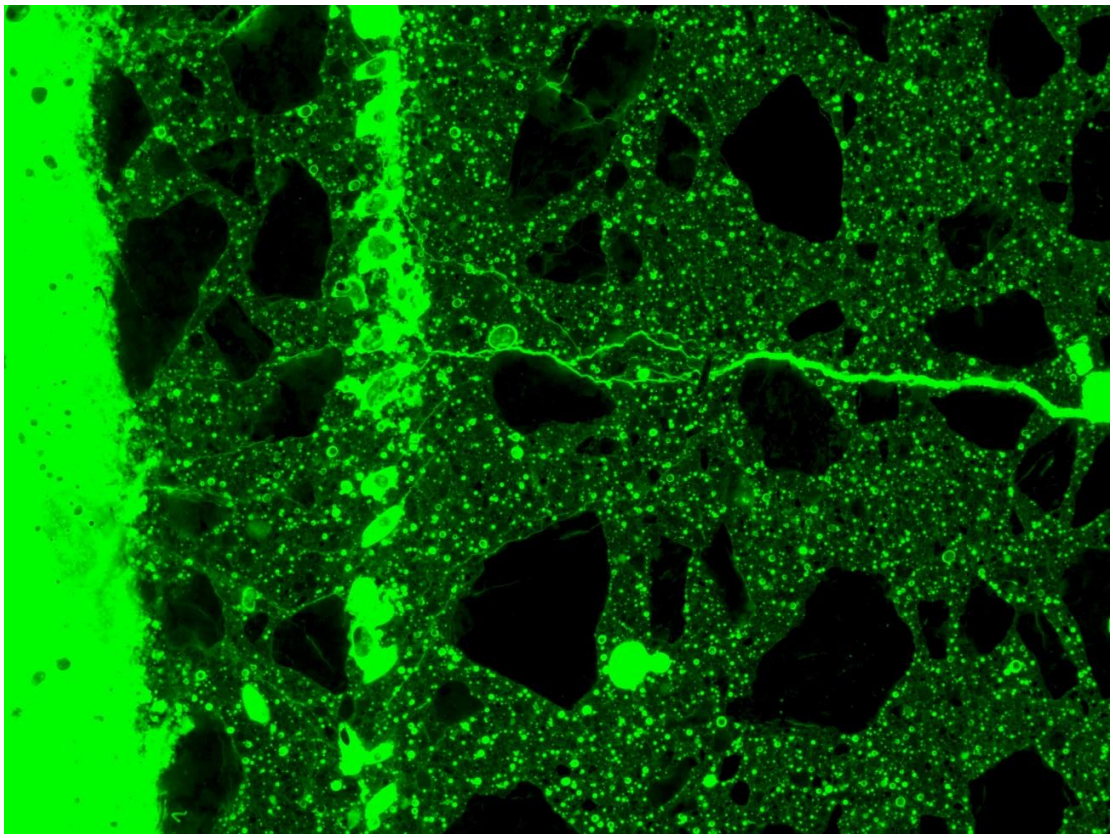

SF2B

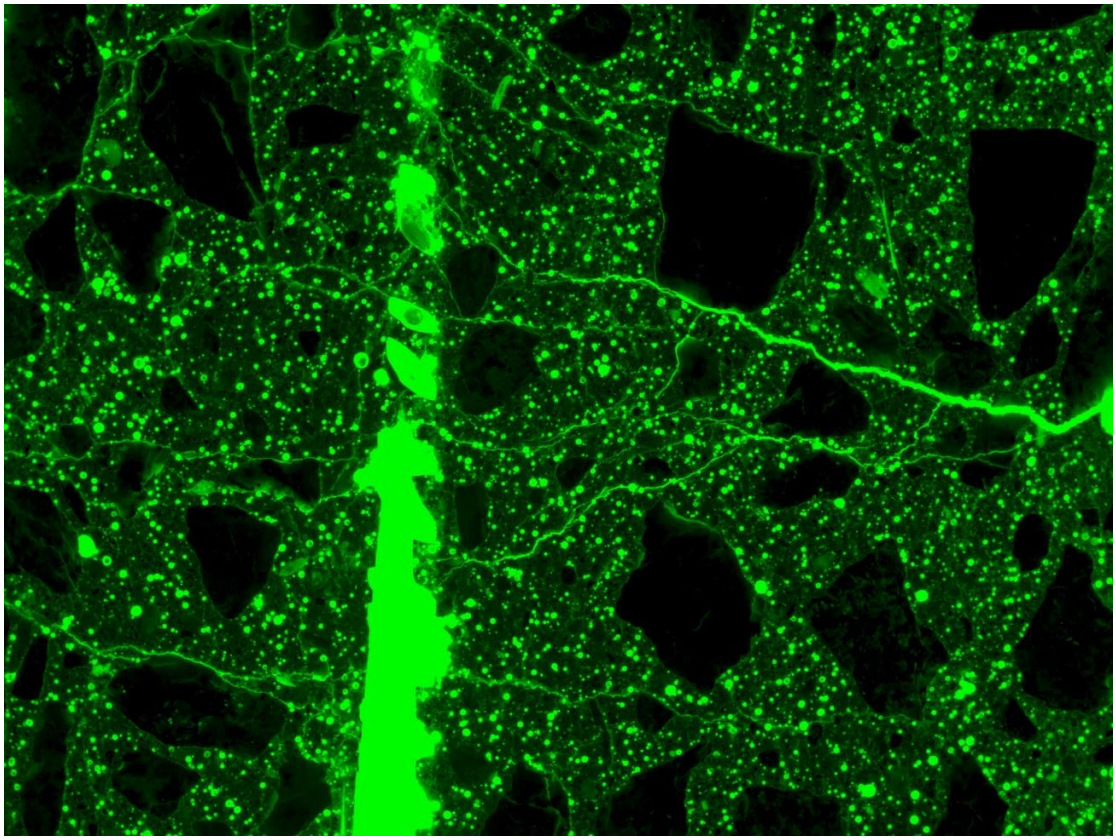

SF3A

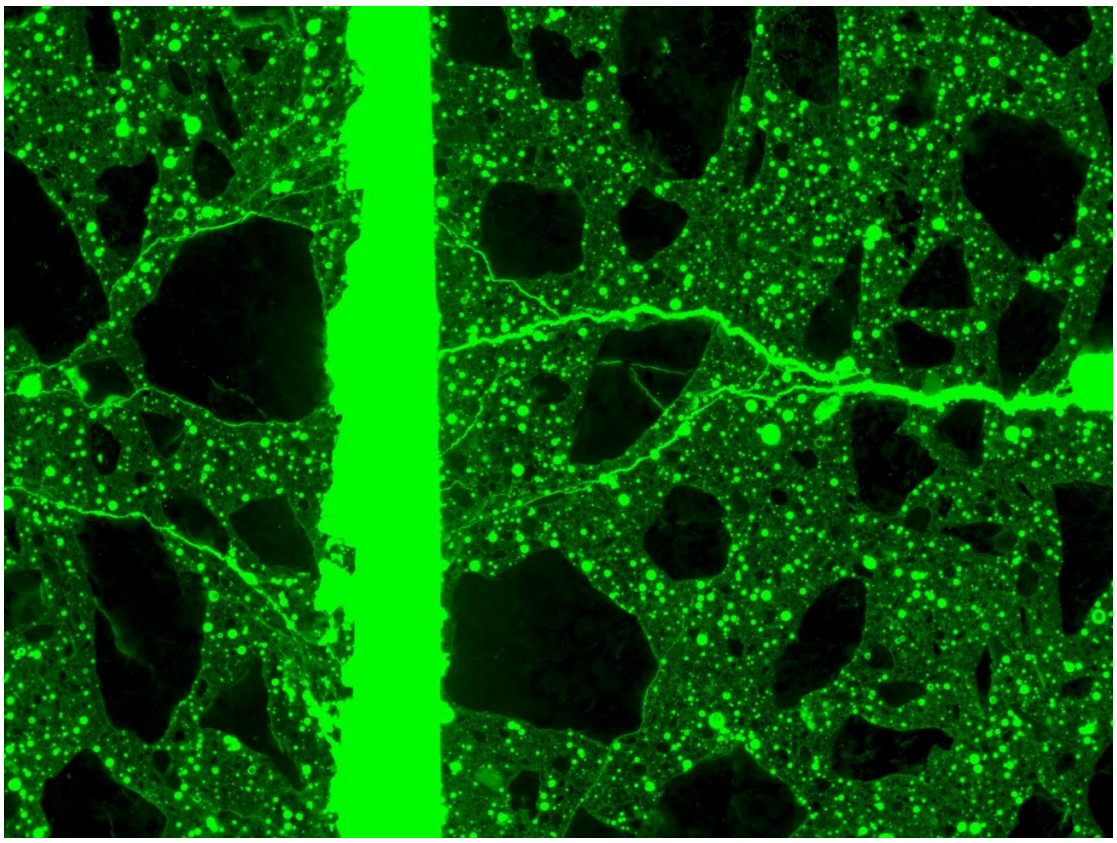

SF3B

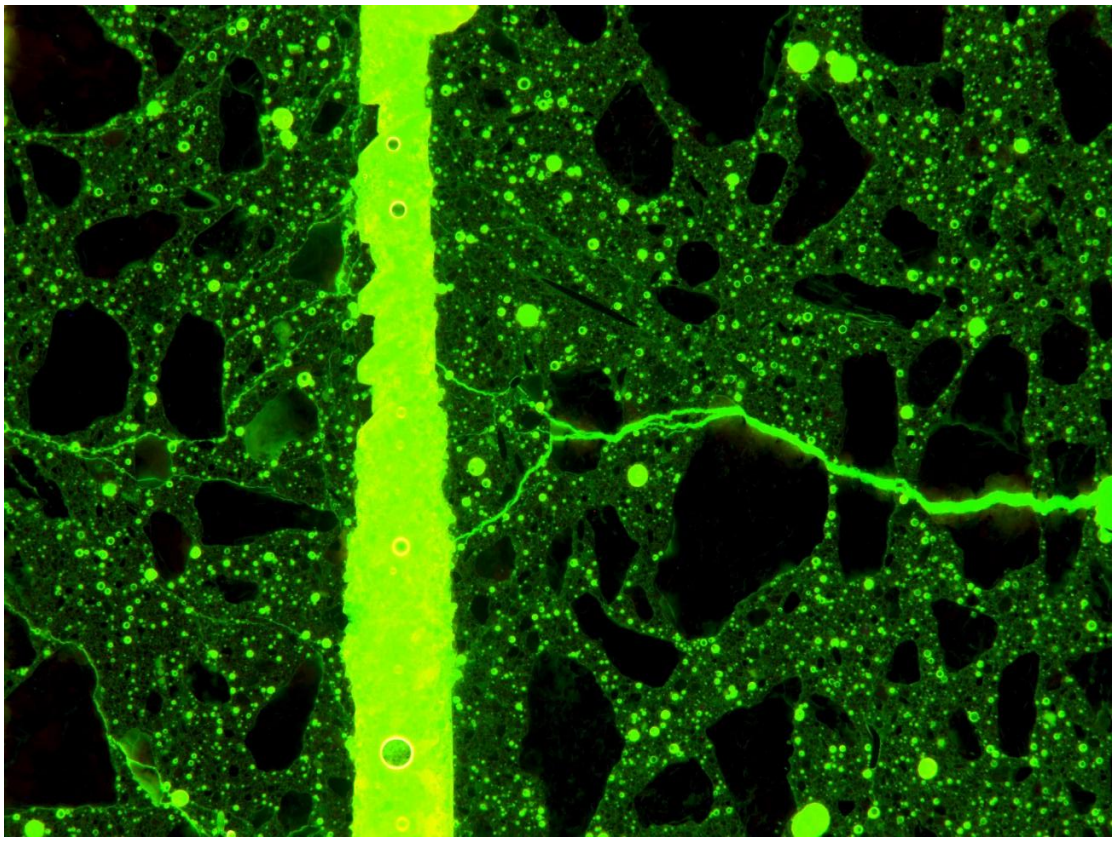

SF4A

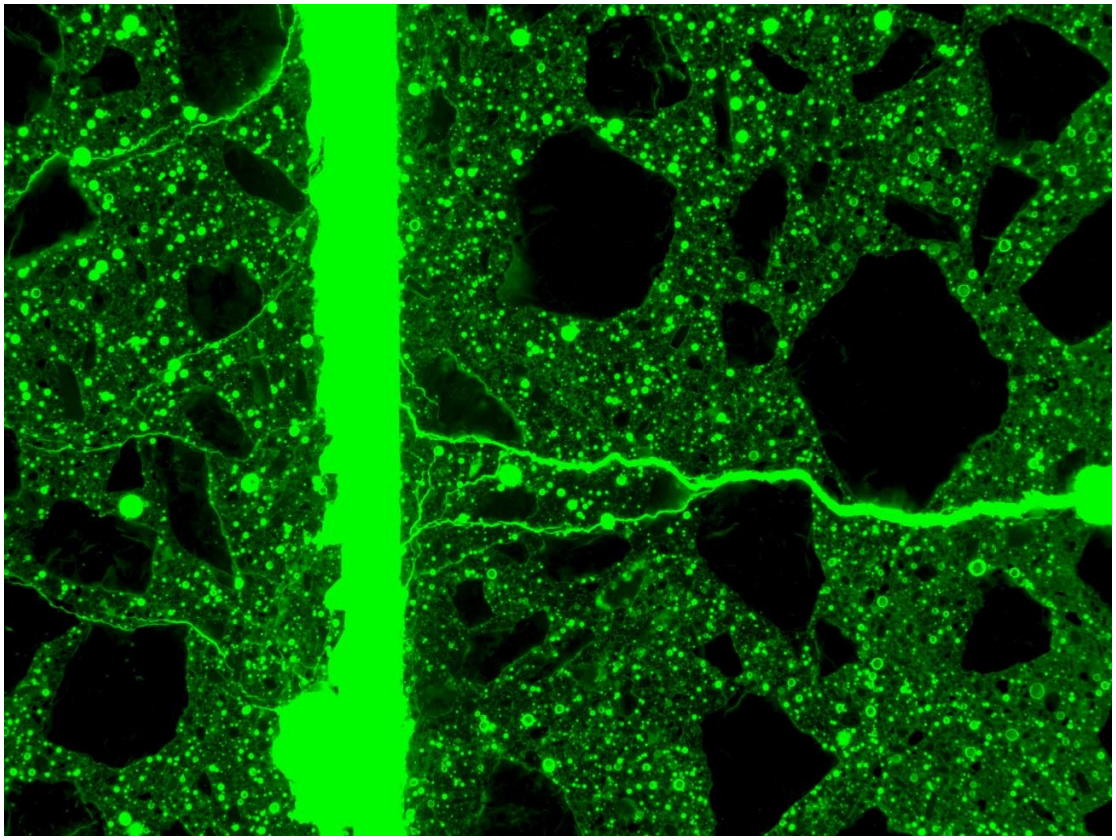

SF4B

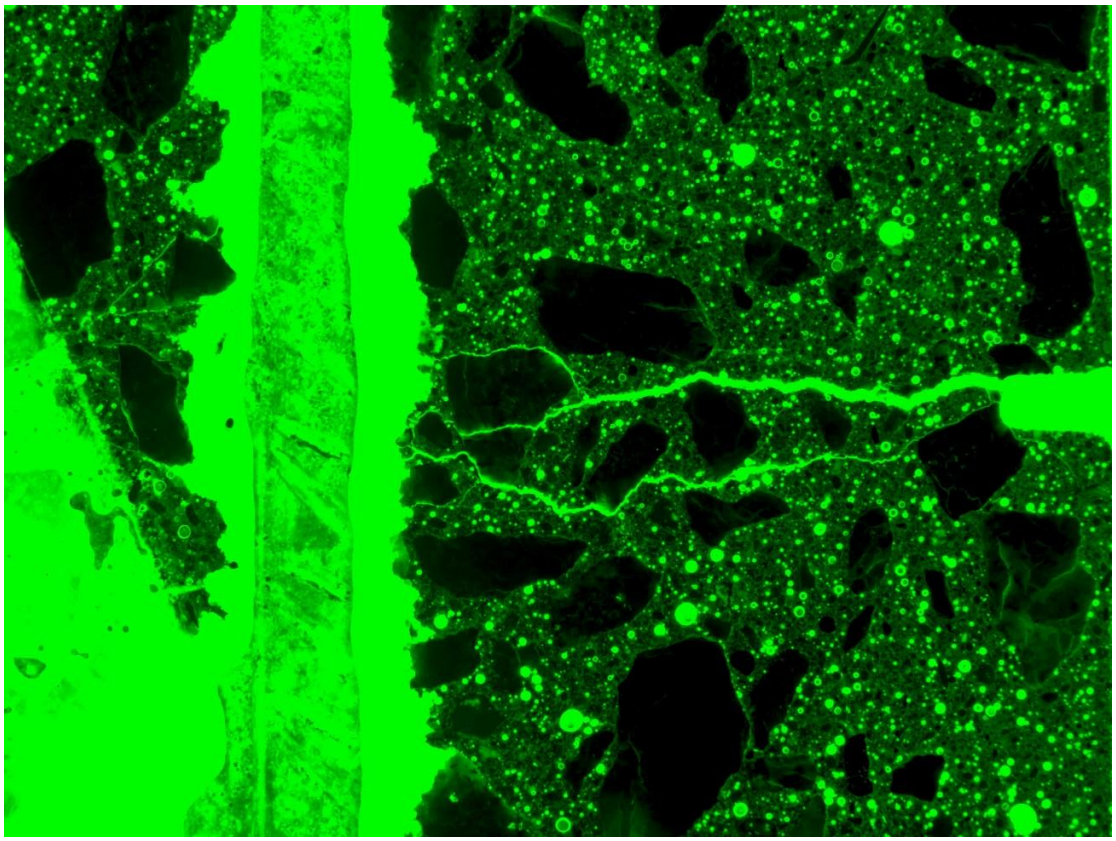

HyFRC

Hy1A

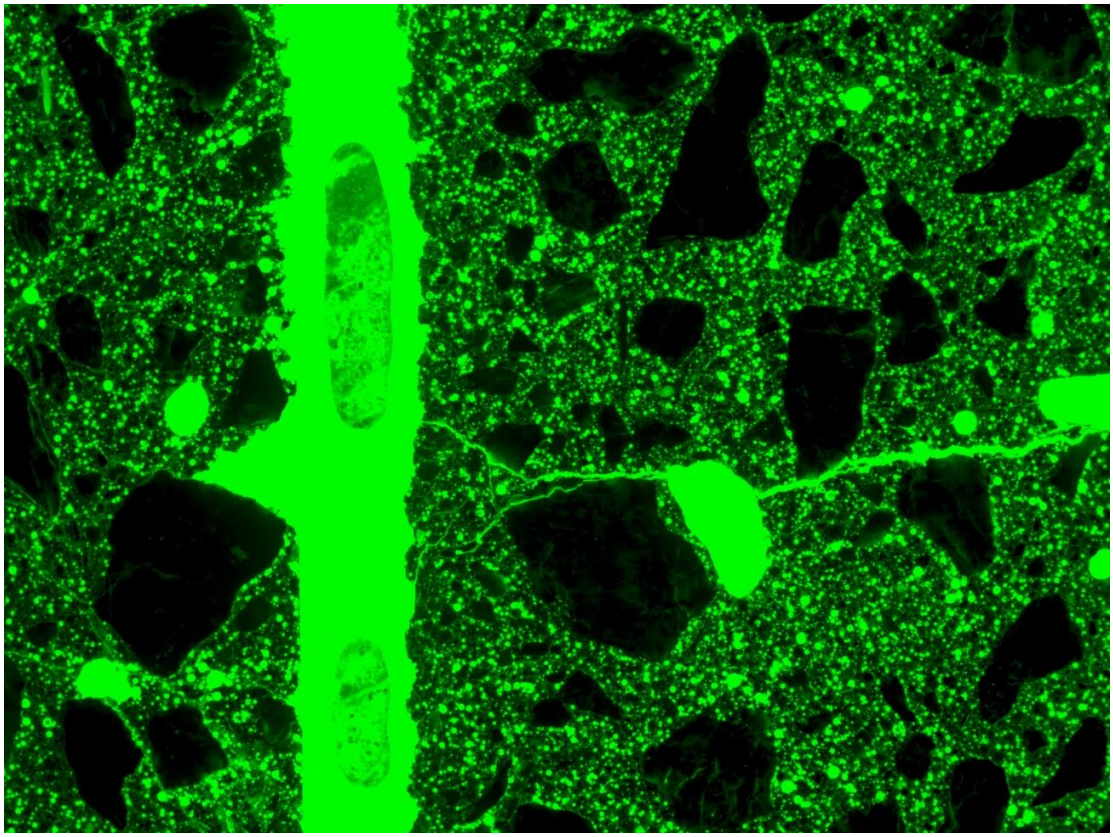

Hy1B

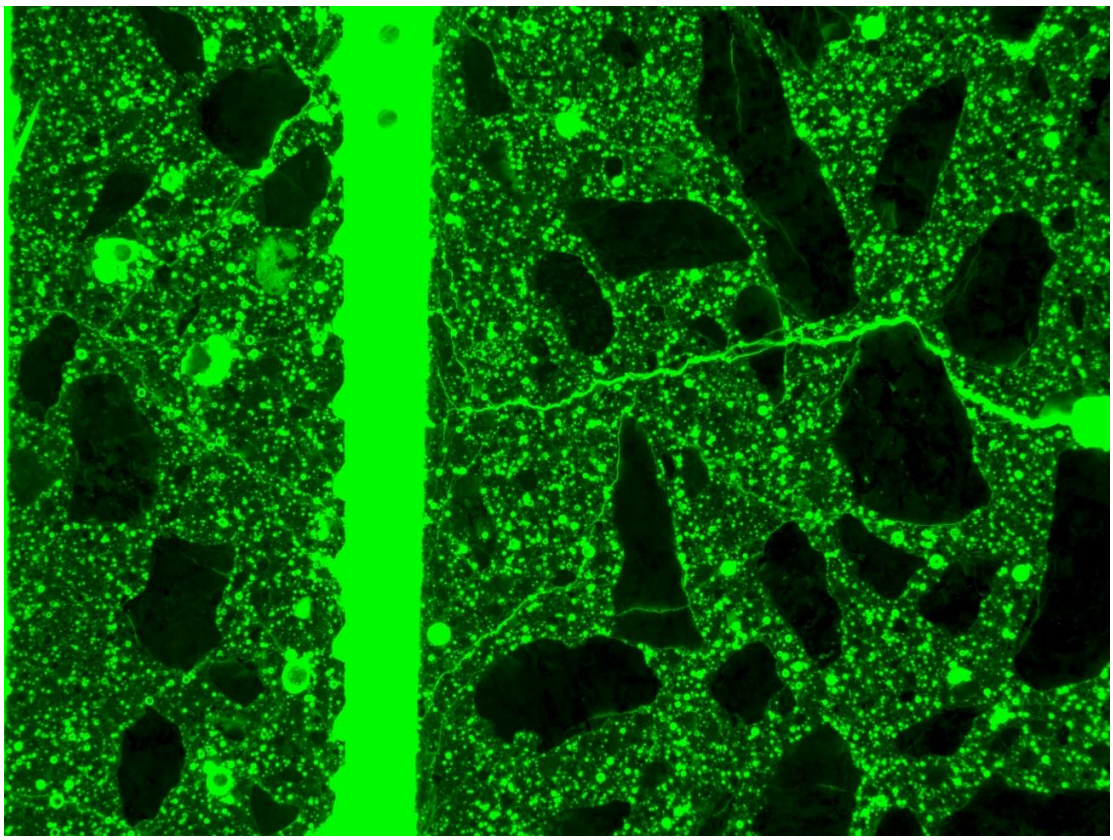

Hy2A

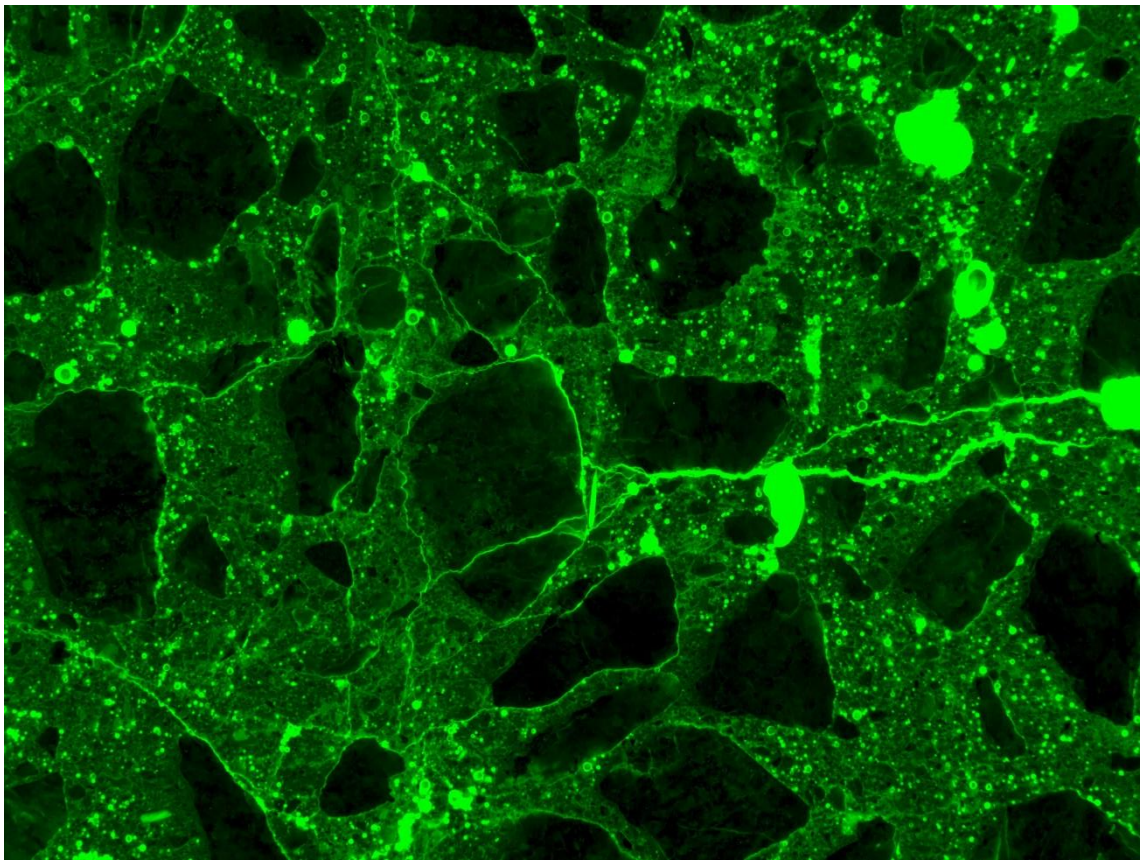

Hy2B

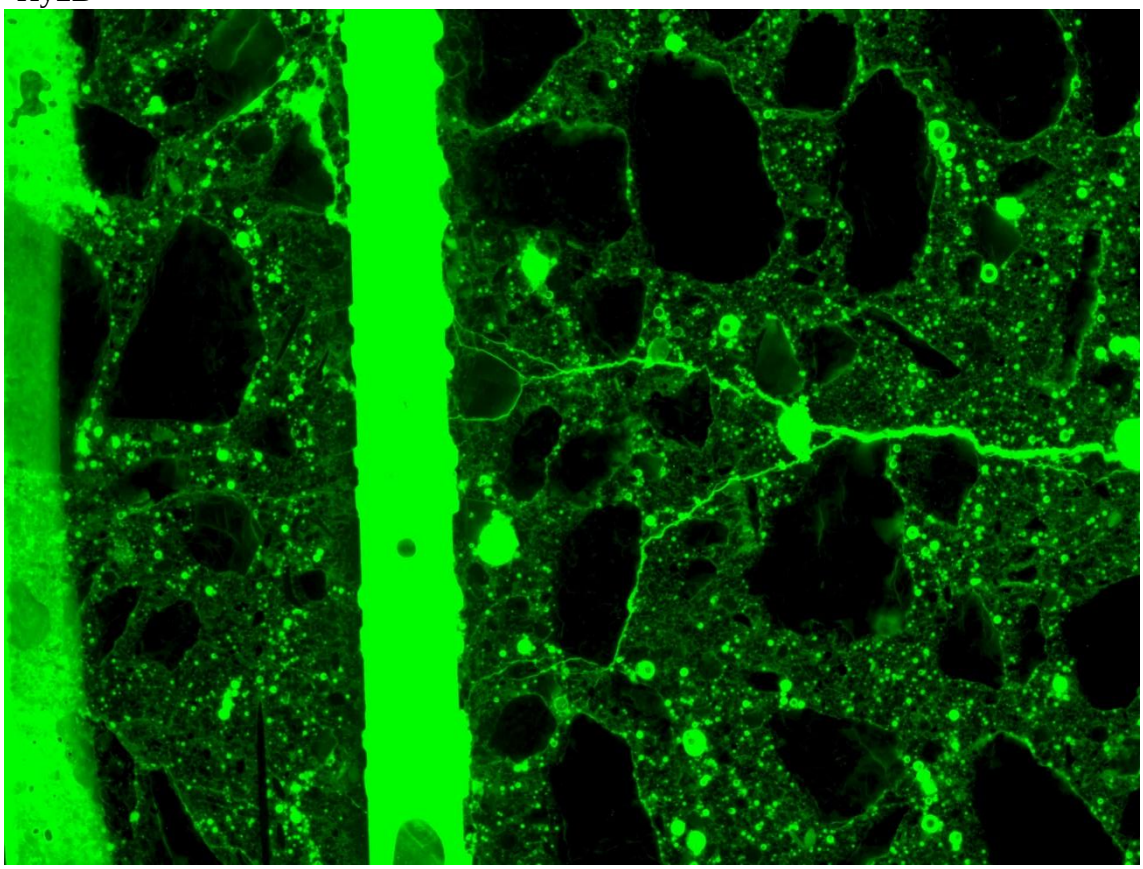

Hy3A

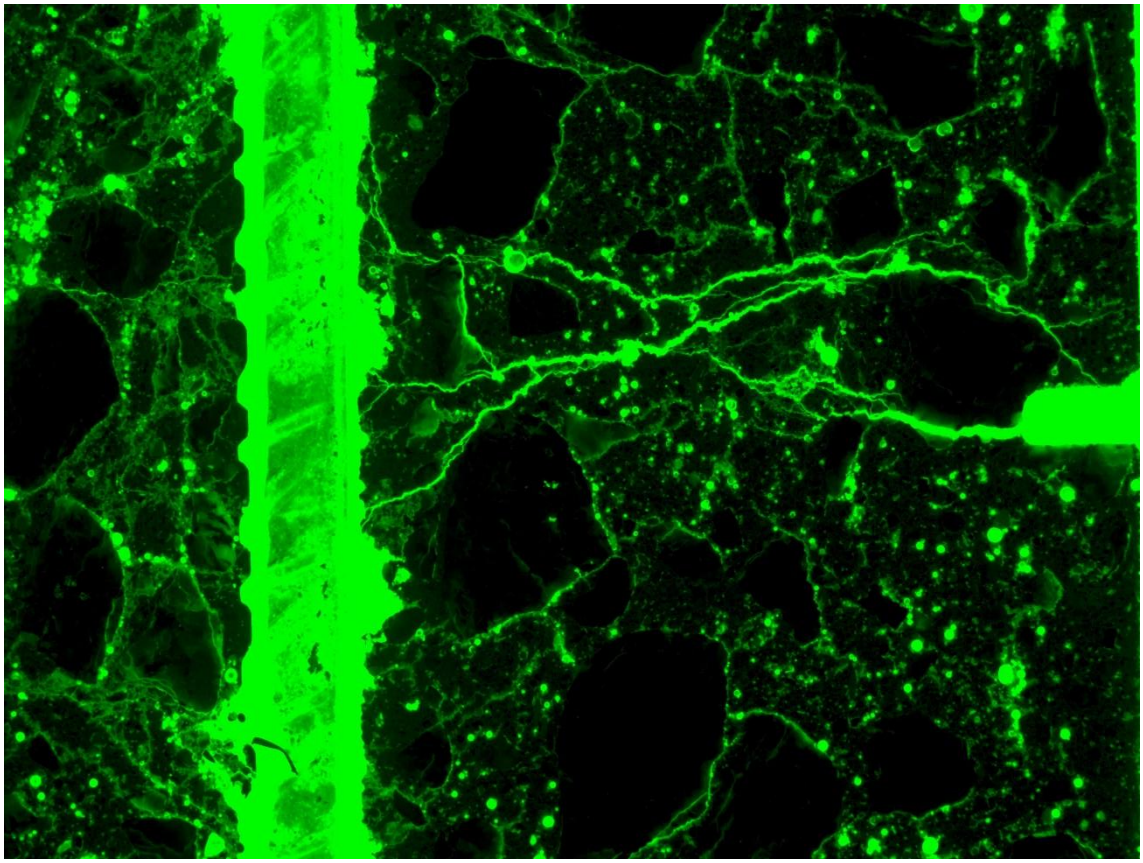

Hy3B

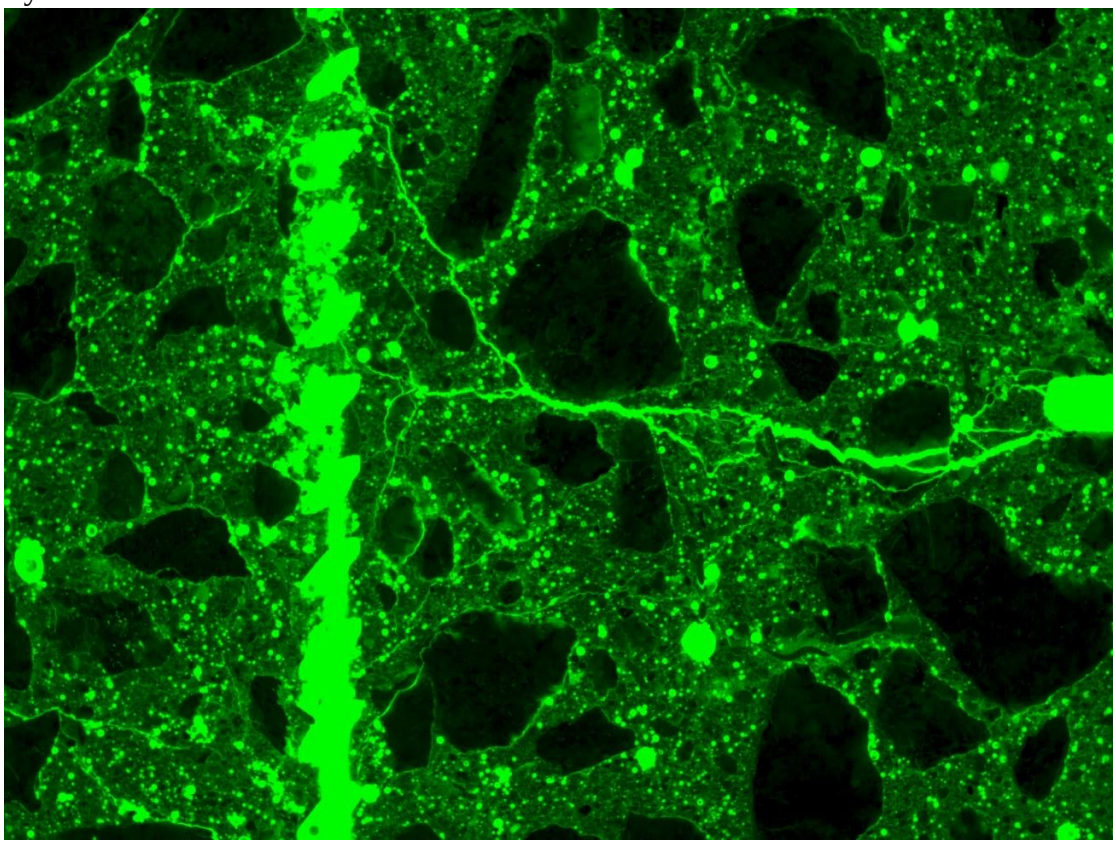

Hy4A

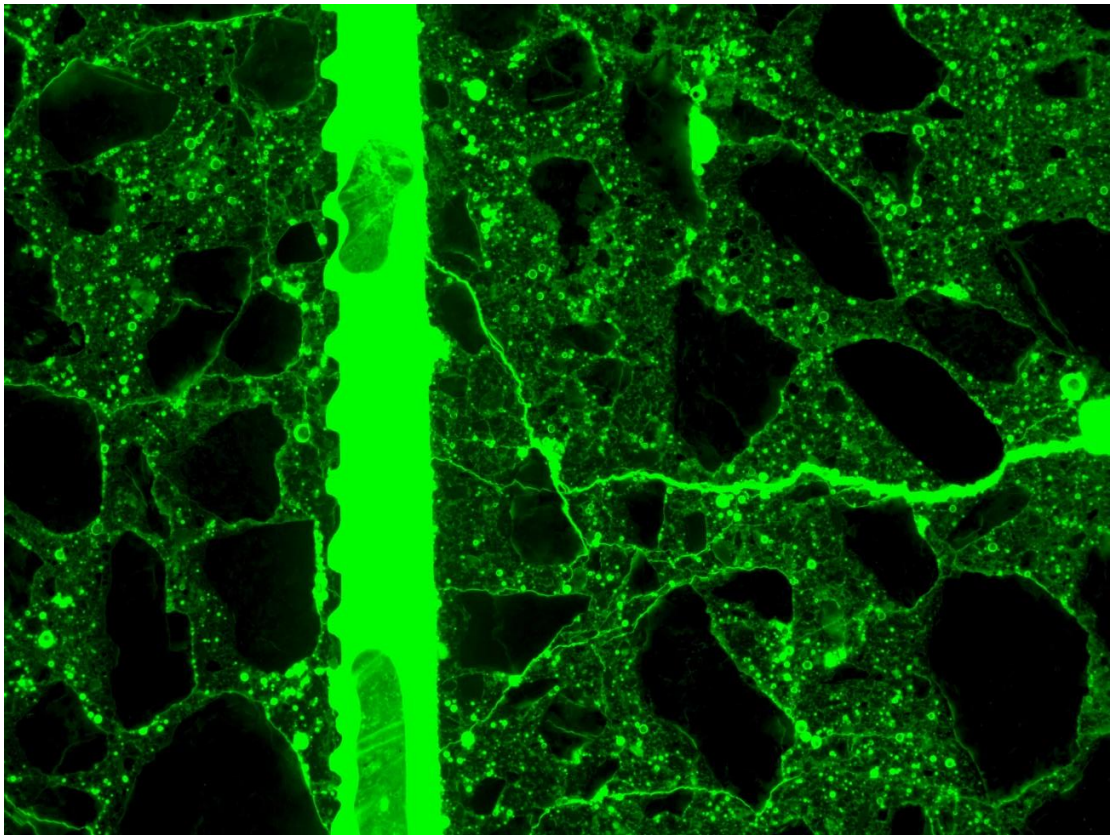

Hy4B